FUTURE COASTLINE RECESSION AND BEACH LOSS IN SRI LANKA





UNIVERSITY OF TWENTE.

UNESCO IHE DELFT

Paul Bakker

July 2018

Future Coastline Recession and Beach Loss in Sri Lanka

Master of Science (MSc) graduation thesis by:
Paul J. J. Bakker

Supervisors:
Rosh W.M.R.J. Ranasinghe, prof.
Pieter C. Roos, dr. ir.

Mentors:
Janaka Bamunawala, ir.
Trang M. Duong, dr. ir.
Keiko Udo, dr. ir.

Examination committee:
Ali Dastgheib, dr. ir.
Rosh W.M.R.J. Ranasinghe, prof. (Chairman)
Pieter C. Roos, dr. ir.

July 2018

Illustrations cover page (f.t.l.t.b.r.):

- Reiger, B. (2016). [Photograph]. Retrieved from: http://www.bertrandrieger.com/folio/691/sri-lanka-2016/page-6.html
- n.d. (2016). [Photograph]. Retrieved from: https://island-spirit.org/sri-lanka/climate-changing-sri-lanka/
- Pushpa Kumara, M.A. & Tharangani Fonseka, R. (2014). *Sea erosion in Ransigamawella, off Wennappuwa* [Photograph]. Retrieved from: http://www.sundaytimes.lk/140824/news/alarm-over-rising-seas-but-villagers-keep-returning-to-risky-shore-114753.html
- Barton, K. (2017). [Photograph]. Retrieved from: https://island-spirit.org/sri-lanka/climate-changing-sri-lanka/
- Sekitar (2012). *Negombo Lagoon by air, Sri Lanka* [Photograph]. Retrieved from: https://www.flickr.com/photos/sekitar/6860657454/

Abstract

Amongst accelerating trends, the response of coastlines to sea-level rise is of major importance to policy makers. This research aims to provides a nation-wide overview of short-term (2050) and long-term (2100) coastline recession and beach loss along the Sri Lankan coast.

Coastline recession estimates have been acquired using the original formulation of the first-pass assessment method for sea-level rise induced coastal erosion known as the Bruun rule, nearshore bathymetry measurements, and mean and likely climate change predictions according to the four Representative Concentration Pathways (RCPs) in the Fifth Assessment Report published by the Intergovernmental Panel on Climate Change. Additionally, future coastline recession at beaches downdrift from several important rivers, and large coastal lakes and lagoons have been assessed using the (reduced) Scale-aggregated Model for Inlet-interrupted Coastlines, and the BQART model determining annual fluvial sediment supplies combined with a sediment trapping efficiency protocol for nested reservoirs.

The nation-wide averaged (representing 48% of the Sri Lankan coast) mean sea-level rise induced long-term coastline recession is 16 m (RCP2.6), 21 m (RCP4.5), 23 m (RCP6.0) or 31 m (RCP8.5). However, significant regional (e.g. South-east vs North-east) in the coastline recession estimates are present. Combined with present beach widths measured from satellite data, the mean Bruun rule coastline recession estimates show considerably reduced future beach widths and the possible disappearance of a vast number of beaches along most of the Sri Lankan coast.

Downdrift from East and North-east coast lagoons that are open or intermittently closed to the ocean, sea-level rise will result in mild to (dangerously) strong local coastline recession. The presence of lagoons in the Jaffna Peninsula is expected to result in local coastline progradation. Projected changes to the terrestrial climate and continuing human development of river catchments will result in increased annual fluvial sediment supplies. However, without limits to future river mining activities, local coastline recessions remain a possibility.

Acknowledgements

This thesis has been written to complete my studies in Water Engineering and Management at the University of Twente and marks the end of the great years I have had in the city of Enschede.

It has been an enticing and challenging puzzle that has introduced me to the wonders of the Sri Lankan coast and the various dimensions to coastal management. Putting all the pieces into place would never have been possible without the invaluable guidance, never ending support and practical feedback by my supervisors Rosh Ranasinghe and Pieter Roos. Furthermore, I would like to thank Janaka Bamunawala for the many discussions, and Ali Dastgheib, Trang Duong and Keiko Udo for their helpful comments.

I have been extremely fortunate with the incredible efforts by Mangala Wickramanayake, Dammith Rupasinghe and all other members of Coastal Research and Design Division at the Coast Conservation Department in Colombo and their kindness during my visit to Sri Lanka. I would also like to express my gratitude to CDR International for their contributions to my thesis.

With this I would like to invite the reader to enjoy the fruits of my hard work.

Paul Bakker

July 2018

Table of Contents

1. Introduction

1.1. Problem Statement

Mitigation of climate change related impacts is a challenge shared by counties all over the globe. Expected to be one of the major drivers of coastline recession, high future sea-level rise rates may have dire global consequences (Ranasinghe & Stive, 2009).

Figure 1: Location of Sri Lanka (black) in the North Indian Ocean and East of the Southern tip of India.

In line with the global trend, the island nation Sri Lanka (Figure 1) has known strong development of its West to South coast responsible for more than 40 percent of the Sri Lankan Gross Domestic Product (CCD, 2006). Moreover, the recent end to the Sri Lankan Civil War and the availability of coastal resources have led to a stark increase in the development of parts of its Eastern coast (Dastgheib et al., 2017). The large built-up areas, (nonregistered) dwellings, (rail)roads and other infrastructure, restrict coastal processes (CCD, 2006; Dastgheib et al., 2017) and are prone to the consequences of coastline recession (Jayathilaka, 2015). Coupled with the low resilience of communities commonly found in developing countries (Duong, 2015), sea-level rise is a significant threat to the Sri Lankan economy and survival of its coastal communities.

In spite of recent efforts by Dastgheib et al., 2017 to gain insight into future sea-level rise induced coastline recession along the Sri Lankan coast, a nationwide overview, useful in drafting preventive and/or mitigation policies, is lacking.

Offering natural harbours, opportunities to the recreation and tourism industry and prime waterfront real estate (Duong, 2015), clusters of coastal development can be found in proximity of the numerous inlet-basin systems along the Sri Lankan coast. Of equal importance is the future state of 103 rivers that reach the Sri Lankan coast. Consequently, possible additional local coastline recession due to the response of rivers and inlet-basin systems to climate change and future anthropogenic changes to catchments must be explored (Bamunawala et al.; CCD, 2006; Ranasinghe et al., 2013; Wickramaarachchi, 2010).

1.2. Research Objective and Research Questions

1.2.1. Research Objective

The goal of this research is threefold. Firstly, it aims to assess the credibility and accuracy of the Bruun rule (Bruun, 1962) in determining future positions of the Sri Lankan coastline. Secondly, this research aims to determine the response of the Sri Lankan coastline to projected sea-level rise trends, climate change related variations in the terrestrial climate, continuing development of catchments and possible future river mining volumes, usable to the Coast Conservation Department Sri Lanka (CCD). Thirdly, it intends to assess the consequence of sea-level rise with regard to the width of Sri Lankan beaches.

1.2.2. Research Questions

To achieve the posed research objectives, this document will answer the following four research questions.

RQ 1: *What is the validity of applying the Bruun rule in assessing the future position of the Sri Lankan coastline?*

RQ 2: *What is the predictive accuracy of the Bruun rule for the Sri Lankan coastline?*

RQ 3: *How far will the Sri Lankan coastline recede due to sea-level rise, and what local influence have rivers and inlet-basin systems?*

RQ 4: *What is the consequence of sea-level rise regarding the width of Sri Lankan beaches?*

1.3. Research Scope

The predictive accuracy of the Bruun rule will be assessed two ways; comparing hindcasted Bruun rule coastline recession estimates for the years 1985 – 2015 with the Satellite Derived Shoreline (SDS) trends by Luijendijk et al. (2018) and comparing Bruun rule coastline recession estimates for the years 2050 and 2110 with the Probabilistic Coastal Recession (PCR) projections in Dastgheib (2017).

Short-term (for the year 2050) and long-term (for the year 2100) coastline recession estimates employ the mean climate change predictions according to the four Representative Concentration Pathways (RCPs) stipulated by the ensemble of climate change models part of the Coupled Model Intercomparison Project Phase 5 (CMIP5). If possible, the 90% likelihood ranges in the climate change predictions have been imposed as well. Both the ensemble means and 90% likelihood ranges have been reproduced after the graphs and figures in IPCC (2013). Estimated anthropogenic changes have been derived from other sources. The calculated trends and coastline recession estimates will consider the start of the year 2016 as the present situation.

To gain further insight into the future behaviour of coastlines downdrift from inlet-basin systems and/or rivers, the Scale-aggregated Model for Inlet-interrupted Coastlines (SMIC) method (Ranasinghe et al. 2013) has been (partially) applied to 10 rivers and 5 large lagoons/coastal lakes together with the BQART model (Syvitski & Milliman, 2007). The 10 rivers have been chosen based on their importance to the sediment budget of the Sri Lankan coast (Dayananda, 1992) and the downdrift presence of coastlines deemed suitable for the application of the Bruun rule. Investigated lagoons/coastal lakes are intermittently closed or permanently open to the ocean, and the ensemble of inlet-basin systems shows variety in basin size, basin shape and annual fresh water input.

1.4. Thesis Outline

The Bruun rule, the SMIC method and the BQART model, the projected climate change driven changes and estimated anthropogenic trends, and the model variables used are described in Chapter 2. Chapter 3 lists the major limitation to the Bruun rule and maps its validity in assessing the future position of the Sri Lankan coastline (RQ 1). Chapter 4 reports the two comparisons performed to assess the accuracy of the Bruun rule in projecting future shoreline positions (RQ 2). 2050 and 2100 coastline recession estimates are presented in Chapter 5 (RQ 3). Using the sea-level rise induced recession estimates, Chapter 6 will discuss the future state of Sri Lankan beaches (RQ 4). Chapter 3 – 6 each have their own conclusion answering the affiliated research question and (except for Chapter 3) listing of limitations. Chapter 7 will once again summarise the answers to the four posed research questions. Limitations have not been given a recap. Finally, Chapter 8 lists recommendations to mitigate the consequences of coastline recession, to supplement coastline recession estimates or to improve the used research method.

Because of the spatial scope, the Sri Lankan coast has been subdivided into eight coastal sectors (modified after Jacobsen et al. (1987)) (Figure 2 and Table 1). Figure 2 also displays most of the spatial locations mentioned in this document.

Table 1: Start and finish of the coastal sectors of Sri Lanka (modified after Jacobsen et al. (1987)*). X and Y coordinates are in decimal degrees and use the WSG84 geographic coordinate system.*

Coastal sector			**X (decimal degrees)**	**Y (decimal degrees)**
Southern	Start:	Galle	80.218	6.023
	Finish:	Tangalle	80.802	6.022
South-eastern	Start:	Tangalle	80.802	6.022
	Finish:	Arugam Bay	81.840	6.839
Eastern	Start:	Arugam Bay	81.840	6.839
	Finish:	Trincomalee Bay	81.279	8.547
North-eastern	Start:	Trincomalee Bay	81.279	8.547
	Finish:	Point Pedro	80.256	9.817
Northern	Start:	Point Pedro	80.256	9.817
	Finish:	Vaddukoddai	79.931	9.779
North-western	Start:	Mannar Island	79.851	9.079
	Finish:	Kandakuliya	79.706	8.143
Western	Start:	Kandakuliya	79.706	8.143
	Finish:	Bentota	79.974	6.463
South-western	Start:	Bentota	79.974	6.463
	Finish:	Galle	80.218	6.023

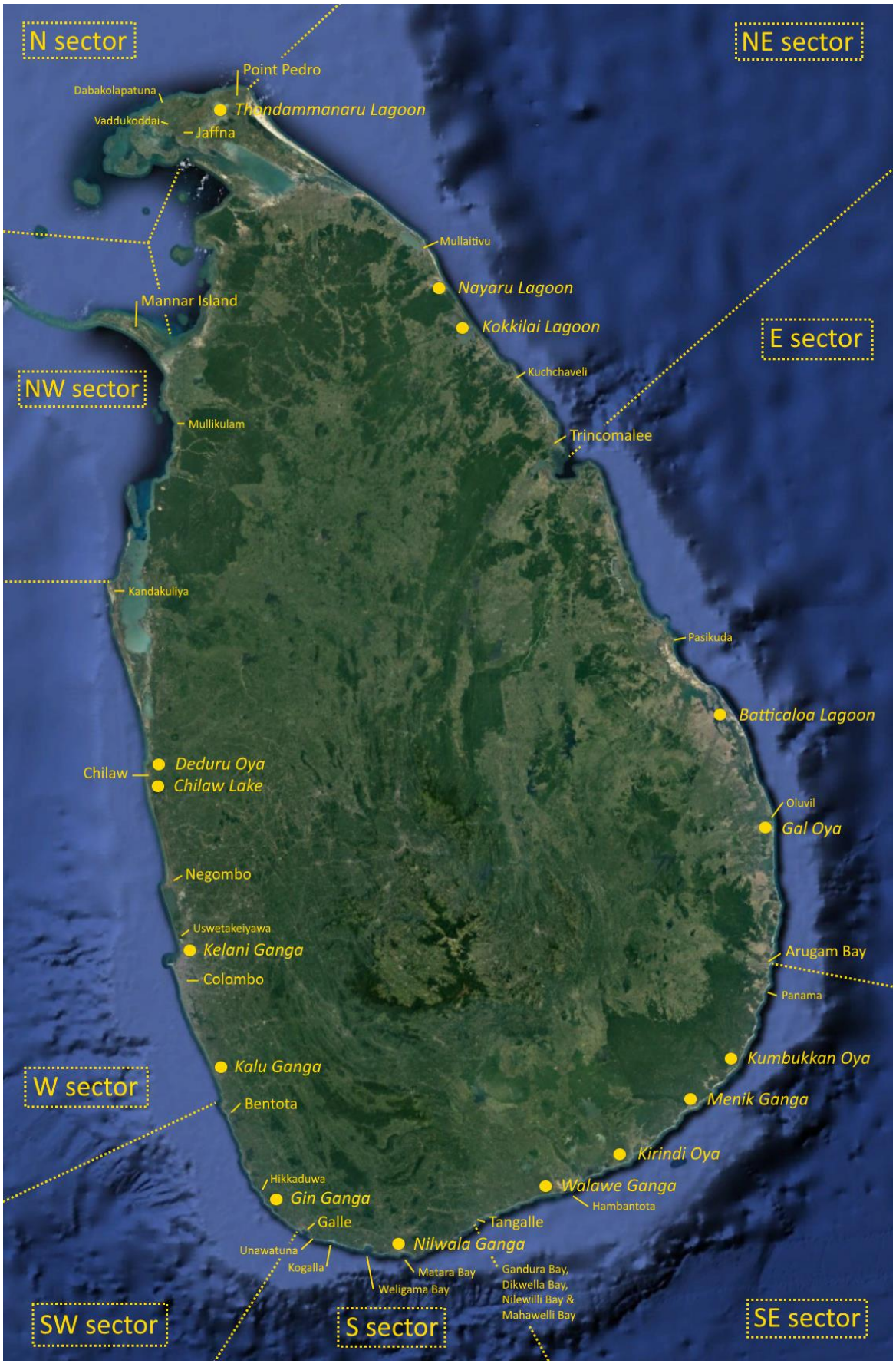

Figure 2: Delineated coastal sectors of Sri Lanka (modified after Jacobsen et al. (1987)*), location of investigated lagoons, coastal lakes and rivers, and spatial locations mentioned in the document* (Baselayer: Google Earth).

2. Research Methodology

Chapter 2 provides the necessary details on the delineation of defined coastal zones (Paragraph 2.2), the calculation methods used (Paragraphs 2.3 – 2.5), future (and past) trends accounted for (Paragraphs 2.6 – 2.8) and the model variables used as input (Paragraph2.9 – 2.11). Paragraph 2.1 outlines the use of each aforementioned paragraph in answering the posed research questions.

2.1. Outline Research Methodology

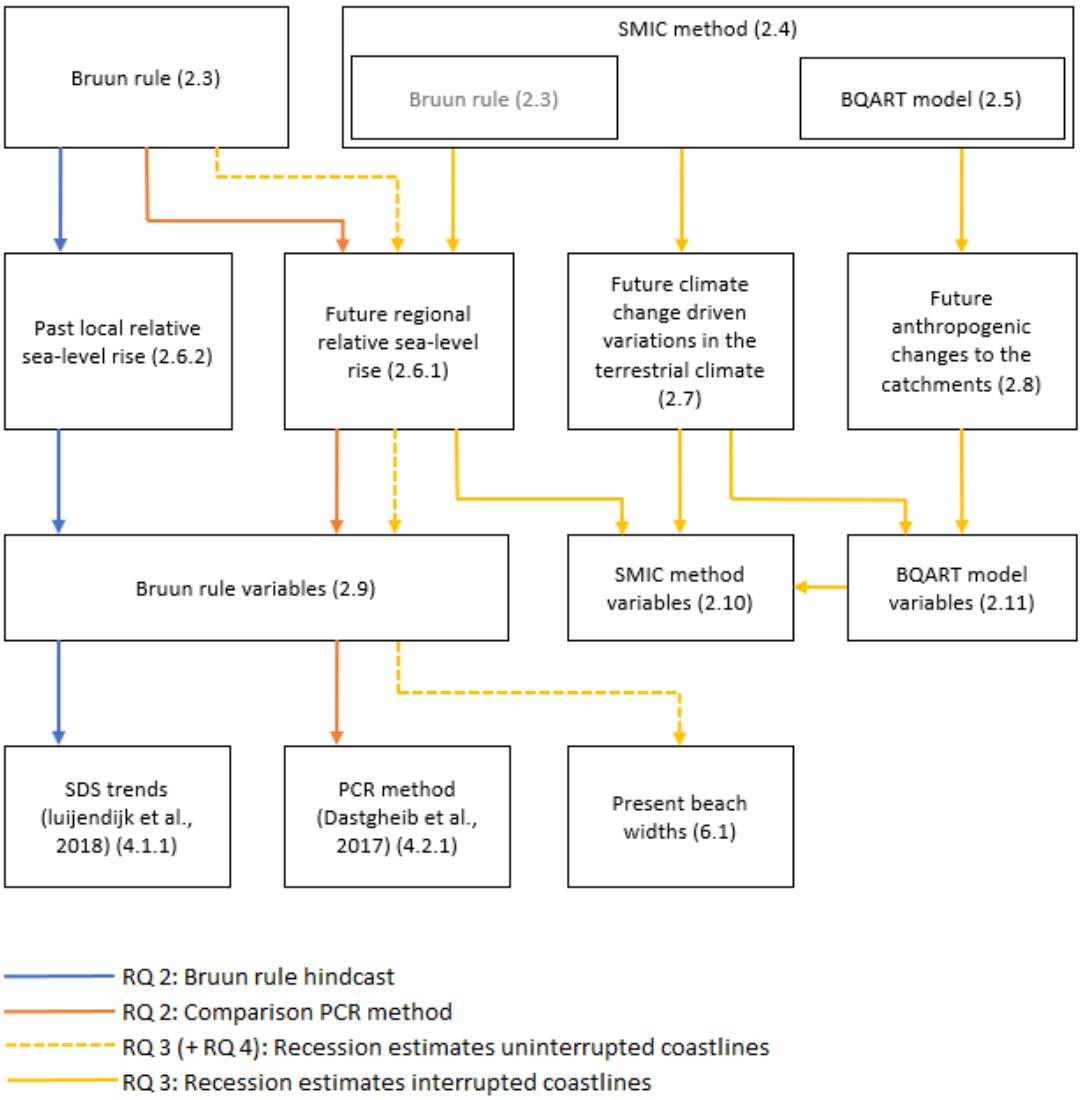

Figure 3: Calculation methods, future (and past) trends, model variables and other data used to answer the posed research questions. Respective paragraph numbers are between brackets.

2.2. Defined Coastal Zones

To estimate sea-level rise induced coastline recession, the Sri Lankan coast has been subdivided into 211 zones deemed suitable for the application of the Bruun rule (indicated by one arrow each in Figure 6).

Because of the complex and significant divergences in the littoral drift of coastal sediments, the Puttalam sandspit (Figure 4) and the Vaddukoddai sandspit have been excluded (Ranasinghe & Stive, 2009) together with the coastline protected from the offshore wave climate by the Puttalam sandspit. The ill-defined muddy (Dayananda, 1992) coast between the Vaddukoddai sandspit and Mannar Island has been omitted too.

Notorious for the offshore loss of coastal sediments to the Trincomalee Canyon (CCD, 2006; Dayananda, 1992), the otherwise suitable sandy coastline inside Trincomalee Bay (Figure 5) has been precluded (after Zhang et al. (2004)).

Lastly, rocky shorefaces, shorelines positioned behind interrupted reefs (Figure 8), influenced by a series of jetties or breakwaters, or protected by revetments have been excluded. However, beaches between breakwaters and jetties that may be assumed embayed

Figure 4: Defined coastal zones (yellow continuous arrows) at the Puttalam sandspit (Baselayer: Google Earth).

Figure 5: Omitted coastline (yellow dotted arrows) inside Trincomalee Bay (Baselayer: Google Earth).

Figure 6: Defined 211 coastal zones deemed suitable for the application of the Bruun rule. Each triangle indicates the middle of a defined coastal zone.

Figure 7: Sandy coastline behind continuous reefs West of the Thondamannaru Lagoon inlet (Google Earth).

Figure 8: Sandy coastline influenced by the construction of a series of small jetties and positioned behind interrupted reefs at Point Pedro (Google Earth).

Figure 9: Defined coastal zones (yellow continuous arrows) between breakwaters and jetties South of the Kalu Ganga river mouth (Baselayer: Google Earth).

Figure 10: The sediment poor and heavily engineered coastline South of the Gin Ganga river mouth and sandspit (Baselayer: Google Earth).

beaches with a closed circulation of coastal sediments (e.g. the beaches South of the Kalu Ganga river mouth (Figure 9) and North of the Negombo Lagoon inlet) have been included.

Defined coastal zones have been delineated using headlands, jetties, breakwaters, river mouths, inlets of intermittently closed to permanently open inlet-basin systems, known nodal points in the littoral drift of coastal sediments as their borders. At all times, a safe distance to river mouths and inlets was maintained.

2.3. The Bruun Rule

Important to many studies regarding the future position of coastlines is the Bruun principle. First described by Bruun (1962), the Bruun principle assumes the persistence of an equilibrium shaped active shoreface, forcing it to move upwards with rising sea-levels. Sediments required to lift the active shoreface are provided through the redistribution of coastal sediments, resulting in a landward migration by the active shoreface. Zhang et al. (2004) attribute the redistribution of shoreface sediments to heavy weather waves. Understandably, the landwards height limit (D_B [m]) and the seawards depth limit (D_C [m]) to the active shoreface are dependent upon their ability to work the coastal sediments.

Provided the assumption regarding the persistence of the equilibrium shaped active shoreface holds, Zhang et al. (2004) explain that sea-level rise induced coastline recession (R_{BE} [m]) can be linked to sea-level rise using, in current literature often referred to as, the Bruun rule.

$$R_{BE} = \frac{L_*}{D_B + D_C} \Delta RSL \qquad (1)$$

With ΔRSL [m] the regional relative increase in sea-level, L_* [m] the cross-shore distance between the positions of the landward and seawards limits to the active shoreface (Figure 11).

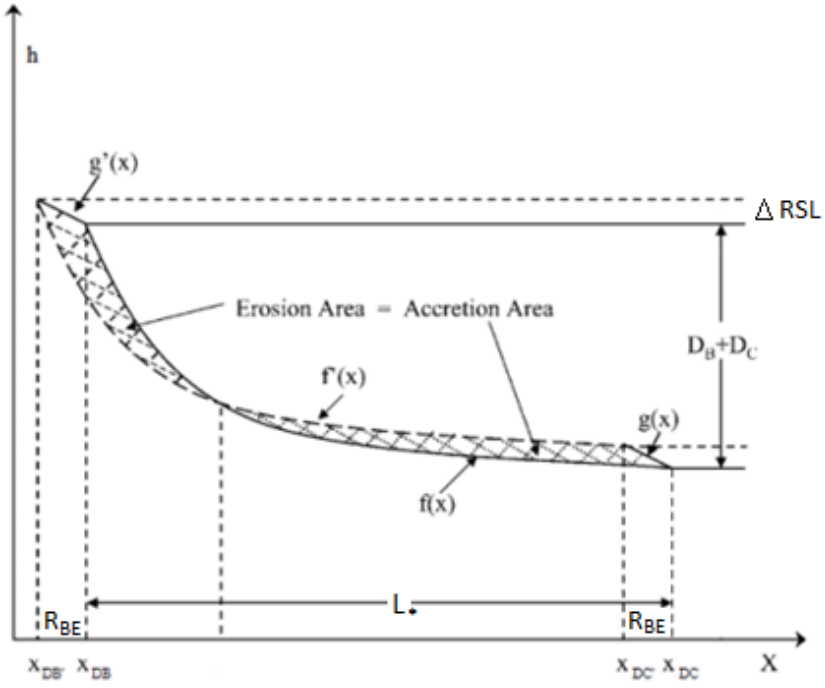

Figure 11: Sea-level rise induced coastline recession according to the Bruun rule for an equilibrium shaped active shoreface f. Modified after Zhang et al (2004).

2.3.1. The Landward Limit to The Active Shoreface

Instead of Equation 1, this research will employ the first proposed wording of the Bruun rule by Bruun (1962).

$$R_{BE} = \frac{L_*}{D_C} \Delta RSL \qquad (2)$$

With L_* the cross-shore distance between the mean sea-level (MSL) mark and the seaward limit to the active shoreface. The diversion from Equation 1 has multiple reasons.

- D_B can be estimated by combining Sunamura (1975), Sunamura (1983), and Takeda and Sunamura (1983). However, the use of non site-specifically calibrated predictors for the beach slope (Velegrakis & Schimmels, 2013) results in an overestimation of surveyed berm heights. The alternative, employing bathymetric and topographic surveys to determine D_B accurately, is a tedious and ambiguous process often hindered by the resolution of available surveys.
- As per the derivation of Dean's equilibrium profile (Dean & Dalrymple, 2001):

$$h = A_{EP}(d_{50})\, x^{2/3} \qquad (3)$$

  with the shape factor A_{EP} [$m^{1/3}$] determined through the mean grain size (d_{50}), the use of Equation 4 is restricted to the shoreface seaward from the MSL mark.
- The persistence of the equilibrium shaped shoreface above MSL is a questionable extension of the assumptions originally part of the Bruun rule. Wet sediments below MSL are more mobile than the dry sediments that (partially) make up the berm. Therefore, the landward migration of the berm is expected to lag that of the MSL mark.
- For high quality cross-shore profiles along the East coast of Sri Lanka, the use of Equation 1 will result in 14% smaller and therefore less conservative coastline recession estimates.

2.3.2. The Seaward Limit to The Active Shoreface

Regarding the depth of closure, Nicholls et al.'s (1996) estimate:

$$D_C = 2.28\, H_{e,t} - 68.5 \left(\frac{{H_{e,t}}^2}{g\, {T_{e,t}}^2} \right) \qquad (4)$$

with g [$m\ s^{-2}$] the gravitational acceleration, $H_{e,t}$ [m] the non-breaking significant wave height that is exceeded 12 hours within a timescale of t years and $T_{e,t}$ [s] the associated wave period, is one of the more often applied estimates for D_C (Ranasinghe & Stive, 2009).

To determine the offshore location of the seaward limit to the active shoreface, the shape of the equilibrium profile is needed. Since the depth of closure is defined as the depth at which no significant change in the profile is observed (Nicholls et al., 1996), present cross-shore profiles are believed useful in providing site-specific values for L_*.

2.4. The SMIC Method

The Scale-aggregated Model for Inlet-interrupted Coastlines (SMIC) method (Ranasinghe et al. 2013) splits the future position of an inlet-interrupted coastline (R_T [m]) into four components.

$$R_T = R_{BE} + R_{BI} + R_{BV} + R_{FS} \qquad (5)$$

With:

- R_{BE} [m]: the response to regional relative sea-level rise according to the Bruun rule;
- R_{BI} [m]: the response to infilling of the basin due to regional relative sea-level rise;
- R_{BV} [m]: the response to future equilibrium basin volumes because of changing flow conditions;
- R_{FS} [m]: the response to a change in fluvial sediment supply.

Without well defined basins, the future locations of coastlines downdrift from investigated rivers is believed predominantly related to the R_{BE} and R_{FS} components of the SMIC method.

2.4.1. Type I and Type II Inlet-basin Systems

Regarding the R_{BI} and R_{BV} components of the SMIC method, it is important to distinguish two types of inlet-basin systems based on their typical shape of the basin (Bamunawala et al., 2018).

Type I: inlet-basin systems without low-lying margins.

Type II: inlet-basin systems containing banks, tidal flats, salt marshes or mild slopes in general.

2.4.2. Basin Infilling Due to Sea-level Rise (R_{BI})

Sea-level rise results in an increase of the basin volume below MSL. To restore its equilibrium volume, the inlet-basin system will increase the bed level of its basin through the import of coastal sediments. The coastline will recede accordingly. For type I inlet-basin systems, R_{BI} is equal to:

$$R_{BI} L_{AC} D_C = 0.5\, \Delta RSL\, A_b \qquad (6)$$

with L_{AC} [m] the length of the affected coastline and A_b [m^2] the present basin surface area. Type II inlet-basin systems require the use of:

$$R_{BI} L_{AC} D_C = 0.5\, [\Delta RSL\, A_b + \Delta V_B(\Delta RSL)] \qquad (7)$$

with ΔV_B [m^3] the additional increase in the basin volume due to a sea-level rise induced increase in basin surface area.

2.4.3. Flow Driven Change in Equilibrium Basin Volume (R_{BV})

Climate change driven variations in flow volumes during ebb tide will force the inlet-basin system to import or export coastal sediments; preserving its equilibrium cross-sectional velocities. Consequences regarding the position of the downdrift coastline are calculated using:

$$R_{BV} L_{AC} D_C = \frac{-\Delta P\, V_B}{P} \qquad (8)$$

with V_B [m^3] the present basin volume, P [m^3] the present mean ebb prism (the sum of the present mean river discharge into the basin during ebb tide (Q_R [m^3])) and the present mean ebb tidal prism (P_T [m^3]), and ΔP [m^3] the future change in the mean ebb prism.

To calculate P_T, Ranasinghe et al. (2013) assume the water level within the basin uniformly moves up and down.

$$P_T = 2a_b\, A_b \qquad (9)$$

With a_b [m] the tidal amplitude within the basin. In the work by O'Neil (1987) the same assumption is used for large inlet-basin systems as well.

Duong (2015) finds a_b using the work by Keulegan (1967). Bamunawala et al.'s (2018) modifications to the SMIC method add the renowned O'Brien (1967) relation between P and the cross sectional surface area of the inlet. Doing so, Bamunawala et al. (2018) allows for the calculation of R_{BV} for type II inlet-basin systems.

Whereas the O'Brien relation holds for systems with a $2.83*10^5\ m^3 < P < 3.11*10^9\ m^3$ (O'Brien, 1967), the work by Keulegan (1967) is based on small inlet-basin systems with a hydraulic radius of the inlet channel smaller than 100 m. For large inlet-basin systems (such as the Alsea river located in the United States of America, and Chilaw Lake, Batticaloa Lagoon, Kokkilai Lagoon, Nayaru Lagoon and Thondamannaru Lagoon in Sri Lanka), calculations using Keulegan (1967) result in an absence of tidal attenuation. Comparing measured water levels during multiple tidal cycles and annual averages of monthly ranges in the tidal amplitudes within the Alsea basin (O'Neil, 1987) with the mean oceanic tidal amplitude (a_o) listed in Engle et al. (2007) also promises the absence of tidal attenuations. Therefore, in the absence of tidal oscillations, computations for large inlet-basin systems can be simplified by assuming a_b equal to a_o.

For type I inlet-basin systems, the ebb tidal prism (P_T) is unaffected by sea-level rise. Therefore, ΔP is directly linked to a change in mean river discharge during ebb tide (Duong, 2015; Ranasinghe et al., 2013). For type II inlet-basin systems, sea-level rise results in an increase in A_b and consequently an increase in P_T (Equation 9). Necessitating a response by the inlet-basin system not only linked to a change in the mean river discharge during ebb tide, but to an increase in P_T as well (Bamunawala, et al. 2018).

2.4.4. Fluvial Sediment Supply (R_{FS})

Lastly, an interrupted coastline will respond to an increase or decrease in the fluvial sediment supply:

$$R_{FS} L_{AC} D_C = \int_0^T \alpha\, \Delta Q_s(t)\, dt \qquad (10)$$

with $\Delta Q_s(t)$ [MT] either the shortage or the surplus in annual fluvial sediment supply and α a coefficient translating MT to m^3. As the deficit or surplus in supplied fluvial sediments to the coast builds over time, $\Delta Q_s(t)$ is integrated from the present to the future year T.

2.5. The BQART Model

The annual fluvial sediment supply can be approximated using the BQART model proposed by Syvitski et al. (2007). With the annual mean temperature in Sri Lanka above 2°C and the absence of ice cover, the annual fluvial sediment supply of a river is approximately:

$$Q_s = \omega B Q^{0.31} A^{0.5} R T \qquad (11)$$

with $\omega = 0.0006$, A [km^2] the catchment area, R [km] the highest point of elevation above MSL inside the catchment, T [°C] the catchment-wide annual mean temperature, and B as in:

$$B = L(1 - TE)E_h \qquad (12)$$

with L the catchment-wide lithology factor ($L = 0.5$ (Syvitski & Milliman, 2007)), TE the catchment-wide sediment trapping efficiency by reservoirs and E_h the catchment-wide anthropogenic factor reflecting the human influence on soil erosion processes.

2.5.1. Trapping Efficiency (TE)

According to Verstraeten and Poesen (2000), empirical models are well suited to determine the annual trapping efficiency of a reservoir (TE_{res}). The applicability of the median reservoir trapping efficiency curve proposed by Brune (1953) is limited to large reservoirs ($V_{res} > 500\ Mm^3$). Small reservoirs ($V_{res} \leq 500\ Mm^3$) require the modified median Brune curve by Heinemann (1981). The catchment-wide trapping efficiency (TE) is determined using Vörösmarty et al. (2003):

$$TE = \frac{\sum_{k=1}^{m}\left(TE_{bas,k}\ Q_{bas,k}\right)}{Q} \qquad (13)$$

with Q_{bas} the annual discharge of the sub-catchment regulated by reservoir k, m the number of controlled sub-catchments draining parallel to one another inside the catchment and Q the annual river discharge. Provided there are no nested reservoirs, $TE_{bas,k}$ is equal to TE_{res}. However, for any reservoir with one or more nested reservoirs, the method proposed by Kummu et al. (2010) should be used.

$$TE_{bas,j} = 1 - \left(1 - TE_{res,j}\right)\frac{Q_{bas,j} - \sum_{k=1}^{m}\left(Q_{bas,j-1,k}\ TE_{bas,j-1,k}\right)}{Q_{bas,j}} \qquad (14)$$

With m the number of sub-catchments regulated by reservoirs found directly upstream (j-1) from the controlling reservoir j.

Future TE_{res} values are decreased by increasing freshwater inputs and reservoir siltation (Verstraeten & Poesen 2000). The latter has been approximated using two BQART model runs; with reservoirs and without reservoirs. The difference between the two is believed the annual catchment-wide volume of reservoir siltation that can be subdivided over the individual reservoirs in the catchment.

2.5.2. River Mining Activities (V_m)

Annual river mining activities (V_m) can be subtracted from the BQART model results (Bamunawala et al., 2018). However, reservoir trapping efficiency calculations show large ($TE_{res} > 0.9$) present and future efficiencies. River mining activities upstream from these reservoirs hardly impact present and future fluvial sediment supplies. Consequently, subtracting V_m from the BQART model results for rivers with large downstream reservoirs and high catchment-wide trapping efficiencies would result in a too large decreases in Q_s. Without a sound approach to include river mining activities in Equation 13 and Equation 14, possible river mining activities in said rivers have been ignored.

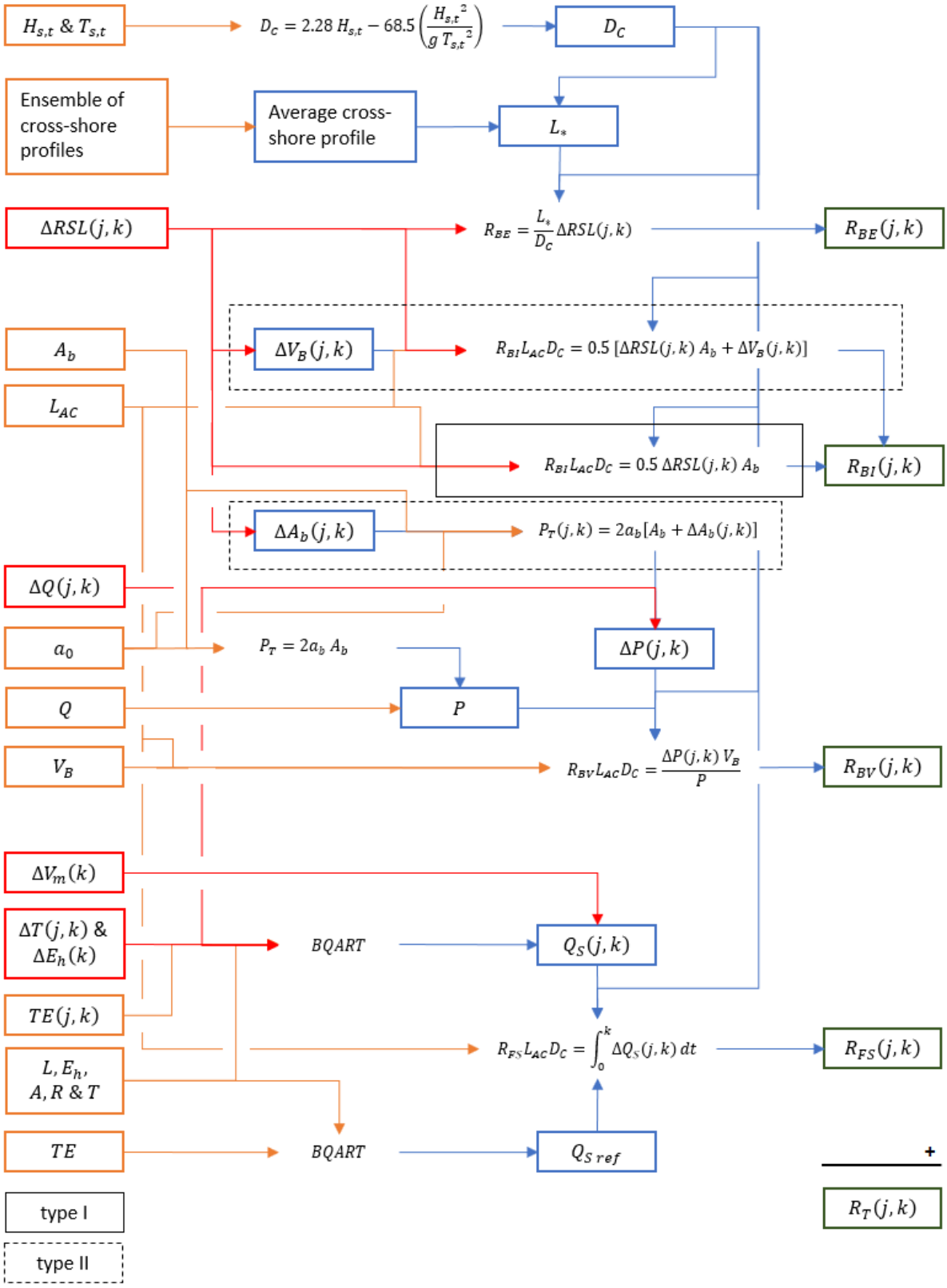

Figure 12: Roadmap describing the equations and variables necessary to determine the future location (RCP j and year k) of an inlet-interrupted coastline.

2.6. Climate Change Related Rise in Sea-level

2.6.1. Future Regional Relative Sea-level Rise (*ΔRSL*)

Without large uninterrupted research quality data records (30 – 35 years or more) describing past regional relative sea-level rise trends along the Sri Lankan coast, model-based projections must be used (Nicholls et al., 2014). Nicholls et al. (2014) break down regional relative sea-level rise into:

$$\Delta RSL = \Delta SL_G + \Delta SL_{RM} + \Delta SL_{RG} + \Delta SL_{RLM} \qquad (15)$$

with ΔSL_G [m] the global change in sea-level, ΔSL_{RM} [m] the regional meteo-oceanic factors (wind fields and related distribution of heat and freshwater, and atmospheric loading), ΔSL_{RG} [m] the regional gravity field changes (linked to the cryosphere and terrestrial water storage), and ΔSL_{RLM} [m] the regional vertical land movements (glacio-isostatic adjustment, tectonic movements and anthropogenic land subsidence rates) (Ballu et al., 2011; IPCC, 2013; Nicholls et al., 2014).

To build the mean, and 95% and 5% likelihood 2100 time series for all four RCPs used in the Bruun rule coastline recession estimates, the approach described in Dastgheib et al. (2017) has been employed. Information regarding the global (ΔSL_G) and regional (ΔSL_{RM}, SL_{RG} and SL_{RLM}) components in Equation 15 originate from Argus et al. (2014), Peltier et al. (2015) and IPCC (2013).

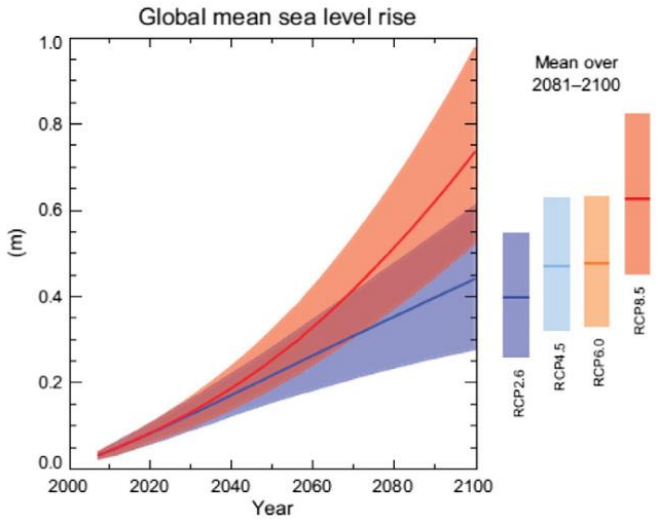

Figure 13: Projected mean global sea-level rise relative to the years 1986 – 2005 imposing either RCP2.6 or RCP8.5. The shaded areas indicate the 90% likelihood ranges (IPCC, 2013).

A second order polynomial is fitted to the global sea-level rise trends plotted in Figure 13.11 in IPCC (2013).

$$\Delta RSL = at^2 + bt + c \qquad (16)$$

With *t* the amount of years since the start of the year 1996. Evaluating Equation 16 at 2056 and 2091 using the values listed in Duong et al. (2016), linearly distributing the regional variations in the sea-level rise projections (Figure 14) over time and adding regional vertical tectonic movements (Figure 15), allows for the determination of *a* and *b*. The value of *c* is found by referencing the regional relative sea-level rise trends to the start of the year 2016.

Linearly distributing the regional variations in sea-level rise projections requires all involved regional processes to contribute in a constant manner despite having different characteristic timescales (IPCC, 2013). Apart from earthquakes, tectonic movements are a slow process and can be considered constant (Nicholls et al., 2014). Over-extraction of coastal aquifers through shallow wells is a possibility (Jayasekera et al, 2011; Jayawardena & Sarathchandra, 1995) and the importance of anthropogenic land subsidence rates in coastline recession studies has been noted by Nicholls et al. (2014), and Udo and Takeda (2017). However, no anthropogenic subsidence rates were found and consequently any possible rates have been omitted.

For the mean RCP8.5 2110 time series required in the comparison with the PCR method, the above has been repeated with the regional components ($\Delta SL_{RM\ 2100} = 0.03$ *m* and $\Delta SL_{RLM} = 0.35$ *mm year*$^{-1}$) listed in Dastgheib et al. (2017).

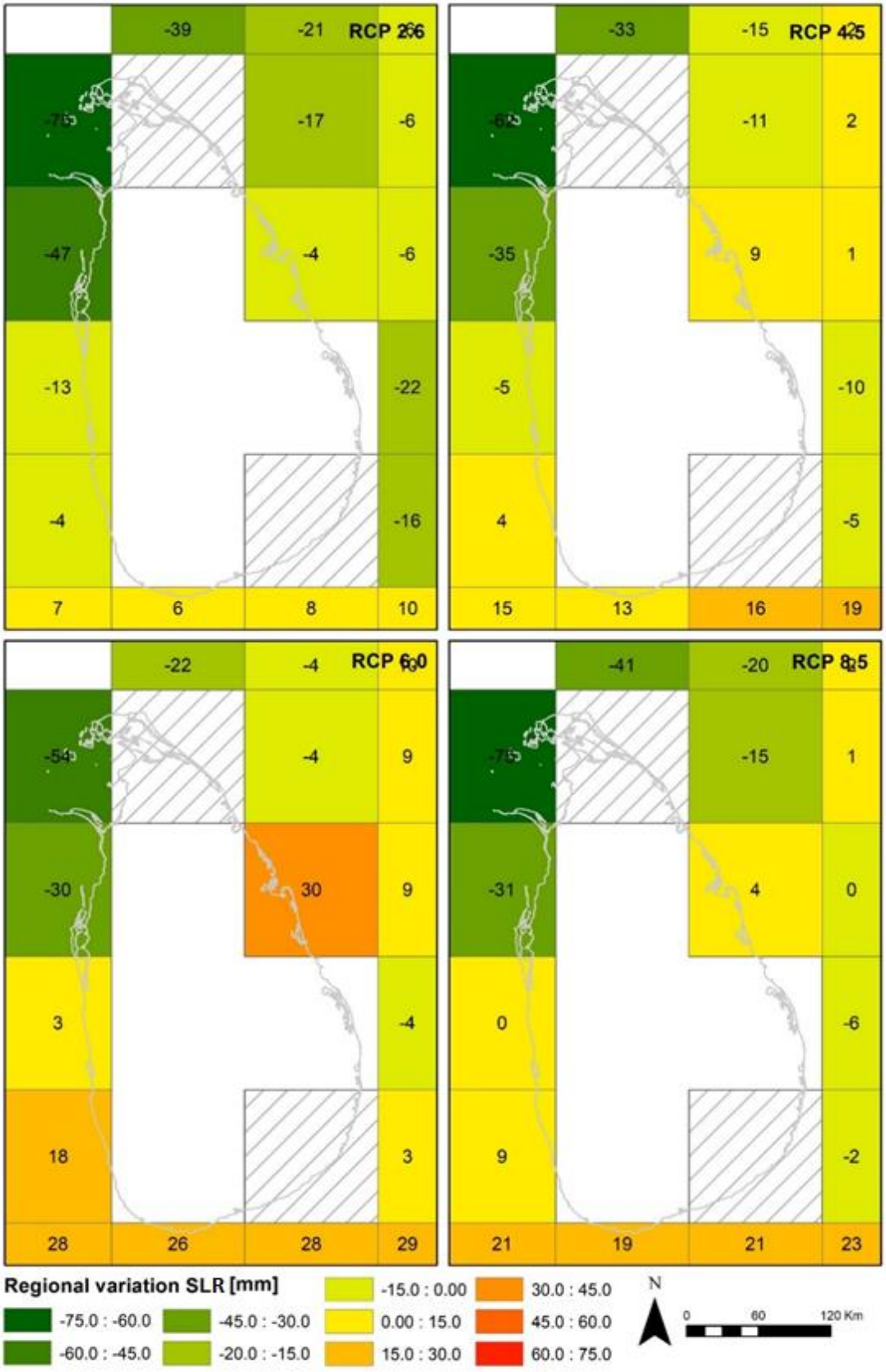

Figure 14:Regional variations [mm] in the mean sea-level rise projections by IPCC (2013) *for the years 2081 – 2100. Values have been acquired by subtracting the global mean sea-level rise trends listed in Duong et al.* (2016) *from the regional mean sea-level rise trends made available in netCDF format by the Integrated Climate Data Center (ICDC, icdc.cen.uni-hamburg.de) University of Hamburg, Hamburg, Germany.*

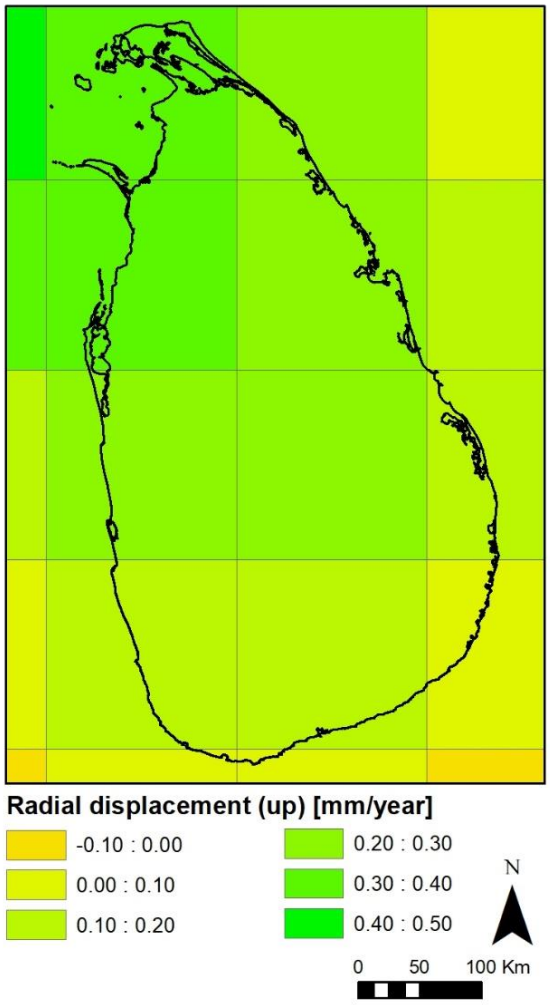

Figure 15: Vertical land movement trends including glacio-isostatic adjustment and tectonic land movements (Argus et al., 2014; Peltier et al., 2015).

2.6.2. Past Local Relative Sea-level Rise (*ΔRSL*)

Past local relative sea-level rise used in the hindcasted Bruun rule coastline recession estimates for the years 1985 – 2015 have been derived from Sea Surface Height satellite measurements downloaded from the E.U. Copernicus Marine Service Information data portal and the vertical land movements according to Argus et al. (2014) and Peltier et al. (2015).

SSH trends have been derived in accordance with the approach used by Luijendijk et al. (2018). First, the SSH time series have been reduced to annual increases in SSH with respect to the year 1985. Because the SSH satellite measurements are limited to the years 1993 – 2015, the time series has been supplemented by assuming no significant sea-level rise before the year 1993 (as reported by Thompson et al. (2016)). A linear fit is applied to the resulting scatter and the resulting SSH trends (Figure 16) are added to the regional vertical land movements according to Argus et al.(2014) and Peltier et al. (2015) (Figure 15).

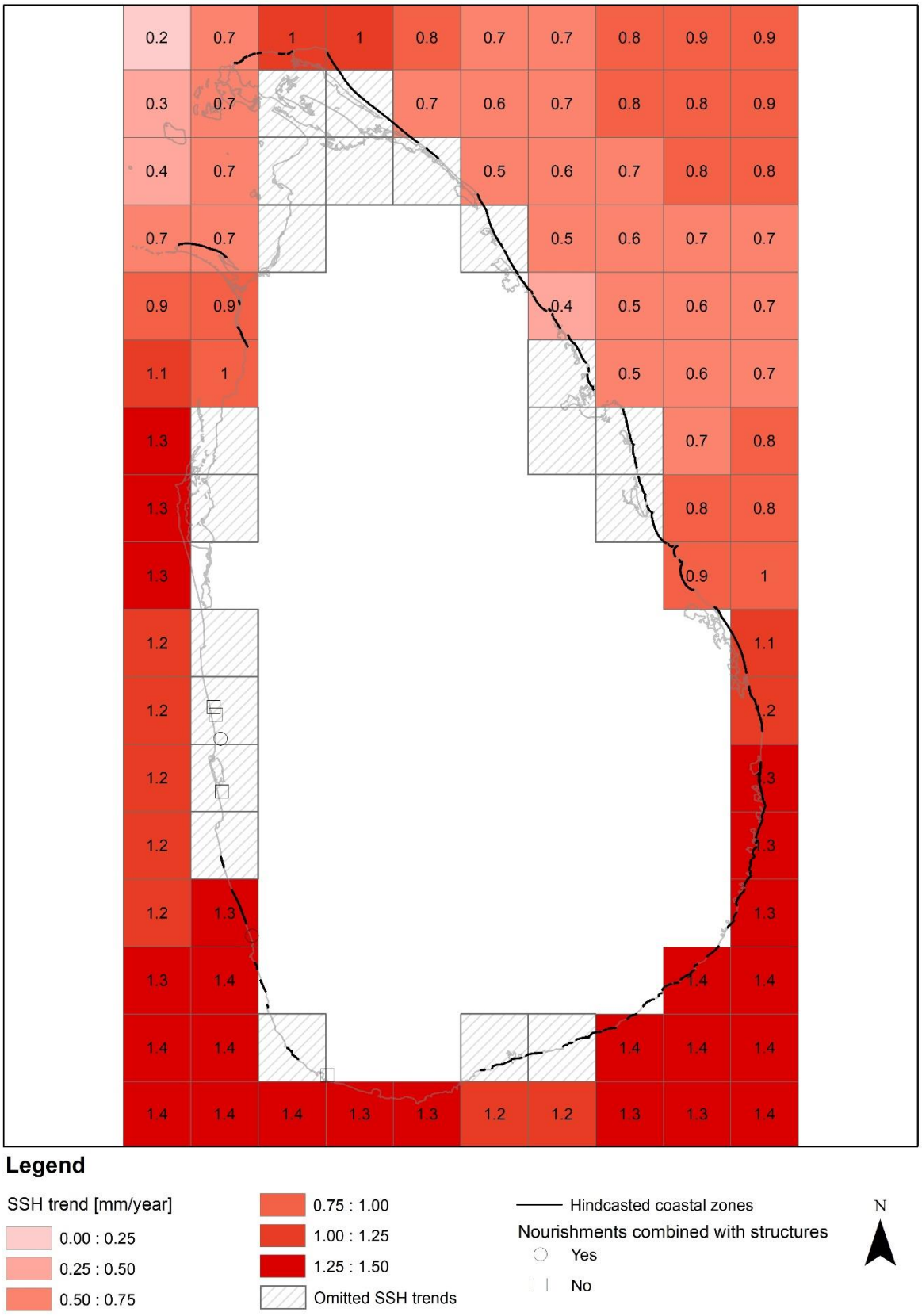

Figure 16: 1985 – 2015 Sea Surface Height (SSH) trends calculated using E.U. Copernicus Marine Service Information. Black solid lines indicate hindcasted defined coastal zones and nourishment schemes completed between the years 1985 – 2015 have been marked using circles (with structures) and squares (without structures).

2.7. Future Climate Change Driven Variations in The Terrestrial Climate

2.7.1. Variations in Annual Mean Temperatures (ΔT)

Because of the size, shape and offshore position of Sri Lanka, the Sri Lankan climate is moderated by its the surrounding waters (Department of Meteorology Sri Lanka, 2016). Therefore, increments in the annual mean temperature have been derived from the projections for the North Indian Ocean in Figure 17 (Figure AI.60 and Figure AI.61 in IPCC (2013)).

The mean (solid lines in Figure 17) annual rate at which T is expected to increase is 0.0036 °C year^{-1} (RCP2.6), 0.014 °C year^{-1} (RCP4.5), 0.020 °C year^{-1} (RCP6.0) or 0.038 °C year^{-1} (RCP8.5). 5% and 95% likelihood bands have been derived from the the two boxplot graphs in Figure 17.

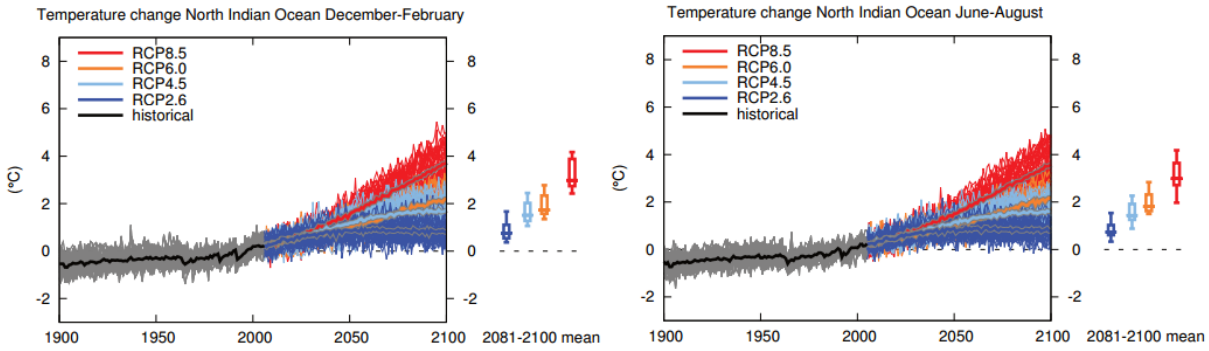

Figure 17: Hindcasted and forecasted mean surface temperature change during the months December – February (left frame) and June – August (right frame) for the North Indian Ocean (solid lines). Boxplot graphs summarising the 2081 – 2100 results of the CMIP5 models are plotted to the right of each frame (Figure AI.60 and Figure AI.61 in IPCC (2013)*).*

2.7.2. Increases in Annual River Discharges (ΔQ)

Future increases in annual river discharges have been estimated using the annual mean runoff change projections in Figure 12.24 in IPCC (2013). The projected changes in daily runoff have been transformed into changes in annual runoff and divided by the amount of years until the end of the 21st century to find the yearly increments of 0.246 mm year^{-1} (RCP2.6 and RCP4.5), 0.740 mm year^{-1} (RCP6.0) or 1.23 mm year^{-1} (RCP8.5). Increases in annual river discharges have been ascertained by multiplying the yearly increment in annual runoff with the catchment areas of investigated rivers.

2.8. Future Anthropogenic Changes to The Catchments

2.8.1. Continuing Development of The River Catchments (ΔE_h)

Land clearance and other future human alterations are believed to increasingly affect soil erosion processes in river catchments. Within the Kalu Ganga catchment several large development projects are planned and a 20% increase in E_h is expected by Bamunawala et al. (2018). Without an alternative, the estimate mentioned in Bamunawala et al. (2018) has been used to describe the middle increase in the catchment-wide anthropogenic factor with respect to the present value (0.24% year^{-1}). Crude lower likelihood (0.12% year^{-1}) and upper likelihood (0.30% year^{-1}) bands have been added.

2.8.2. Increases in River Mining Activities (ΔVm)

Rapidly increasing since early 2000 and linked to economic growth (Jayathilaka, 2015), river mining activities are expected to continue to increase. Bamunawala et al. (2018) estimate a 25% growth in river mining activities before the end of the 21st century. Assuming a linear relationship, said estimate results in a 0.30% year^{-1} increase in possible river mining activities with respect to the present situation.

2.9. Bruun Rule Variables

2.9.1. Historic Wave Climate ($H_{s,t}$ & $T_{s,t}$)

The non-breaking significant wave height ($H_{s,t}$) and associated wave period ($T_{s,t}$) in Nicholls et al.'s depth of closure estimate have been based on the significant wave height and the related mean wave period in the ERA-Interim reanalysed wave data (Dee et al., 2011) from the year 1979 untill the year 2015. Inland values and values believed too close to the shore to provide accurate wave conditions have been omitted.

The 1985 – 2015 Bruun rule hindcast (paragraph 4.2.3) uses the significant wave height that is recorded for 12 hours during its 30 years timespan and the associated recorded mean wave period. After Udo and Takeda (2017), depth of closure values used in the comparison with the PCR method (Paragraph 4.2.3) and the Bruun rule coastline recession presented in Chapter 5 use the significant wave height for 6 hours and the related mean wave period (Figure 18).

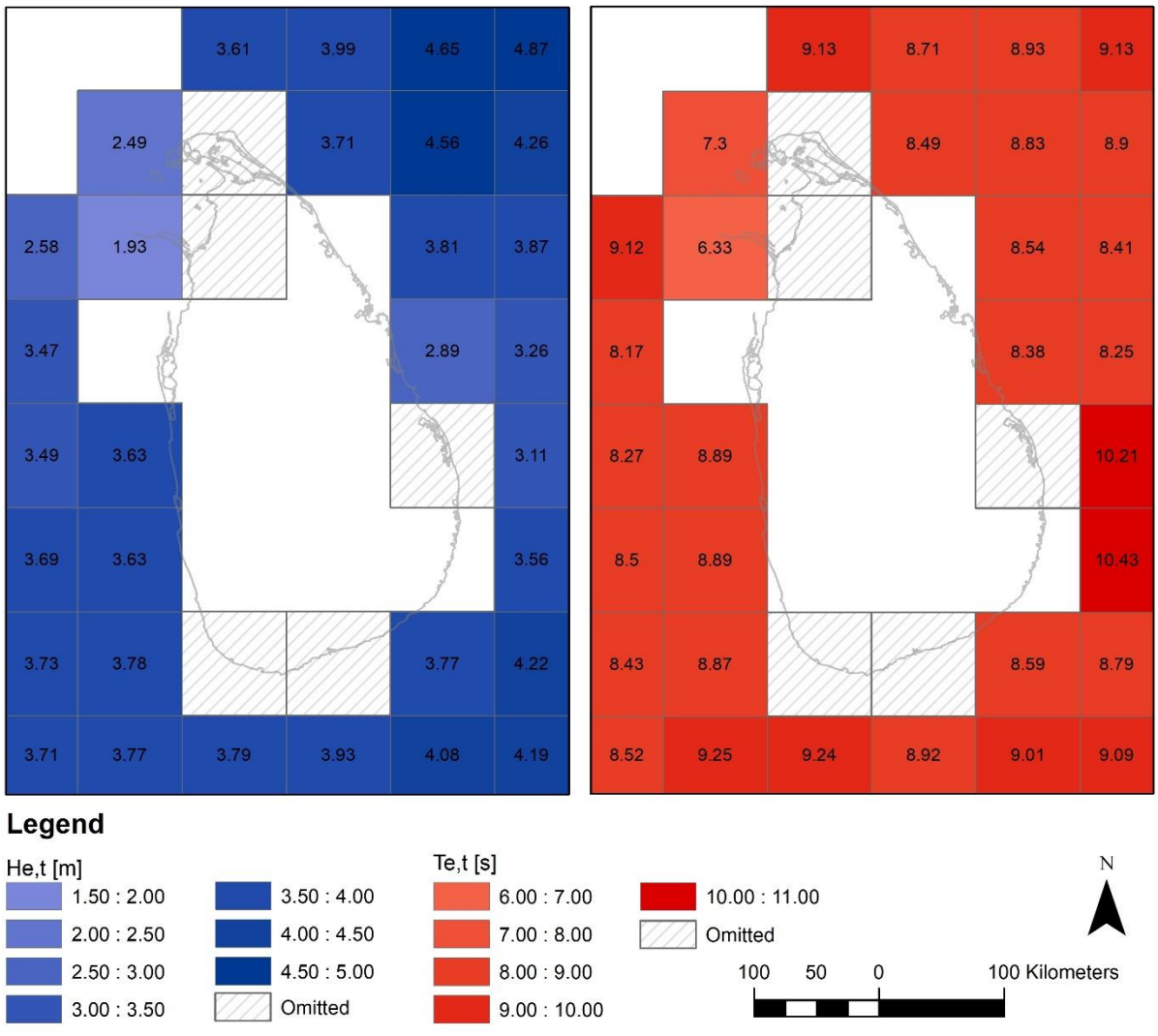

Figure 18: The significant wave height during 6 hours between 1979 – 2015 ($H_{e,t}$) and the related mean wave period ($T_{e,t}$) according to the offshore ERA-Interim reanalysed wave data (Dee et al., 2011).

2.9.2. Active Shoreface Dimensions (L_*)

2.9.2.1. Acquisition of Cross-shore Profile Measurements

Cross-shore profiles have been extracted from bathymetry maps and *xyz* datafiles from the CCD, and supplemented with a small collection of transects from CDR-International. The measurements have been assumed perpendicular to the coast and clear artefacts (e.g. loops in the measurements, turns at the beginning and/or end of transects and double takes) have either been solved manually or resulted in the omission of an entire transect. To avoid the use of unfit transects (e.g. the nearshore shape is influenced by revetments, breakwaters or headlands) only bathymetry measurements that line up with defined coastal zones have been included. An exception was made for measurements near Jaffna, Koggala and Hambantota. The sheer scarcity of measurements in these areas necessitated the use of measurements outside defined coastal zones. The measurements at Hambantota predate the second construction phase of the harbour.

At Mannar Island, Jaffna and Mullaitivu, cross-shore profile measurements were incomplete. The missing depths between MSL and -2 to -3 m + MSL have been determined using Dean's equilibrium profile, the average median grain sizes listed in IHE-Delft (2016) and the look-up table for the shapefactor in Dean and Dalrymple (2001). Shape factors for Mannar Island, Jaffna and Mullaitivu are 0.1482 ($d_{50} = 420\ \mu m$), 0.1410 ($d_{50} = 380\ \mu m$) and 0.1578 ($d_{50} = 480\ \mu m$). Obvious mismatches between Dean's equilibrium profile and bathymetry measurements have been linked to cross-shore profile measurements missing the entire final approach of MSL and respective transects have been omitted. Remaining mismatches are believed to be solved by taking the average cross-shore profile of multiple transects.

2.9.2.2. Cross-shore Profile Measurements Allocation

The positions of the resulting 273 suitable cross-shore profiles is depicted in Figure 20. Roughly half the defined coastal zones has one or more cross-shore profiles within their longshore limits. All other zones have been assigned representative cross-shore profiles (Figure 20).

Between Galle and Tangalle (~60 km gap), the cross-shore profiles at Unawatuna and Kogalla have been assigned to respectively sheltered and exposed beaches. Between Tangalle and Oluvil (~160 km gap), bathymetry measurements at Tangalle and Hambantota have been used to draw approximate cross-shore profiles for sheltered and exposed beaches, and a combination of the two. Closer to Oluvil, the cross-shore profile at Oluvil has been used as well. To the North of Chilaw (~70 km gap), the bathymetry measurements along the Chilaw – Negombo coastline have been reused.

2.9.2.3. Determining L_*

The offshore location of the depth of closure (L_*) has been measured from average cross-shore profiles drawn for each defined coastal zone (Figure 19).

Average cross-shore profiles that do not reach the estimated depth of closure have been extended to include the depth of closure assuming a constant slope seaward from the last visible change in the slope of the average cross-shore profile. West of Point Pedro, L_* has been truncated to the offshore position of the reefs (approximately 65 m) and the affiliated depth value have been used as the depth of closure.

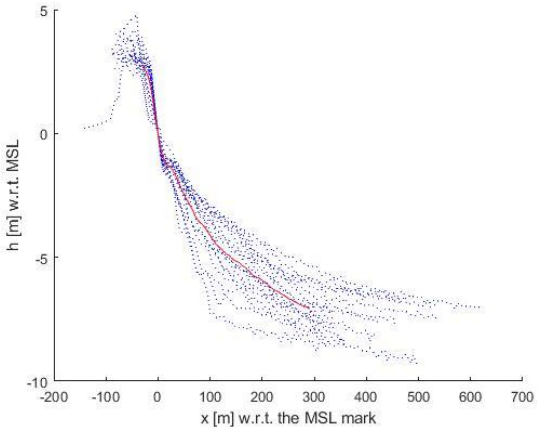

Figure 19: The average cross-shore profile (red) for the Chilaw – Negombo coastline drawn using individual transects (blue).

Figure 20: Use and location of suitable transects. Cross-shore measurements that required supplements provided by Dean's equilibrium profile have been marked with an 'x'.

2.10. SMIC Method Variables

Table 2: Present SMIC method model variables: length of affected coastline (L_{AC}), annual river discharge (Q), mean oceanic tidal amplitude (a_o), basin surface area (A_b) and basin volume (V_B).

	L_{AC} [m]	Q [Mm³]	a_o [m]	A_b [km²]	V_B [Mm³]
Type I *lagoons/Coastal lakes*					
Chilaw lake	20000	-	0.33	5.3	18.6
Batticaloa Lagoon	10400	1460	0.26	83.2	291
Kokkilai Lagoon	11400	358	0.39	47.6	71.4
Type II *lagoons*					
Nayaru Lagoon	20000	87	0.41	7.1	9.94
Thondamannaru Lagoon	5500	-	0.43	8.9	22.3
Rivers					
Deduru Oya	20000	1180			
Kelani Ganga	-	5570			
Kalu Ganga	-	7600			
Gin Ganga	-	1970			
Nilwala Ganga	1200	1410			
Walawe Ganga	-	1680			
Kirindi Oya	3400	305			
Menik Ganga	7800	215			
Kumbukkan Oya	3100	250			
Gal Oya	20000	148			

2.10.1. Present Mean River Discharges During Ebb Tide (Q_R)

Annual discharges by the tributaries of Batticaloa Lagoon, Kokkilai Lagoon and Nayaru Lagoon have been reproduced after those listed in Silva et al. (2013). Without tributaries, Thondamannaru Lagoon is believed to receive no annual freshwater input. Likewise, with the Deduru Oya river bypassing Chilaw Lake, the latter will experience a negligible annual freshwater input.

Concerning the annual river discharges, the values by the Survey Department of Sri Lanka (1983) have been used. For eight out of the ten rivers, recent discharge measurements for one year have been acquired by the CCD. However, concerns about their accuracy regarding the interannual mean could not be addressed. Moreover, in combination with Table 5, the use of said discharge measurements for heavily controlled catchments does not result in catchment-wide trapping efficiencies conform the condition ($0 \leq TE < 0.9$) set by Syvitski et al. (2016).

2.10.2. Mean Oceanic Tidal Amplitudes (a_o)

Although the M2 tidal constituent explains most of the tidal range in the waters surrounding Sri Lanka, the tide is considered mixed semi-diurnal (Wijeratne & Pattiaratchi, 2017). Using the amplitude and phase maps for the tidal constituents M2, S2, N2, K1 and O1, and the amplifications by the coastal shelf in Sindhu and Unnikrishnan (2013), columns two and three in Table 3 have been determined. Values for Chilaw Lake after from Wijeratne (n.d.). The individual tidal constituents have been added using:

$$a(t) = \sum a_n \cos(\sigma_n t - \vartheta_n) \qquad (17)$$

with $a(t)$ the tidal amplitude at a moment t in time, and a_n the amplitude, σ_n the period and ϑ_n the phase of tidal constituent n. Since M2 is the main tidal constituent, the tidal period of M2 has been

employed to find the compounded tidal amplitudes and mean oceanic tidal amplitude for one simulated year.

Table 3: Tidal constituents according to Sindhu and Unnikrishnan (2013) *and Wijeratne* (n.d.)*, and resulting mean oceanic tidal amplitude (a_0) at Chilaw Lake, Batticaloa Lagoon, Nayaru Lagoon, Kokkilai Lagoon and Thondamannaru Lagoon.*

	Constituent	Amplitude (a_n) [m]	Phase w.r.t *M2* (ϑ_n) [°]	(a_0) [m]
Chilaw Lake	*M2*	0.36	-	0.33
	S2	0.22	47	
	K1	0.18	-2	
	O1	0.06	13	
Batticaloa Lagoon	*M2*	0.225	-	0.26
	S2	0.10	20	
	N2	0.055	-10	
	K1	0.04	190	
	O1	0.02	180	
Kokkilai Lagoon	*M2*	0.35	-	0.39
	S2	0.12	20	
	N2	0.08	-10	
	K1	0.04	190	
	O1	0.02	185	
Nayaru Lagoon	*M2*	0.375	-	0.41
	S2	0.125	20	
	N2	0.08	-10	
	K1	0.045	190	
	O1	0.02	185	
Thondamannaru Lagoon	*M2*	0.40	-	0.43
	S2	0.10	25	
	N2	0.09	-5	
	K1	0.045	190	
	O1	0.02	185	

2.10.3. Present (A_b, V_B) and Future Basin Surface Areas and Basin Volumes (ΔA_b, ΔV_B)

Present basin surface areas have been measured from satellite images. For type II inlet basin systems, the basin surface area varies with each satellite image taken. Here, the satellite image showing roughly the average amount of basin surface area has been used. Present basin volumes have been acquired by multiplying A_b with the average depths (3.5 m, 1.5 m, 1.4m, 2.5 m) estimated from bathymetry maps regarding Chilaw Lake and Batticaloa Lagoon, Kokkilai Lagoon, Nayaru Lagoon, and Thondamannaru Lagoon (Personal communication Silva, 2018).

Because of the negligible (fluctuations in) salinity levels in the Southernmost part of the Batticaloa Lagoon basin (Silva et al., 2013) and since this sub-basin is connected to the remainder of Batticaloa lagoon via a narrow channel, the Southernmost part of Batticaloa Lagoon is not believed to move with the oceanic tide. However, It does receive a freshwater input. According to O'Neil (1987), and Stive and Rakhorst (2008), the mean freshwater input during ebb tide is small compared to the mean ebb tidal prism. Therefore, A_b and V_B have been based on the Northern parts of Batticaloa Lagoon. Thondamannaru Lagoon is a similar large system of which only the Western part is connected to the ocean.

Due to its vertical accuracy (Wickramagamage et al., 2012), the NASA Shuttle Radar Topography Mission (SRTM) Digital Elevation Model (Jarvis et al., 2008) cannot be used to determine ΔA_b and ΔV_B. Instead, the tidal flats within Nayaru Lagoon and Thondamannaru Lagoon are assumed to have a constant slope up to a height of 1 m + MSL at the landward edge of the tidal flat.

2.11. BQART Model Variables

Table 4:Present BQART model variables: catchment-wide anthropogenic factor (E_h), catchment-wide trapping efficiency (TE), catchment area (A), relief (R), catchment-wide annual mean temperature (T) and (assumed) annual volume of legally mined river sediments (V_m legal).

Catchment	E_h	TE (present)	A [km²]	R [km]	T [°C]	$V_{m\ legal}$ [m]
Deduru Oya	1.05	0.105	2681	1.24	26.9	154000
Kelani Ganga	1.09	0.0867	2397	2.31	26.8	462000
Kalu Ganga	0.939	0.0800	2778	2.18	25.3	423000
Gin Ganga	0.909	0.0	976.6	1.34	25.9	109000
Nilwala Ganga	0.878	0.0	1010	0.98	26.3	71900
Walawe Ganga	0.892	0.499	2532	2.35	25.9	-
Kiridi Oya	0.897	0.668	1205	1.94	26.4	-
Menik Ganga	0.741	0.0	1248	2.02	26.1	77000
Kumbukkan Oya	0.728	0.0	1201	1.50	26.6	58800
Gal Oya	0.834	0.784	1741	1.46	26.9	-
Batticaloa Lagoon	0.888	0.166	2965	0.84	27.9	46800
Kokkilai Lagoon	0.823	0.293	1384	0.25	29.0	10300
Nayaru Lagoon	0.805	0.0	328.0	0.12	29.6	21800

2.11.1. Catchment-wide Anthropogenic Factors (E_h)

According to Syvitski et al. (2016) the optimal range for E_h is between 0.3 and 2.0. Instead of the three categories proposed by Syvitski et al. (2016), the approach by Bamunawala et al. (2018) has been adopted. Bamunawala et al. (2018) base their E_h value on the Global Human Footprint Index (GHFI) by the Wildlife Conservation Society - WCS and Center for International Earth Science Information Network - CIESIN - Columbia (2005). The GHFI for the Batticaloa Lagoon tributaries is shown in Figure 21. E_h values have been found by scaling the catchment-wide relative impact according to the GHFI, to the range proposed by Syvitski et al. (2016).

2.11.2. Basin-wide Trapping Efficiency (*TE*)

Reservoir capacities have been acquired from the Department of Irrigation Sri Lanka (2018) and Global Energy Observatorium (2018). Without measured annual reservoir inflows, Q_{bas} has been approximated using:

$$Q_{bas} = RR\ \frac{P_{bas}\ A_{bas}}{1.0\ E^5} \qquad (18)$$

with *RR* the catchment-wide run-off coefficient according to the Survey Department Sri Lanka (1983), P_{bas} [mm] the subcatchment-wide annual precipitation (estimated using Figure 1 in Department of Meteorology Sri Lanka (2016)) and A_{bas} [ha] the surface area of the upstream subcatchment. Subcatchment surface areas have been delineated using river network information from the Department of Irrigation Sri Lanka and the SRTM Digital Elevation Model. For Kokkilai Lagoon and Batticaloa Lagoon, *RR* values have been calculated using an estimate of the catchment-wide annual precipitation (Figure 1 in Department of Meteorology Sri Lanka (2016)) and the annual freshwater inputs listed in Silva et al (2013).

Table 5: Variables used for the calculation of the present and future catchment-wide trapping efficiencies: subcatchment-wide annual precipitation (P_{bas}), subcatchment surface area (A_{bas}), catchment-wide run-off coefficient (RR), annual reservoir inflow (Q_{bas}) and reservoir capacity (V_{res}).

Catchment	Reservoir name	P_{bas} [mm]	A_{bas} [ha]	RR	Q_{bas} [Mm³]	V_{res} [Mm³]
Deduru Oya	Hakwatuna Res.	1656	6330	0.27	28	24.26
	Kimbulwana Res.	1750	9980		47	8.49
	Batalagoda Res.	1750	4540		21	5.95
	Magalla Res.	1375	11140		41	9.15
Kelani Ganga	Wimalasurendra Res.	2708	14410	0.64	249	44.8
	Canyon Dam Res.	3563	12550		286	123.4
Kalu Ganga	Kukule Ganga Res.	3875	30830	0.64	765	58
Walawe Ganga	Mau Ara Res.	1469	23600	0.35	121	40.96
	Samanalawewa Res.	2825	23650		234	278
	Udawalawe Tank	1893	81830		542 + $Q_{Samanalawewa\ Res.}$	267
Kirindi Oya	Handapanagala Res.	1750	5500	0.16	15	7.13
	Lunugamwehera Res.	1500	84100		201 + $Q_{Mau\ Ara\ Res.}$	225.09
Gal Oya	Namal Oya Res.	1750	5560	0.05	5	53.44
	Nenayaka Samudraya Res.	2150	98670		106	947.10
	Pallan Oya Res.	1750	9260		8	113.39
	Ekgal Oya Res.	1750	3630		3	28.91
Batticaloa Lagoon	Navakiri Res.	1750	18470	0.28	91	65.19
	Unnichchai Res.	1750	24230		119	67.67
	Rugam Res.	1750	10340		51	22.88
Kokkilai Lagoon	Padaviya Res.	1375	54390	0.15	112	104.55

2.11.3. Catchment Surface Area (*A*) and Relief (*R*)

Catchment surface areas have been extracted from the river catchments polygons by the Department of Irrigation Sri Lanka. The highest point of elevation within said river catchment polygons has been found using the SRTM Digital Elevation Model. An example of the SRTM Digital Elevation Model for the tributaries of Batticaloa Lagoon is shown in Figure 22.

2.11.4. Catchment-wide Annual Mean Temperatures (*T*)

Catchment-wide annual mean temperatures have been estimated using the annual mean temperatures for the years 1961 – 1990 (middle frame of Figure 2 in Department of Meteorology Sri Lanka (2016)). However, according to Figure 17, the annual mean temperature in the North Indian Ocean has since elevated by 0.8 °C. The acquired catchment-wide annual mean temperatures have been increased accordingly.

2.11.5. Annual River Mining Activities (V_m)

The present annual volume of legally mined river sediments ($V_{m\ legal}$) within the Kalu Ganga river catchment is 423060 m³ (Bamunawala et al., 2018). Consequently, its present annual fluvial sediment supply according to the BQART model is decreased by 58%.

Assuming the Geological Survey and Mines Bureau of Sri Lanka issues river mining permits based on the fluvial sediment yield of rivers and the demand exceeds supply, the present percentage for the Kalu Ganga river has been used to estimate possible legal river mining activities within the catchments of other rivers. To include possible illegal river mining activities (0.5 times $V_{m\ legal}$ (Bamunawala et al. 2018)) $V_{m\ legal}$ has been increased up to $V_{m\ total}$ by including $V_{m\ illegal.}$ Except for the Kalu Ganga river, both river mining volumes ($V_{m\ legal}$ and $V_{m\ total}$) are very crude estimates of possible present river mining activities and should be considered as such.

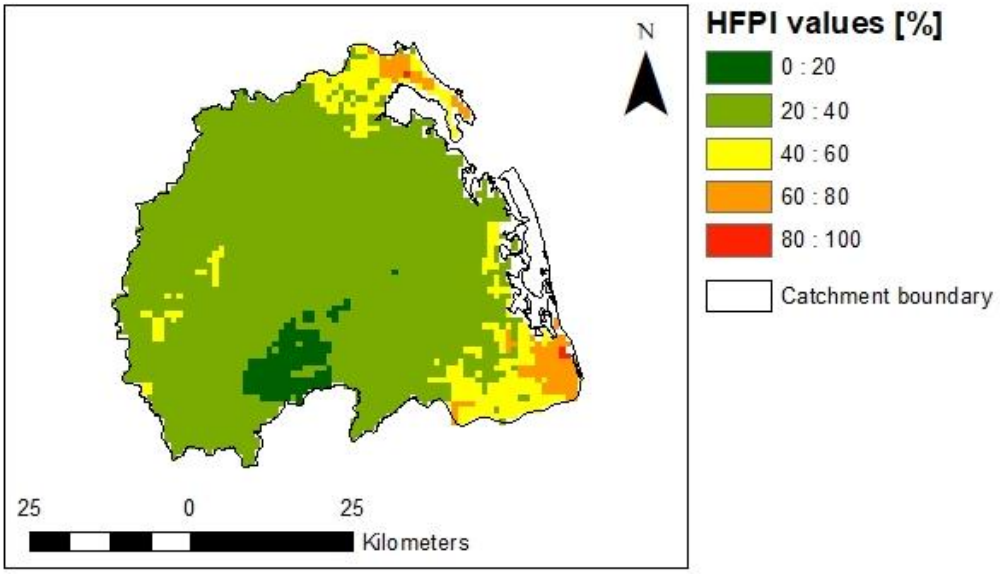

Figure 21: Relative human impact for the tributaries of Batticaloa Lagoon according to the HFPI (Wildlife Conservation Society - WCS and Center for International Earth Science Information Network - CIESIN - Columbia, 2005).

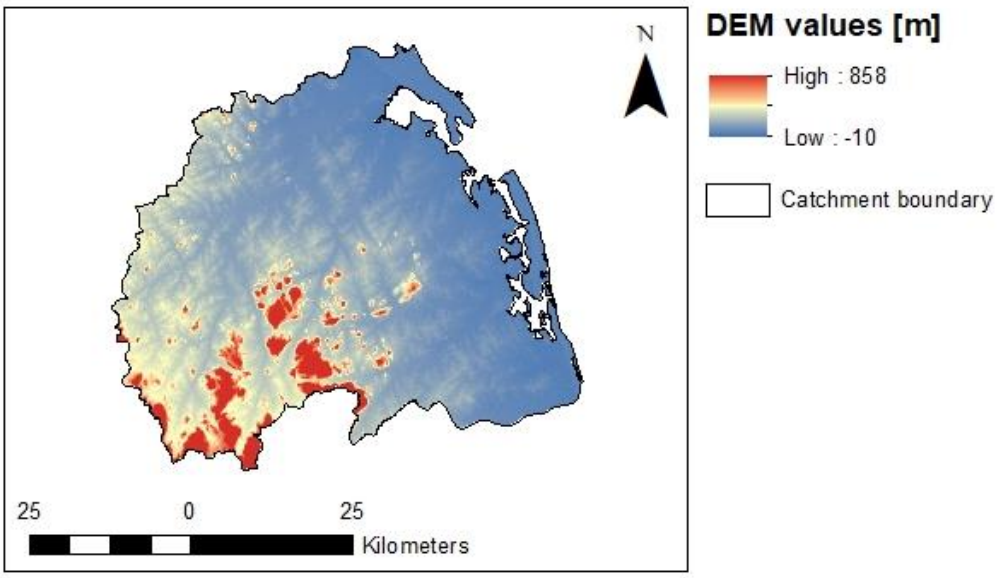

Figure 22: Heights above MSL within the tributaries of Batticaloa Lagoon according to the SRTM Digital Elevation Model (Jarvis et al., 2008).

3. Validity of The Bruun Rule

The validity of the Bruun rule in coastline recession studies is often criticised in literature. By answering research question 1: "*What is the validity of applying the Bruun rule in assessing the future position of the Sri Lankan coastline?"* this chapter will provide the reader with information regarding the necessary assumptions and their consequences regarding the validity of a coastline recession study using the Bruun rule performed for the Sri Lankan coast.

3.1. Limitations to The Use of The Bruun Rule

3.1.1. Availability of Erodible Sediments

Firstly, the Bruun rule is only applicable to sandy coastlines. That is, coastlines with enough available erodible sediments to accommodate an upwards and landwards shift by the active shoreface. This prerequisite renders the Bruun rule invalid for rocky shorefaces.

Apart from said rocky shorefaces, coastlines protected by means of revetments, jetties, seawalls and other coastal structures radically depart from the assumptions by the Bruun rule (Zhang et al., 2004). Similarly, Toimil et al. (2017) carefully select beaches without coastal structures or structures placed sufficiently far back no influence on coastline recession is expected. In addition, investigating future beach widths and amongst others the consequences of sea-level rise to the stability of seawalls and revetments, Udo and Takeda (2017) consider the Bruun rule valid from the present until the moment in time the landward limit to the active shoreface reaches a (soft) barrier.

3.1.2. Upland Topography

Secondly, in their case against the use of the Bruun rule, Cooper and Pilkey (2004) mention the influence of the slope of the land over which the active shoreface migrates. The Bruun rule assumes its estimates unaffected, however the amount of recession is easily demonstrated to be inversely proportional to the upland slope or affected by any upland topography for that matter.

3.1.3. Persistence of an Equilibrium Shaped Active Shoreface

Thirdly, in the derivation of the Bruun rule by Zhang et al. (2004) the persistence of the equilibrium shape of the active shoreface is an important assumption. Consequenly, there are prerequisites regarding the wave climate and grain size distribution; both constant in time (Cowell et al., 2006; Dean, 1995). Whereas studies regarding the latter are non-existent, projections of the future wave-climates along the Sri Lankan coast have been found in IPCC (2013) (Table 6). However, together with Nicholls et al.'s depth of closure estimate, Equation 3 does not allow for the incorporation of changing annual wave climate variables.

Table 6: Projected change in annual wave climate variables for the Sri Lankan coast according to Figure 13.26 in IPCC (2013).

Annual mean wave climate variables	Min. value of change	Max. value of change
Significant wave height (H_s)	-3%	-1%
Wave period (T_M)	-0.13 s	+0.05 s
Wave direction (φ_M)	-9°	-4°

3.1.4. Coastal Sediment Balance

Finally, the Bruun rule describes the redistribution of shoreface sediments and requires the assumption that no coastal sediments are lost or added to the sediment balance of a beach. CCD (2006) lists several sinks and sources of which offshore, onshore, and littoral transports of coastal sediments are considered most important. With the seaward limit to the active shoreface calculated using Nicholl et al.'s (1996) depth of closure estimate, a constant coastal sediment balance can only be attained by enforcing zero divergences in the littoral drift of coastal sediments.

3.2. Modifications of The Bruun Rule

To decrease the amount of assumptions involved with the application of the Bruun rule, researchers have presented numerous modifications of the method. Below, a short summary of the more important modifications is provided.

3.2.1. Upland Topography

Komar (1983) presents a generalisation of the Bruun rule applicable to both barrier beaches (found along the South-east, East and North-east coast of Sri Lanka) and mainlands beaches (found along the South and South-west coast). Moreover, at mainland beaches, Edelman (1976) employs a variable berm height to account for the flat topography landward from the berm.

3.2.2. Protected Shorelines

From the moment in time the landward limit to the active shoreface reaches a hard barrier and onwards, Dean (1991) proposes the use of virtual active shoreface origins to determine the scour affiliated with the persistence of the equilibrium profile. The calculations by Dean (1991) are intricate and the use of the Bruun principle at shorelines protected by seawalls and revetments is sternly rejected by Cooper and Pilkey (2004).

3.2.3. Sediment Sinks and Sources

A comprehensive effort to incorporate the longshore and cross-shore transports of coastal sediments through the coastal sediment balance has been made by Cowell et al. (2003). A condensation is found in Le Cozannet et al. (2016):

$$R_T = \frac{L_*}{D_C}\Delta RSL + R_{cross-shore} + R_{longshore} \qquad (19)$$

with $R_{cross\text{-}shore}$ and $R_{longshore}$ the horizontal migration by the active shoreface due to respective processes resulting in the gain or loss of coastal sediments.

Onshore loss of coastal sediments through overwash and aeolian transport may again become available to the active shoreface as it migrates landward (Jayathilaka, 2015). Therefore, as opposed to the offshore loss of coastal sediments, subtracting onshore transported coastal sediments from the coastal sediment balance is a first approximation. To address the onshore loss of coastal sediments more accurately, Rosati et al. (2013) present a modification of the Bruun rule that includes overwash and aeolian transport rates.

3.3. Validity of The Bruun Rule along The Sri Lankan Coastline

Given the right context, the use of each modification of the Bruun rule is justifiable. However, the complexity of the calculations, difficulty of delineation correct active shoreface dimensions and/or the amount of required information increases with each modification employed. Moreover, the modifications by Komar (1983), Edelman (1976) and Rosati et al. (2013) include the berm height.

To qualitatively adjudge the validity of the Bruun rule (Bruun, 1962), the presence of sink and source terms for uninterrupted sandy coastlines by Le Cozannet et al. (2016), and for interrupted sandy coastlines (Ranasinghe et al., 2013) have been mapped (Figure 23). Appendix A provides a textual explanation per coastal sector.

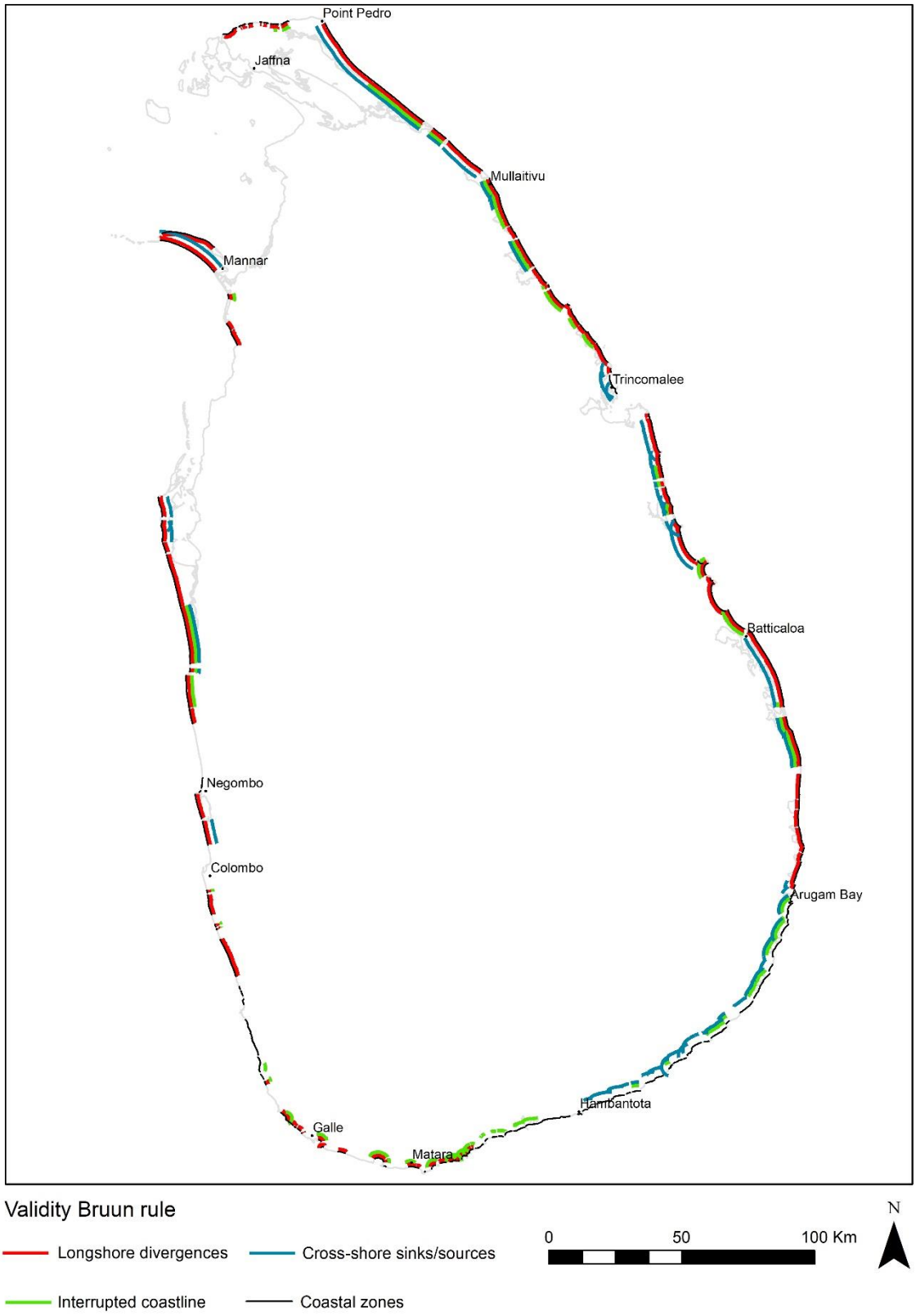

Figure 23: The location of defined coastal zones (black), expected divergences in the littoral drift of coastal sediments (red) and cross-shore transports of coastal sediments (blue), and influence areas of rivers and inlet-basin systems (green) along the Sri Lankan coast.

3.4. Conclusions

Due to limitations inherent to the Bruun rule (Bruun, 1962) the validity of the method is reduced to a first-pass assessment of sea-level rise induced coastline recession. Moreover, the validity of a coastline recession study using the Bruun rule is subject to the presence of cross-shore processes, longshore processes, rivers or inlet-basin systems influencing the coastal sediment balance.

Of the entire Sri Lankan coastline (1534 km in length (CCD, 2006)) only 708 km allows for the application of the Bruun rule to derive sea-level rise induced coastline recession estimates. The many divergences in the littoral drift of coastal sediments explain a significant part of the past coastal morpho-dynamics. Cross-shore transport of coastal sediments, rivers and inlet-basin systems also influence considerable parts of the Sri Lankan coast. Consequently, a coastline recession study based on the Bruun rule accounts for only one of many processes that have determined past coastal morpho-dynamics and may continue to explain future coastline positions.

Table 7: Total length of Sri Lankan coastline deemed suitable for the application of the Bruun rule and lengths of the suitable coastline affected by cross-shore or longshore processes working the coastal sediment balance, or downdrift from rivers and/or inlet-basin systems. Percentages are with respect to the total length of suitable coastline.

	Cross-shore transports of coastal sediments	Divergences in the littoral drift of coastal sediments	Influenced by rivers and/or inlet-basin systems
Cross-shore transports of coastal sediments	362 km (51%)	272 km (38%)	142 km (20%)
Divergences in the littoral drift of coastal sediments	272 km (38%)	549 km (78%)	175 km (25%)
Influenced by rivers and/or inlet-basin systems	142 km (20%)	175 km (25%)	230 km (32%)

Length of coastline affected by all three	103 km (15%)	Length of coastline affected by none	54 km (7.6%)

Total length suitable coastline	708 km

Total length Sri Lankan coastline	1534 km

4. Predictive Accuracy of The Bruun Rule

Chapter 4 will seek to provide an answer to research question 2: "*What is the predictive accuracy of the Bruun rule for the Sri Lankan coastline?"*. To do so, two comparisons have been performed. Firstly, a hindcast of the Bruun rule for the years 1985 – 2015 using the Satellite Derived Shoreline trends by Luijendijk et al. (2018). Secondly, a comparison between Bruun rule estimates and Probabilistic Coastal Recession (PCR) method derived coastline recession projections in Dastgheib et al. (2017). A conclusion has been written including both comparisons at once.

4.1. Bruun Rule Hindcast

Hindcasted Bruun rule coastline recession estimates for the years 1985 - 2015 have been compared with the Satellite Derived Shoreline (SDS) trends by Luijendijk et al. (2018) averaged per defined coastal zone.

4.1.1. The SDS Dataset

The SDS trends have been computed by Luijendijk et al. (2018) using a linear fit to a scatter of cross-shore satellite derived shoreline locations plotted to the moment in time the measurements have been taken. Time values are in years with respect to the year 1985. Shoreline locations have been referenced to an origin landwards from the shoreline. Therefore, a positive trend indicates shoreline progradation.

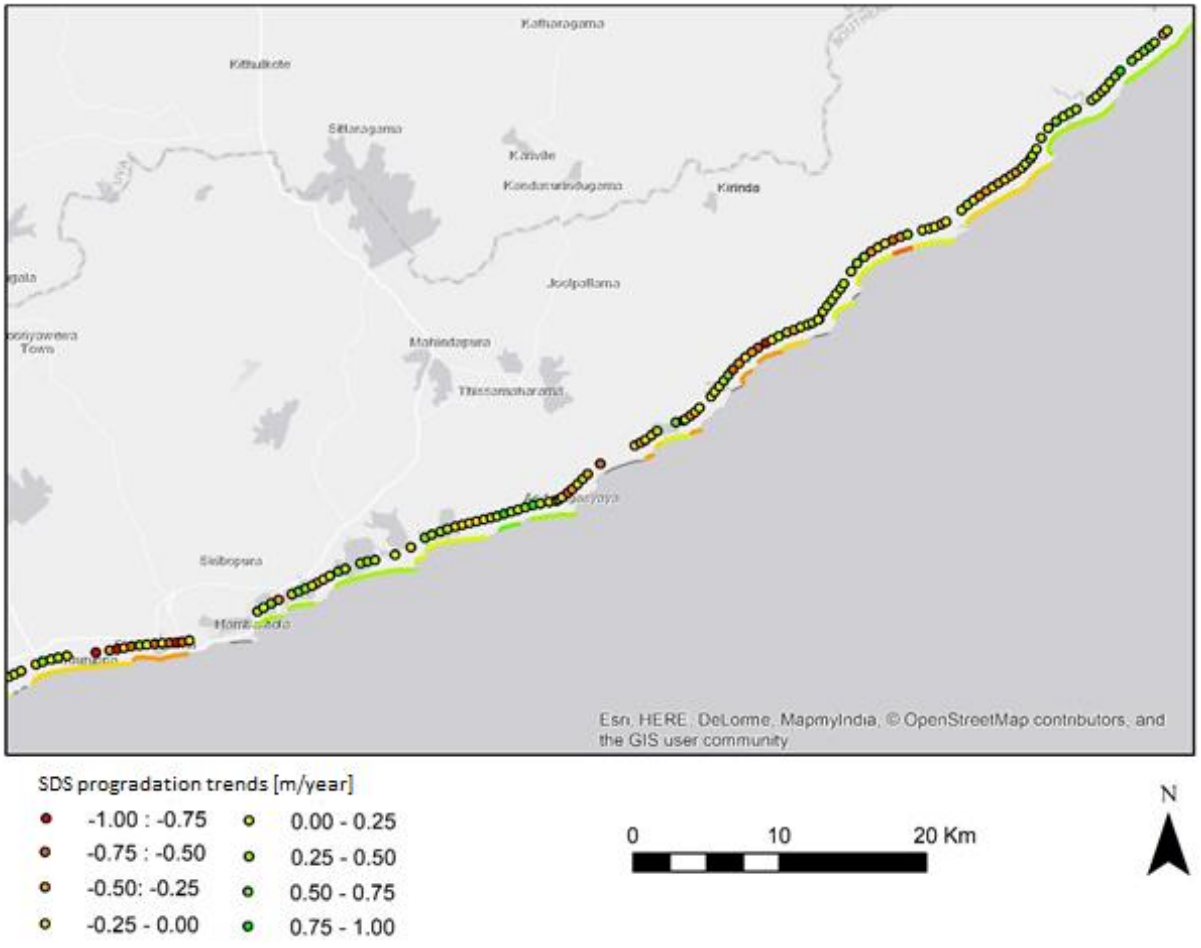

Figure 24: Satellite derived shoreline trends for every 500m of coastline (Luijendijk et al., 2018) , and calculated average trend per defined coastal zone between Tangalle and Yala.

To arrive at zonal averages, the SDS data points have manually been allocated to the defined coastal zones. Regarding small defined coastal zones this process is troublesome because the distinction between a suitable data point (within the reach of a defined coastal zones) and a not suitable data point (e.g. positioned at a headland) is hard to make. Consequently, defined coastal zones with a small longshore length have often been omitted. Moreover, defined coastal zones that contain few SDS data points with respect to their longshore length, have a skewed longshore distribution of SDS data points or are affected by (updrift) anthropogenic changes to the coast are believed to have distorted SDS trends and have been excluded as well. Distinguished antropogenic changes are the construction of harbours, jetties and breakwaters, and beach nourishments. Whereas nourishments performed without the construction coastal structures may influence multiple downdrift defined coastal zones, the effect of nourishments combined with coastal structures is believed restricted to the immediate area.

4.1.2. Results

The comparison between past 1985 – 2015 coastline recession trends according to the Bruun rule and past 1985 – 2015 coastline recession according to the SDS trends has been summarised using a scatter plot (Figure 25). According to the SDS trend, 60% of the hindcasted coastline (Figure 16) progradated between the years 1985 and 2015 (bottom half of Figure 25). In general, the receding coastlines are significantly underestimated by the Bruun rule.

4.1.3. Limitations

Verification of the SDS trends using the Uswetakeiyawa 1999 – 2010 erosion study by the CCD was not successful. Moreover, the SDS trends are based on a linear fit. Thompson et al. (2016) show that past sea-level rise trends in the North Indian Ocean are non-linear. The used sea-level rise trends have been calculated matching the approach by Luijendijk et al. (2018) and therefore assume a past linear increase in sea-level.

Between the years 1985 and 2015, the derived linear sea-level rise trends and affiliated estimated sea-level rise induced coastline recessions are small. Consequently, it is hard to differentiate the Bruun principle from other processes (e.g. divergences in the littoral drift of coastal sediments, cross-shore transports of coastal sediments and interannual variability of storms) (Le Cozannet et al., 2016; Ranasinghe & Stive, 2009).

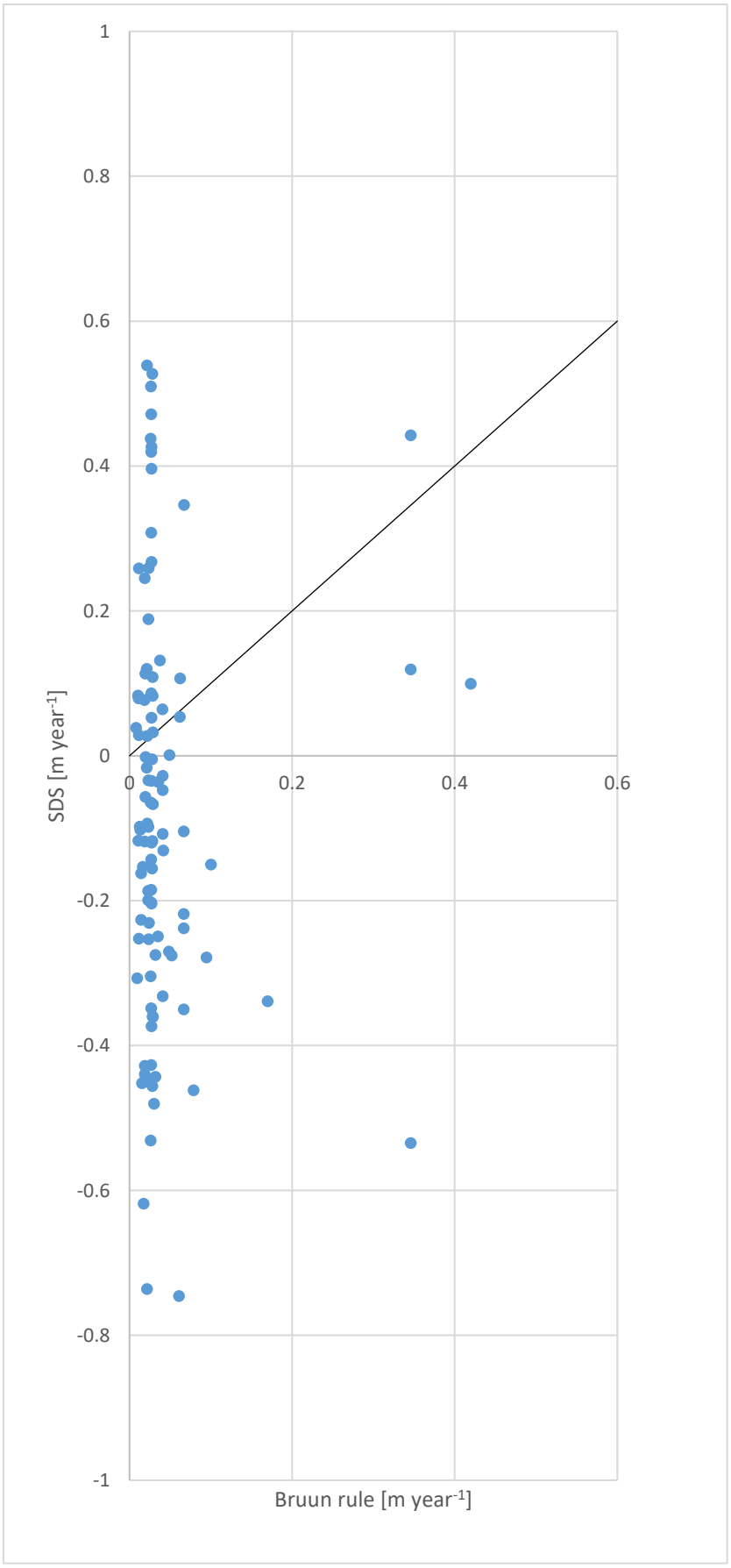

Figure 25: 1985 – 2015 Bruun rule coastline recession estimates plotted against 1985 – 2015 Satellite Derived Shoreline (SDS) trends (Luijendijk et al., 2018).

4.2. Comparison with The Probabilistic Coastal Recession Method

The second comparison will use the stochastic coastline recession projections in Dastgheib et al. (2017). Said projections have been computed using the Probabilistic Coastal Recession (PCR) method which is believed more accurate than the Bruun rule (Ranasinghe et al., 2012). Spanning 85 transects in 72 km of uninterrupted coastline (Figure 26), the work by Dastgheib et al. (2017) incorporates steeply and mildly sloping shorefaces, and shorefaces with various berm heights.

Since Ranasinghe and Stive (2009), and Zhang et al. (2004) state that the Bruun rule is only capable of providing an average coastline recession estimates for defined coastal zones, the comparison between the Bruun rule and the PCR method has been performed on both a transect and a zonal basis. Zonal Bruun rule coastline recession estimates have been calculated using average cross-shore profiles and PCR projections have been averaged for each coastal zone delineated by Dastgheib et al. (2017) (Figure 26).

Figure 26: Spatial scope of the two study areas Tincomalee – Kuchchaveli (left frame) and Karaitivu – Batticaloa (right frame). Coastal zones defined by Dastgheib et al. (2017) *have been numbered and the positions of transects part of the PCR analysis are shown using dots* (Dastgheib et al., 2017).

4.2.1. The PCR Method

The PCR method is a process based model that can be used to attain stochastic coastline recession projections. The PCR method believes present coastline positions the result of storm eroding the beach and beach recovery and sea-level rise induced coastline recession the result of both inundation and the increase of beach erosion due to an increased exposure to storms (Ranasinghe et al., 2012).

A deterministic time series describing coastline recession over time requires (Da Cruz, 2018):

1. the generation of a time series of storms using site-specific storm (season) characteristics;
2. the increase in sea-level each time a storm occurs;
3. the projection of future coastline locations because of storm erosion (erosion model) and beach recovery between storms (beach recovery rate);
4. the calculation of coastline recession projections as the difference between the projected coastline locations and the initial coastline position.

To attain stochastic coastline recession projections, Dastgheib et al. (2017) employ a Monte Carlo simulation repeating the steps by Da Cruz (2018) approximately 100.000 time per transect in Figure 26. Each time, a new time series of storms is randomly generated from site-specific stochastic storm (season) characteristics based on 30 years of offshore ERA-interim reanalysed wave data transformed to nearshore wave conditions. Doing so, no change in the future wave climate is assumed.

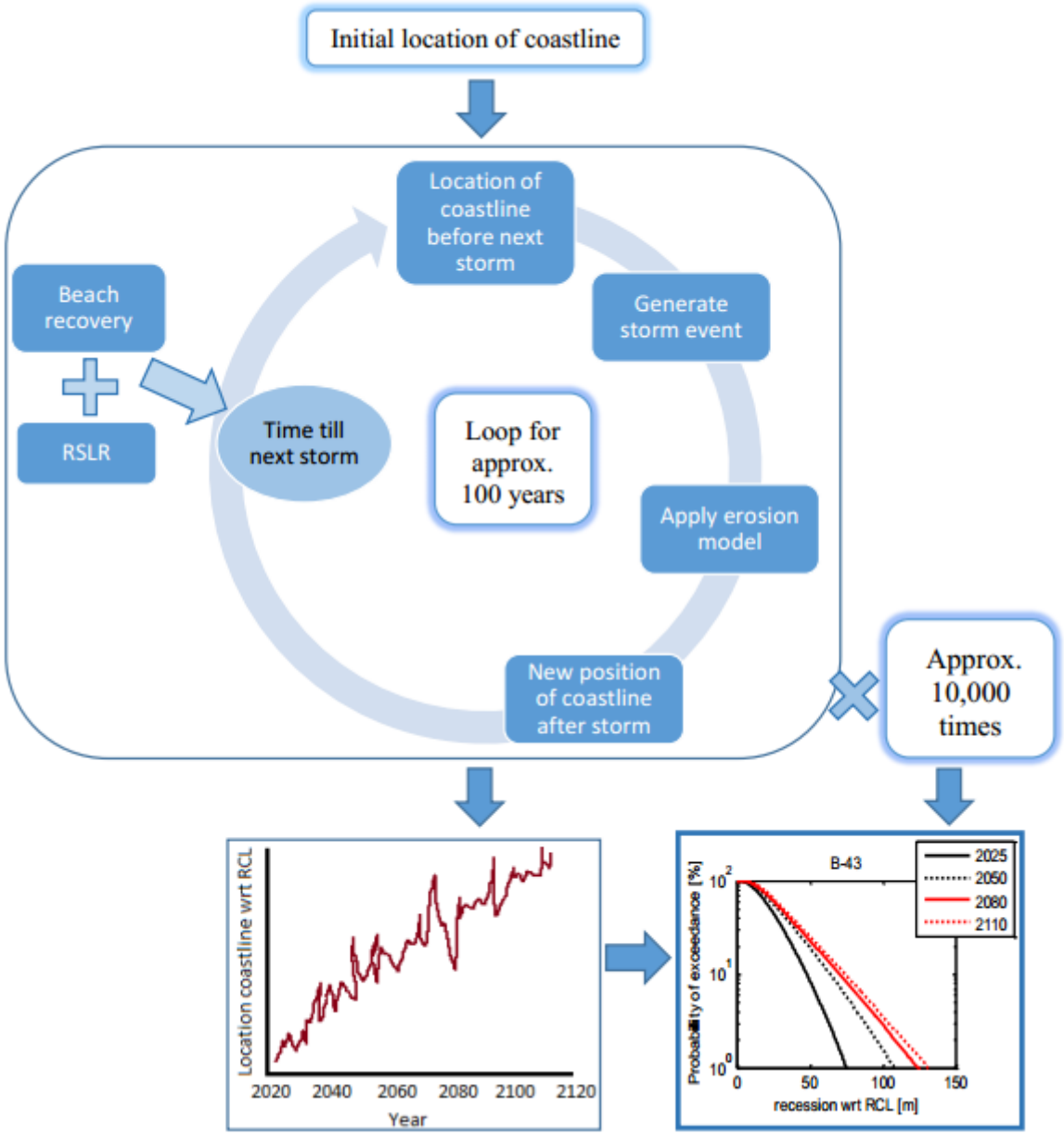

Figure 27: The process behind the calculation of stochastic coastline recession projections using the PCR method (Da Cruz, 2018).

4.2.1.1. Erosion model

Several erosion models can be applied to derive erosion volumes from storm conditions (Da Cruz, 2018). In Dastgheib et al. (2017) the predictive function by Mendoza and Jiménez (2006) is employed:

$$\Delta V = C1\, JA\, dt + C2 \qquad (20)$$

with *C1* and *C2* model parameters calibrated for each defined coastal zone in Figure 26 and *JA* a predictor (Jiménez et al., 1993), which includes the beach slope. Beach slopes have been measured from recent surveys by the CCD.

4.2.1.2. Interpretation of PCR method derived coastline recession projections

An empirical cumulative distribution function is fitted to the results of the Monte Carlo analysis. Exceedance probabilities (vertical axis in the bottom right frame of Figure 27) depict the chance that the annual position of the shoreline is landward from a certain distance to the reference coastline (horizontal axis in the bottom right frame of Figure 27) at a certain year. In Dastgheib et al. (2017) the annual position corresponds with the maximum recorded distance to the reference coastline. High exceedance probabilities equal small coastline recession projections and low exceedance probabilities equal large coastline recession projections. Here the exceedance probability (10%, 50% or 99%) and the year (2050 or 2110) are defined, and the corresponding projected position of the shoreline is sought.

4.2.1.3. Horizontal Migration of The MSL Mark

The PCR projections in Dastgheib et al. (2017) depict the future position of the MSL mark with respect to the past 1% probabilistic wave runup line during 30 years of simulations. With the Bruun rule estimate the landward migration of the MSL mark, the PCR projections must be modified to express the same value. Consequently, additional information regarding the exact geographic location of the MSL mark in the PCR projections, the cross-shore position of the MSL in the profile drawings used in the PCR analysis, the exact geographic location of the origin in the profile drawings and the distance between the PCR projections and the transect origin is required.

4.2.2. Results

According to Figure 28, the 2110 annual landward migration of the MSL mark exceeded in 50% of the PCR method runs is always greater than the coastline recession estimate provided by the Bruun rule. The underestimation of by the Bruun rule persists into the highest (99%) exceedance probability. Differences between the Bruun rule coastline recession estimates and the PCR method projections increase with shorter timescales (Figure 29).

The variability in the 2110 PCR method derived coastline recessions associated with 50% probability of occurrence devided by the 2110 Bruun rule coastline recession estimate scatter is best reduced by substracting an exponential line based on the slope of the active shoreface. The remaining variability can be decreased further by taking the zonal averages (Figure 30). The relative difference between the PCR method and the Bruun rule increases with approximately the same magnitude as the slope of the active shoreface. Creating the same plots for the 2110 PCR method derived coastline recessions associated with 99% probability of occurance results in a ‘consistent’ (0 - 50%) relative underestimation of the PCR method results by the Bruun rule (Figure 31).

Figure 28: 10% (orange), 50% (blue) and 99% probabilistic coastal recession projections according to the PCR method for the year 2110 plotted against the 2110 Bruun rule coastline recession estimates.

Figure 29: 10% (orange), 50% (blue) and 99% probabilistic coastal recession projections according to the PCR method for the year 2050 plotted against the 2050 Bruun rule coastline recession estimates.

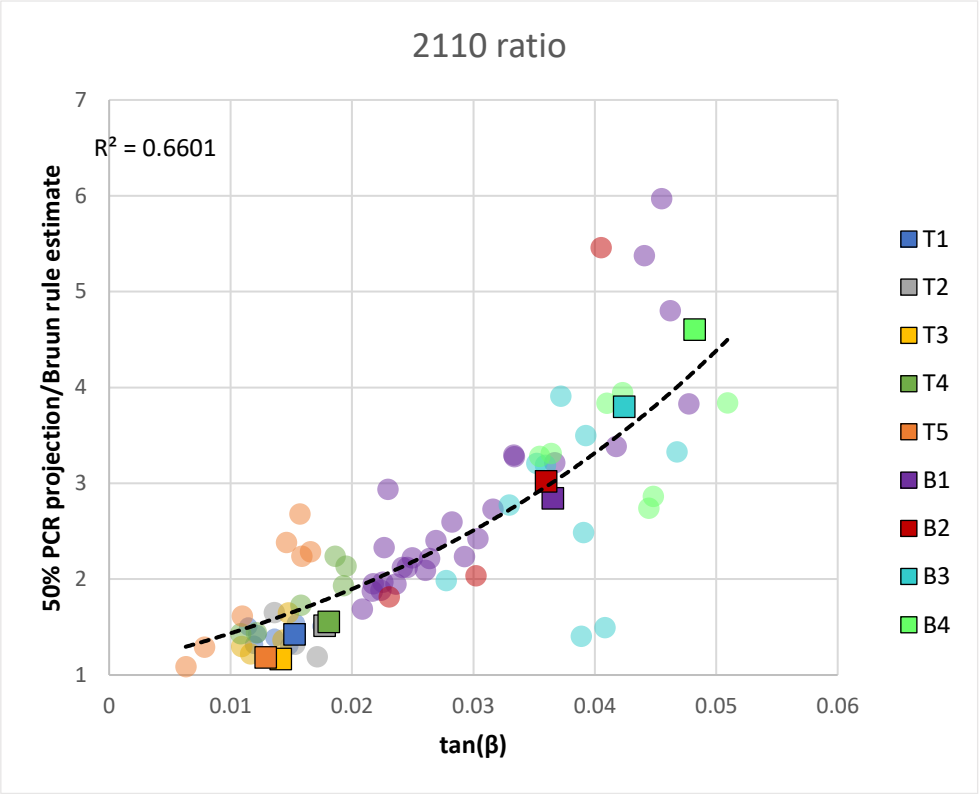

Figure 30: 50% probabilistic coastal recession projections for the year 2110/2110 Bruun rule coastline recession estimate ratios for defined coastal zones (squares) T1, T2, T3, T4, T5, B1, B2, B3 and B4 plotted against their average active shoreface slope. Ratios of their separate transects have been included using bullets.

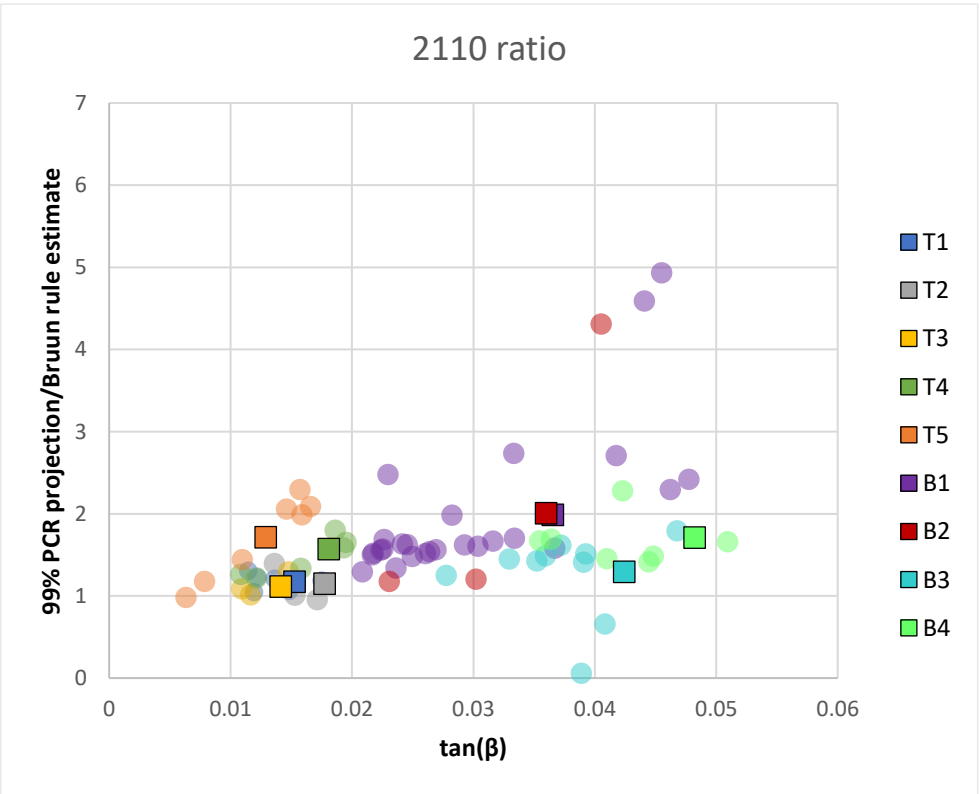

Figure 31: 99% probabilistic coastal recession projections for the year 2110/2110 Bruun rule coastline recession estimate ratios for coastal zones (squares) T1, T2, T3, T4, T5, B1, B2, B3 and B4 plotted against their average active shoreface slope. Ratios of their separate transects have been included using bullets.

4.2.3. Limitations

Firstly, the PCR projections have been computed using the most landward recorded positions of the coastline in 2050 and 2110. Toimil et al. (2017) use the Bruun rule coastline recession estimates as the landward shift of the average coastline position. Similarly, Ranasinghe et al. (2012) make their comparison using the two-year average coastline position. Doing so, Ranasinghe et al. (2012) arrive at very different results (*Bruun rule coastline recession estimates > PCR method derived coastline recessions associated with 1% probability of occurance*). Yet, since more differences between the comparison in this document and the comparison by Ranasinghe et al. (2012) have been found (the use of Larson et al. (2004) instead of the predictor by Mendoza and Jiménez (2006) and the use of Dean's equilibrium profile (Dean & Dalrymple, 2001) as an alternative to actual cross-shore profile measurements) it is unclear how much of the difference can be attributed to the inclusion of intra-annual variabilities in coastline positions.

Secondly, whilst comparing the Bruun rule with the PCR method, the latter is assumed to return values in (better) agreement with reality. In the absence of subsequent topography and bathymetry measurements, the erosion predictor in Dastgheib et al. (2017) has been calibrated using the volumes of eroded sediments according to XBEACH (Roelvink et al., 2009). Consequently, the accuracy of the calibrated erosion predictor is subject to the accuracy of the XBEACH model (or morphological models in general).

Thirdly, apart from their parallel use in coastline recession risk assessments, the Bruun rule and PCR method use decisively different approaches. The PCR method believes coastline recession the result of an increase in exposure to storms due to sea-level rise (Ranasinghe et al., 2012). Consequently, the PCR method does not allow the active shoreface to move vertically. Although the Bruun rule often is criticized because of its simplistic representation of sea-level rise induced coastline recession and the heedless application of the Bruun rule in risk assessments, the vertical migration of the active shoreface with sea-level rise, known as the Bruun principle, is recognised even by Cooper and Pilkey (2004). Admittedly, there are some common grounds. Both methods are a function of the severity of wave attack and, depending on the predictor, the PCR method employs the slope of the the uppermost part of the active shoreface. Still, because the Bruun rule and PCR method describe two very different processes, the fairness of a comparison between the two methods is open to debate.

4.3. Conclusions

The predictive accuracy of the Bruun rule depends on the interpretation of the Bruun rule coastline recession estimates.

Reasonably probable future annual coastline locations appear mostly the result of annual storm erosion instead of sea-level rise induced coastline recession described by the the Bruun principle.With regard to the accuracy of the Bruun rule in predicting the sea-level rise induced recession of the average position of the coastline, the Bruun rule hindcast and the comparison between the Bruun rule coastline recession estimates and the PCR method results in Dastgheib et al. (2017) are inconclusive.

The accuracy of the SDS dataset could not be verified and the linear fit used by the SDS dataset does not recognise the non-linear increase in sea-level between the years 1985 and 2015. Moreover, the Bruun principle is likely obscured by other local scale processes that have determined past coastline positions. Bruun rule coastline recession estimates show better agreement with high exceedance probability PCR method derived coastline recessions and said high exceedance probability projections are more comparable to the average location of the coastline than the low exceedance probability projections. However, the difference between the average coastline position and the definition of the annual location of the coastline in Dastgheib et al. (2017) cannot be bridged.

5. Coastline Recession Projections

This chapter will provide an answer to research question 3: "*How far will the Sri Lankan coastline recede due to sea-level rise, and what local influence have rivers and inlet-basin systems?*". Firstly, nation-wide averaged Bruun rule coastline recession estimates and averages per coastal sector will be provided in Paragraph 5.1. Longshore variations in Bruun rule coastline recession estimates within the coastal sectors will be discussed as well. Paragraph 5.2 continues with the expected coastline recessions downdrift from investigated inlet-basin systems and rivers. Limitations are mentioned in Paragraph 5.3 and conclusions have been written in Paragraph 5.4.

5.1. Bruun Rule Coastline Recession Estimates

5.1.1. Nation-wide Projections and Projections per Coastal Sector

Because of the spatial scale of the research, results cannot be presented on a zonal basis. Instead, results for the years 2050 and 2100 have been averaged to nation-wide coastline recession estimates and averages per coastal sector in Figure 2. Both calculations use weights related to lengths of the defined coastal zones included:

$$\bar{R}_{BE} = \frac{\sum_{i=1}^{n} L_i \, R_{BE,i}}{\sum_{i=1}^{n} L_i} \qquad (21)$$

$$\sigma_{R_{BE}} = \sqrt{\frac{\sum_{i=1}^{n} L_i \, (R_{BE} - \bar{R}_{BE})^2}{\frac{n-1}{n} \sum_{i=1}^{n} L_i}} \qquad (22)$$

with L_i [m] the longshore length of a defined coastal zone i, $R_{BE,i}$ [m] the Bruun rule coastline recession estimate for said defined coastal zone and n the amount of defined coastal zones within the coastal sector.

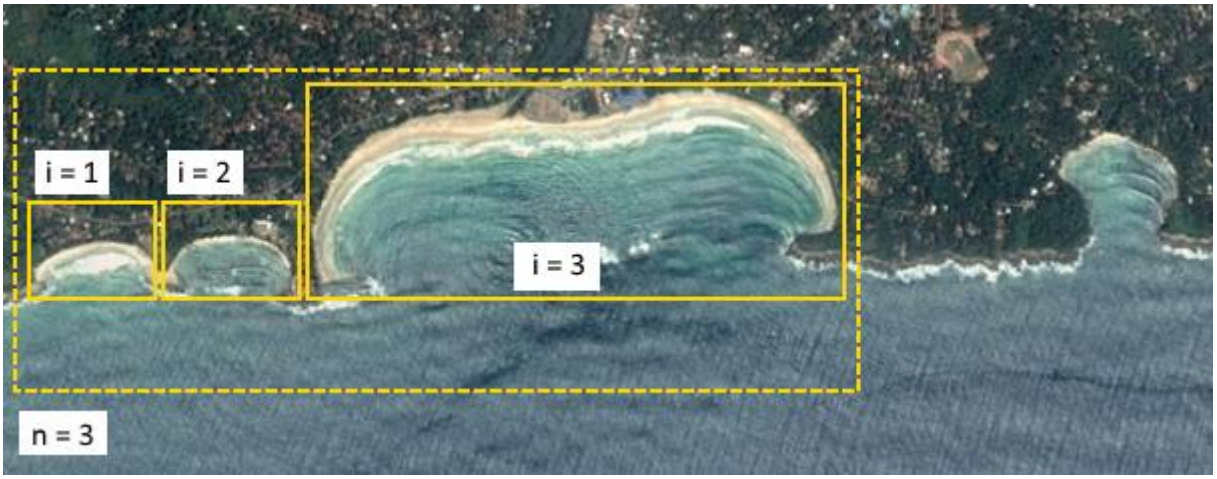

Figure 32: A hypothetical coastal sector (dashed square) with 3 coastal zones (solid squares) (Baselayer: Google Earth).

With increasing timescales, the 2100 nation-wide averaged Bruun rule coastline recession estimates shows increasing differences between climate change scenarios RCP2.6, RCP.4.5 and RCP6.0, and RCP8.5. RCP4.5 and RCP6.0 coastline recession estimates remain almost indistinguishable. Table 8 shows that the 90% likelihood ranges in the sea-level rise projections (shaded areas in Figure 13) result in considerable ranges in coastline recession estimates regardless of the imposed RCP.

Table 8: Nation-wide averaged coastline recession estimates [m] according to the Bruun rule per RCP in IPCC (2013). The importance of uncertainties in the CMIP5 sea-level rise projections are shown using the 90% likelihood ranges.

	2050		2100	
	Mean [m]	*Likely range [m]*	*Mean [m]*	*Likely range [m]*
RCP2.6	6	3 : 9	16	7 : 25
RCP4.5	7	4 : 10	21	10 : 32
RCP6.0	7	4 : 10	23	12 : 34
RCP8.5	9	5 : 13	31	18 : 45

The average coastline recessions estimates per coastal sector (Table 9) show that sea-level rise induced coastline recession should not be presented on a nation-wide scale alone. Significant differences in the short-term and long-term projections between (for example) the South-eastern and Eastern coastal sectors, or South-eastern and North-eastern coastal sectors are present.

Table 9: Average 2050 and 2100 coastline recession estimates according to the Bruun rule per coastal sector as delineated in Figure 2 and per RCP in IPCC (2013). The importance of uncertainties in the CMIP5 sea-level rise projections are shown using the 90% likelihood ranges.

		2050		2100	
	Coastal sector	*Mean [m]*	*Likely range [m]*	*Mean [m]*	*Likely range [m]*
RCP2.6	*Southern*	7	4 : 10	17	10 : 26
	South-eastern	3	2 : 4	8	4 : 12
	Eastern	5	3 : 8	14	6 : 22
	North-eastern	8	4 : 12	21	8 : 33
	Northern	10	5 : 15	27	12 : 41
	North-western	8	4 : 12	22	9 : 34
	Western	6	3 : 9	17	7 : 26
	South-western	5	3 : 8	14	6 : 22
RCP4.5	*Southern*	7	4 : 11	22	11 : 33
	South-eastern	4	2 : 5	10	5 : 15
	Eastern	6	3 : 9	18	9 : 27
	North-eastern	9	5 : 13	27	13 : 42
	Northern	12	6 : 17	36	18 : 56
	North-western	10	5 : 14	30	15 : 45
	Western	7	4 : 10	21	11 : 33
	South-western	6	3 : 9	18	9 : 27
RCP6.0	*Southern*	7	4 : 11	24	13 : 34
	South-eastern	4	2 : 5	11	6 : 16
	Eastern	6	3 : 9	20	11 : 29
	North-eastern	9	5 : 14	30	15 : 44
	Northern	12	6 : 18	40	21 : 59
	North-western	10	5 : 14	32	17 : 48
	Western	7	4 : 11	23	12 : 34
	South-western	6	3 : 9	20	11 : 29
RCP8.5	*Southern*	9	5 : 13	32	19 : 45
	South-eastern	4	3 : 6	15	9 : 22
	Eastern	8	4 : 11	27	15 : 38
	North-eastern	11	6 : 17	40	21 : 58
	Northern	15	8 : 22	56	32 : 81
	North-western	12	7 : 18	46	26 : 66
	Western	9	5 : 13	32	19 : 46
	South-western	8	4 : 11	27	16 : 38

5.1.2. Intra-sectoral Variations in Bruun Rule Coastline Recession Estimates

Inspection of the Bruun rule coastline recession estimates per defined coastal zone shows remaining variations within certain coastal sectors. Said intra-sectoral variations have been indicated using a weighted standard deviation (Equation 22), and minimum and maximum coastline recession estimates for the years 2050 and 2100 (Table 10).

Within the Eastern coastal sector a changing response to sea-level rise is expected. From Arugam Bay (Elephant Point) till Pasikuda Headland, the average estimated mean 2100 coastline recession is 8 m (RCP2.6), 11 m (RCP4.5), 12 m (RCP6.0) or 16 m (RCP8.5). Between Pasikuda Headland and the Northern limit to Thennadi Bay (Figure 33) the average mean 2100 coastline recession estimate is 62 m, 80 m, 89 m or 117 m. North of Thennadi Bay, the average mean 2100 Bruun rule coastline recession estimate is 18 m, 24 m, 26 m or 35 m.

Figure 33: Shorelines deemed suitable for the application of the Bruun rule from Pasikuda Headland up to and including Thennadi Bay (yellow arrows) (Base layer: Google Earth).

In general, the use of transects from Trincomalee Bay – Kuchchaveli and Mullaitivu amounts to minor longshore differences in the Bruun rule coastline recession estimates. However, steep active shorefaces at Manayaweli Bay and Dutch Bay result in the minimum coastline recession estimates listed for the North-eastern coastal sector in Table 10. The maximum values in Table 10 are found at the beach immediately North of Black Bay.

Bruun rule coastline recession estimates along the Northern coast of Sri Lanka are depend upon the presence of continuous nearshore reefs. Shorelines positioned behind said reefs are expected to recede according to the minimum values in Table 10. Without, shallow nearshore depths result in the maximum coastline recession estimates listed in Table 10. Estimates for Mannar Island show a similar two-faced response to sea-level rise; small coastline recession estimates along the South and large coastline recession estimates along the North side of Mannar Island.

Inspection of the Bruun rule coastline recession estimates along the West coast of Sri Lanka reveals a decrease in the expected sea-level rise induced coastline recession North from Chilaw. The good coverage provided by bathymetry measurements and the relatively small size of defined coastal zones result in a highly variable coastline response to sea-level rise along the South-west coast of Sri Lanka. Smoothening of the coastline recession estimates places larger recession estimates towards the North of the coastal sector and shows small coastline recession estimates at the sediment poor coastline near Hikkaduwa.

Table 10: Intra-sectoral variations in the Bruun rule coastline recession estimates per RCP in IPCC (2013) shown using the minimum and maximum mean coastline recession estimates, and the weighted standard deviation of the mean coastline recession estimates. The standard deviations for coastal sectors with few transects have been greyed out.

		2050		2100	
	Coastal sector	*Standard deviation [m]*	*Min : Max recession [m]*	*Standard deviation [m]*	*Min : Max recession [m]*
RCP2.6	*Southern*	0.9	4 : 7	2.3	9 : 18
	South-eastern	0.3	2 : 6	0.9	6 : 15
	Eastern	5.1	2 : 30	13.6	5 : 81
	North-eastern	1.3	4 : 13	3.5	12 : 34
	Northern	5.9	6 : 18	15.9	16 : 48
	North-western	6.4	3 : 17	17.3	9 : 45
	Western	1.8	2 : 11	4.9	4 : 29
	South-western	1.8	2 : 9	4.7	6 : 23
RCP4.5	*Southern*	1.0	4 : 8	2.9	12 : 23
	South-eastern	0.4	3 : 7	1.1	8 : 19
	Eastern	5.9	2 : 35	17.5	7 : 104
	North-eastern	1.6	4 : 15	4.5	15 : 44
	Northern	7.1	7 : 21	21.7	21 : 65
	North-western	7.7	4 : 20	23.6	12 : 61
	Western	2.1	2 : 13	6.1	5 : 37
	South-western	2.0	3 : 10	6.0	8 : 30
RCP6.0	*Southern*	1.0	4 : 8	3.2	13 : 25
	South-eastern	0.4	3 : 7	1.3	9 : 21
	Eastern	6.2	2 : 37	19.4	7 : 115
	North-eastern	1.7	5 : 17	5.1	17 : 49
	Northern	7.1	7 : 22	23.7	23 : 71
	North-western	7.8	3 : 20	25.9	13 : 67
	Western	2.1	2 : 13	6.7	6 : 40
	South-western	2.1	3 : 10	6.6	8 : 32
RCP8.5	*Southern*	1.2	5 : 10	4.2	18 : 34
	South-eastern	0.5	3 : 8	1.7	12 : 29
	Eastern	7.3	3 : 43	25.5	10 : 152
	North-eastern	1.9	6 : 22	6.3	23 : 65
	Northern	8.9	9 : 27	33.3	32 : 100
	North-western	9.7	5 : 25	36.2	19 : 94
	Western	2.6	2 : 16	9.0	8 : 55
	South-western	2.6	3 : 12	8.9	12 : 44

5.2. Coastline Recession Downdrift from Inlet-basin Systems and Rivers

Future shortages in the coastal sediment budgets due to the presence of inlet-basin systems or rivers have been enclosed in Appendix C. Shortages in fluvial sediment supplies after accounting for possible future volumes of legally ($V_{m\ legal}$) and illegally ($V_{m\ total}$) mined river sediments are shown in Appendix D. For investigated inlet-basin systems and rivers with adjacent defined coastal zones, the graphs in Appendix C and Appendix D have been translated to coastline recession.

5.2.1. Southern Coastal Sector

Nilwala Ganga

Figure 34: Longshore limits to and length of the coastline affected by the Nilwala Ganga river (Baselayer: Google Earth).

Table 11: 2050 and 2100 coastline recession downdrift from the Nilwala Ganga river according to the reduced SMIC method. Uncertainties in climate change projections and continuing development of the river catchment are shown together with the effect of possible future legal + illegal river mining activities ($V_{m\ total}$). Values in the $V_{m\ total}$ column are the 95% likelihood : mean : 5% likelihood SMIC projections minus river mining volumes. Changes from progradation to recession due to $V_{m\ total}$ total have been underscored.

	2050			**2100**		
	Mean [m]	*5% - 95% range [m]*	*$V_{m\ total}$ [m]*	*Mean [m]*	*5% - 95% range [m]*	*$V_{m\ total}$ [m]*
RCP2.6	-14	-5 : -18	16 : 7 : 3	-110	-45 : -148	81 : 16 : -22
RCP4.5	-16	-7 : -21	14 : 5 : 0	-128	-61 : -165	65 : -2 : -39
RCP6.0	-19	-10 : -23	11 : 2 : -2	-145	-78 : -183	48 : -19 : -57
RCP8.5	-24	-15 : -29	6 : -3 : -8	-181	-106 : -225	20 : -55 : -99

5.2.2. South-eastern Coastal Sector

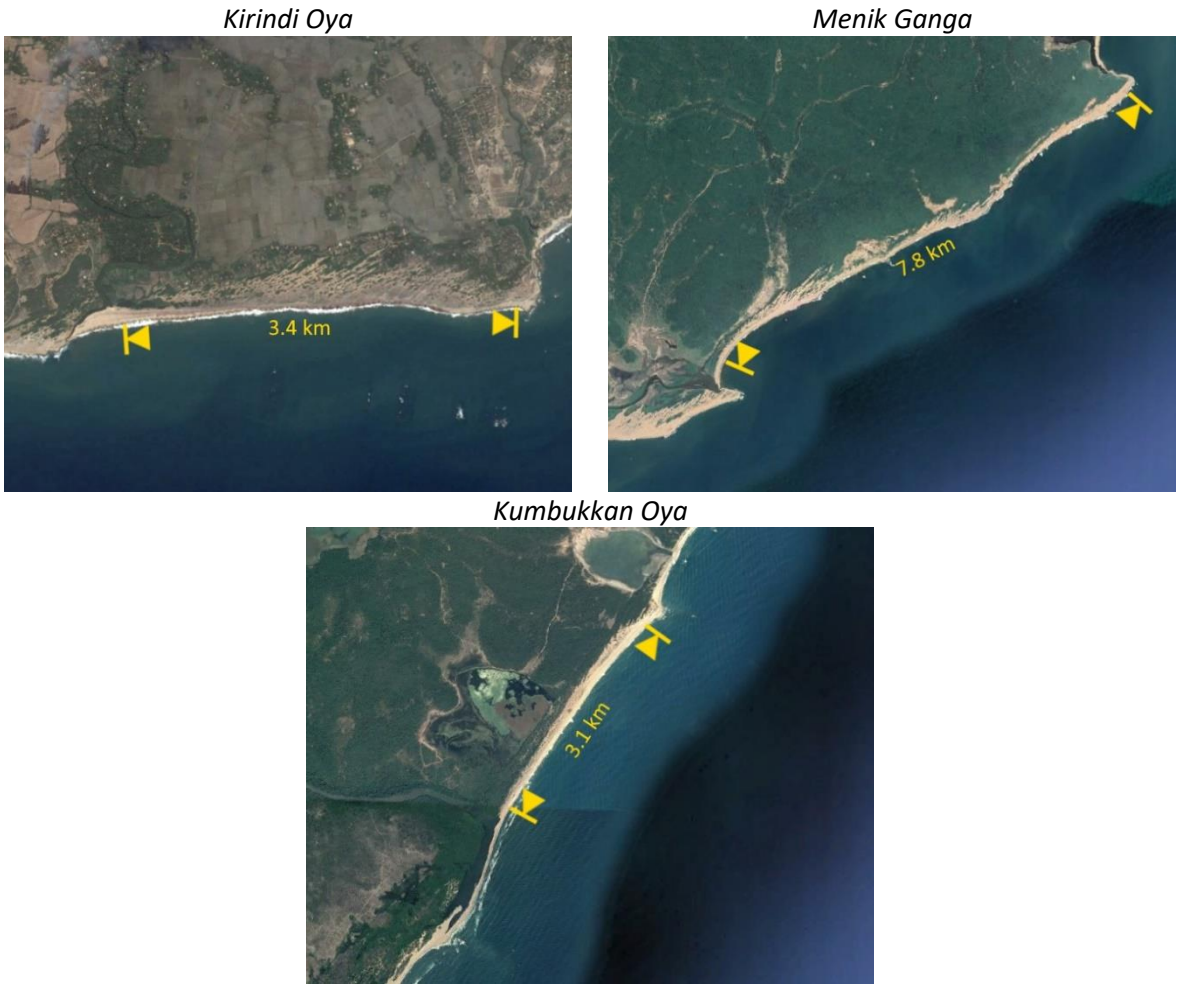

Figure 35: Longshore limits to and lengths of the coastlines affected by the Kirindi Oya, Menik Ganga and Kumbukkan Oya rivers (Baselayer: Google Earth).

Table 12: 2050 and 2100 coastline recession downdrift from the Kirindi Oya, Menik Ganga and Kumbukkan Oya rivers according to the reduced SMIC method. Uncertainties in climate change projections and continuing development of the rivers catchments are shown together with the effect of possible future legal + illegal river mining activities ($V_{m\ total}$). Values in the $V_{m\ total}$ column are the 95% likelihood : mean : 5% likelihood SMIC projections minus river mining volumes. Changes from progradation to recession due to $V_{m\ total}$ total have been underscored.

		2050			2100		
	River	*Mean [m]*	*5% - 95% range [m]*	*$V_{m\ total}$ [m]*	*Mean [m]*	*5% - 95% range [m]*	*$V_{m\ total}$ [m]*
RCP2.6	*Kirindi Oya*	-1	0 : -1	-	-16	-8 : -20	-
	Menik Ganga	-1	0 : -1	4 : 3 : 3	-17	-9 : -21	12 : 4 : 0
	Kumbukkan Oya	-5	-2 : -6	5 : 2 : 1	-40	-19 : -52	22 : 1 : -11
RCP4.5	*Kirindi Oya*	-1	-1 : -1	-	-18	-9 : -21	-
	Menik Ganga	-1	-1 : -1	3 : 3 : 3	-19	-10 : -22	11 : 2 : -1
	Kumbukkan Oya	-5	-3 : -7	4 : 2 : 0	-45	-23 : -57	18 : -4 : -16
RCP6.0	*Kirindi Oya*	-2	-2 : -2	-	-25	-16 : -29	-
	Menik Ganga	-2	-2 : -2	2 : 2 : 2	-28	-19 : -32	2 : -7 : -11
	Kumbukkan Oya	-8	-5 : -9	2 : -1 : -2	-61	-39 : -74	2 : -20 : -33
RCP8.5	*Kirindi Oya*	-3	-3 : -3	-	-34	-24 : -38	-
	Menik Ganga	-4	-4 : -4	0 : 0 : 0	-39	-28 : -43	-7 : -18 : -22
	Kumbukkan Oya	-11	-8 : -13	-1 : -4 : -6	-83	-57 : -97	-16 : -42 : -56

5.2.3. Eastern Coastal Sector

Figure 36: Longshore limits to and lengths of the coastlines affected by the Gal Oya river and Batticaloa Lagoon (Baselayer: Google Earth).

Table 13: 2050 and 2100 coastline recession downdrift from the Gal Oya river and Batticaloa Lagoon according to the (reduced) SMIC method. Uncertainties in climate change projections and continuing development of the Gal Oya river and the tributaries of Batticaloa lagoon are shown shown together with the effect of possible future legal + illegal river mining activities ($V_{m\ total}$). Values in the $V_{m\ total}$ column are the 95% likelihood : mean : 5% likelihood SMIC projections minus river mining volumes. Changes from progradation to recession due to $V_{m\ total}$ total have been underscored.

		2050			2100		
	Inlet-basin system/River	*Mean [m]*	*5% - 95% range [m]*	*$V_{m\ total}$ [m]*	*Mean [m]*	*5% - 95% range [m]*	*$V_{m\ total}$ [m]*
RCP2.6	*Gal Oya*	2	1 : 3	-	5	2 : 7	-
	Batticaloa Lagoon	89	39 : 142	41 :91 : 144	223	80 : 368	92 : 235 : 380
RCP4.5	*Gal Oya*	3	2 : 4	-	7	4 : 10	-
	Batticaloa Lagoon	104	51 : 156	53 : 106 : 158	291	134 : 459	146 : 303 : 471
RCP6.0	*Gal Oya*	3	1 : 4	-	6	3 : 9	-
	Batticaloa Lagoon	103	49 : 159	51 : 105 : 161	310	149 : 476	161 : 322 : 488
RCP8.5	*Gal Oya*	3	2 : 4	-	8	4 : 13	-
	Batticaloa Lagoon	119	56 : 181	58 : 121 : 183	405	213 : 610	225 : 417 : 622

5.2.4. North-eastern Coastal Sector

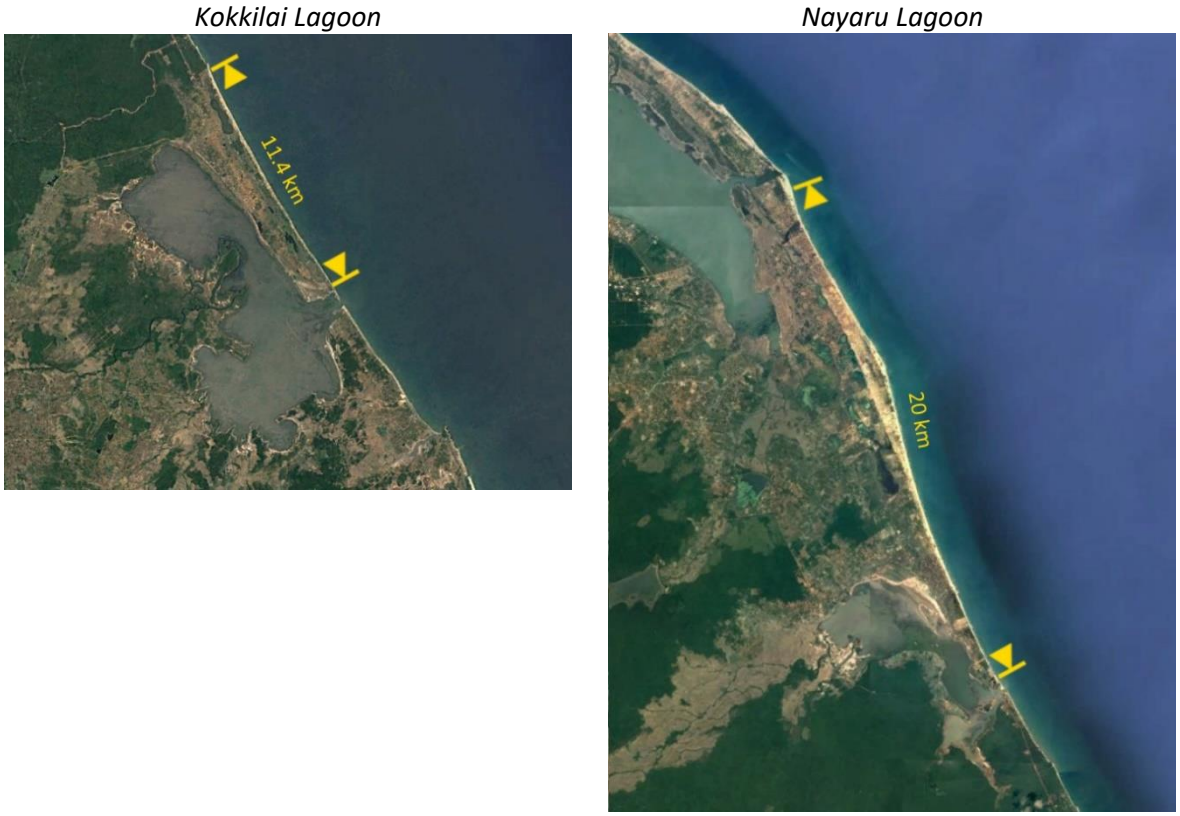

Figure 37: Longshore limits to and lengths of the coastlines affected by Kokkilai Lagoon and Nayaru Lagoon (Baselayer: Google Earth).

Table 14: 2050 and 2100 coastline recession downdrift from Kokkilai Lagoon and Nayaru Lagoon according to the SMIC method. Uncertainties in climate change projections and continuing development of tributaries are shown together with the effect of possible future legal + illegal river mining activities ($V_{m\ total}$). Values in the $V_{m\ total}$ column are the 95% likelihood : mean : 5% likelihood SMIC projections minus river mining volumes. Changes from progradation to recession due to $V_{m\ total}$ total have been underscored.

		2050			2100		
	Inlet-basin system	*Mean [m]*	*5% - 95% range [m]*	*$V_{m\ total}$ [m]*	*Mean [m]*	*5% - 95% range [m]*	*$V_{m\ total}$ [m]*
RCP2.6	*Kokkilai Lagoon*	45	22 : 69	22 : 45 : 69	119	50 : 187	52 : 121 : 189
	Nayaru Lagoon	8	4 : 12	4 : 8 : 12	21	8 : 34	8 : 21 : 34
RCP4.5	*Kokkilai Lagoon*	52	27 : 76	27 : 52 : 76	153	75 : 235	77 : 155 : 237
	Nayaru Lagoon	9	5 : 13	5 : 9 : 13	27	13 : 44	13 : 27 : 44
RCP6.0	*Kokkilai Lagoon*	52	27 : 77	27 : 52 : 77	164	85 : 244	87 : 166 : 246
	Nayaru Lagoon	9	4 : 13	4 : 9 : 13	29	15 : 46	15 : 29 : 46
RCP8.5	*Kokkilai Lagoon*	64	34 : 93	64 : 34 : 93	225	128 : 326	130 : 227 : 328
	Nayaru Lagoon	11	6 : 16	6 : 11 : 16	42	23 : 63	23 : 42 : 63

5.2.5. Northern Coastal Sector

Thondammanaru Lagoon

Figure 38: Longshore limits to and length of the coastline affected by Thondammanaru Lagoon (Baselayer: Google Earth).

Table 15: 2050 and 2100 coastline recession downdrift from Thondammanaru Lagoon according to the SMIC method.

	2050		**2100**	
	Mean [m]	*5% – 95% range [m]*	*Mean [m]*	*5% - 95% range [m]*
RCP2.6	-134	-70 : -193	-333	-155 : -459
RCP4.5	-159	-85 : -227	-424	-231 : -506
RCP6.0	-160	-84 : -232	-450	-267 : -508
RCP8.5	-197	-109 : -278	-506	-386 : -444

5.2.6. Western Coastal Sector

Deduru Oya and Chilaw Lake

Figure 39: Longshore limits to and length of the coastline affected by the Deduru Oya river and Chilaw Lake
(Baselayer: Google Earth).

Table 16: Compounded 2050 and 2100 coastline recession downdrift from the Deduru Oya river and Chilaw Lake according to the SMIC method. Uncertainties in climate change projections and continuing development of the Deduru Oya river catchment are shown together with the effect of possible future legal + illegal river mining activities ($V_{m\ total}$). Values in the $V_{m\ total}$ column are the 95% likelihood : mean : 5% likelihood SMIC projections minus river mining volumes. Changes from progradation to recession due to $V_{m\ total}$ total have been underscored.

	2050			**2100**		
	Mean [m]	*5% - 95% range [m]*	*$V_{m\ total}$ [m]*	*Mean [m]*	*5% - 95% range [m]*	*$V_{m\ total}$ [m]*
RCP2.6	2	0 : 9	3 : 5 : 12	-5	-16 : 23	1 : 12 : 40
RCP4.5	2	0 : 11	3 : 5 : 14	-6	-15 : 29	2 : 11 : 46
RCP6.0	2	-1 : 11	2 : 5 : 14	-6	-18 : 26	-1 : 11 : 43
RCP8.5	2	-1 : 13	2 : 5 : 16	-7	-19 : 35	-2 : 10 : 52

5.3. Limitations

5.3.1. Used Depth of Closure Estimates

There are two notable limitations with regard to the used depth of closure estimates. Whereas, Nicholls et al. (1996) only specify the use of the non-breaking significant wave heights, Hallermeier (1980) states that local (significant) wave conditions should be used. Without wave conditions available on a more refined grid, the offshore ERA-Interim reanalysed significant wave height and related mean wave period have been used. Due to refraction or diffraction, and attenuation or dissipation of waves it is unclear how representative the offshore ERA-Interim reanalysed wave data are with respect to wave conditions closer to the coastline. Consequences of said lack of nearshore wave data are the large coastline recession estimates along the Northern coast of Mannar Island (IHE-Delft, 2016). Moreover, the large Bruun rule coastline recession estimates near Pasikuda Headland may also be the result of a difference between the actual and the imposed wave climate.

Secondly, the ERA-Interim reanalysed wave data has a timespan limited to 35 years. Coastline recession estimates that use Nicholls et al.'s depth of closure estimate and surpass said timespan require an extrapolation of the wave data. Udo and Takeda (2017) increase the coverage of their five-year nearshore wave data by decreasing the duration in Nicholls et al.'s depth of closure estimate from 12 hours to 3 hours. The same method has been used to increase the timespan of the ERA-Interim dataset. However, said approach is easy thinking and the anticipated increase in coverage is unlikely attained.

Nicholls et al.'s depth of closure estimates draws a progressively conservative bound to observed values with increasing timescales. However, since Nicholls et al.'s depth of closure estimate is based on the effect of surface waves on an annual timescale, the witnessed progressive overestimation of D_C is (partially) reserved for macro timescale (10 – 100 year) processes transporting coastal sediments in the cross-shore direction (Nicholls et al., 1998).

5.3.2. Calculated Catchment Wide Trapping Efficiencies

The calculated reservoir and catchment-wide trapping efficiencies assume the annual river discharge unaffected by the construction and operation of reservoirs. Still, it is common knowledge that the retention of water and use of water for irrigation purposes result in higher evaporation rates and water losses. Consequently, the actual catchment-wide trapping efficiencies are lower than those calculated using Vörösmarty et al. (2003).

5.3.3. Use of The GHFI

The three E_h categories by Syvitski et al. (2016) have been substituted with the GHFI by assuming a catchment-wide 1% GHFI equal to a 0.3 E_h value and equating a catchment-wide 100% GHFI with a 2.0 E_h value. However, the ensemble of river catchments from which the BQART model has been derived unlikely contains these extreme catchment-wide GHFI values. Consequently, the used GHFI scaling is open to debate.

5.3.4. Assumed Dynamic Equilibrium of Interrupted Coastlines

The assumption that the present coastline has fully adapted to any past changes to the coastal and terrestrial climate is of great importance to the SMIC method calculations. Said assumption will hold for the R_{BE} and R_{BV} components of the SMIC method and since past sea-level rise is negligible with regard to projected sea-level rise trends, it can be extended to include the R_{BI} component.

Regarding the R_{FS} component of the SMIC method, Ranasinghe et al. (2013) assume the terrestrial climate not yet affected by climate change. However as stated in Paragraph 2.11.4, the mean annual temperature in Sri Lanka has already increased by 0.8 °C. Moreover, present fluvial sediment supplies

are heavily influenced by humankind. To include the fluvial sediment supply, the coastline must have again reached an equilibrium with regard to these changes. Thus, past deviations from pristine conditions do not influence future recession by coastlines and are limited to the yellow shaded areas in Figure 40.

CCD (2006) is inconclusive, but the absence of significant negative SDS trends (Luijendijk et al., 2018) at the beaches downdrift from the Deduru Oya, Kalu Ganga, Nilwala Ganga, Kirindi Oya, Menik Ganga and Gal Oya rivers suggest the coast is indeed able to reach said new equilibrium. The 'recession front' moving away from the Maha Oya river mouth in the longshore direction (mentioned in Wickramaarachchi (2010)) can be the result of the annual volume of mined river sediments or the increase in annual river mining activities alone.

However, the believed tendency of coastlines to reach dynamic equilibriums affects projections as well. In Equation 10, the fluvial sediment supply at the start of the year 2016 is considered the reference annual fluvial sediment supply. Therefore, the integral describes the red shaded area in Figure 40. Assuming a dynamic equilibrium, the reference annual fluvial sediment is no longer a constant and lags the projected annual supply of fluvial sediments. Consequenly, the red shaded area in Figure 40 should be smaller and the SMIC method overestimates the amount of coastline recession linked to changes in the fluvial sediment supply.

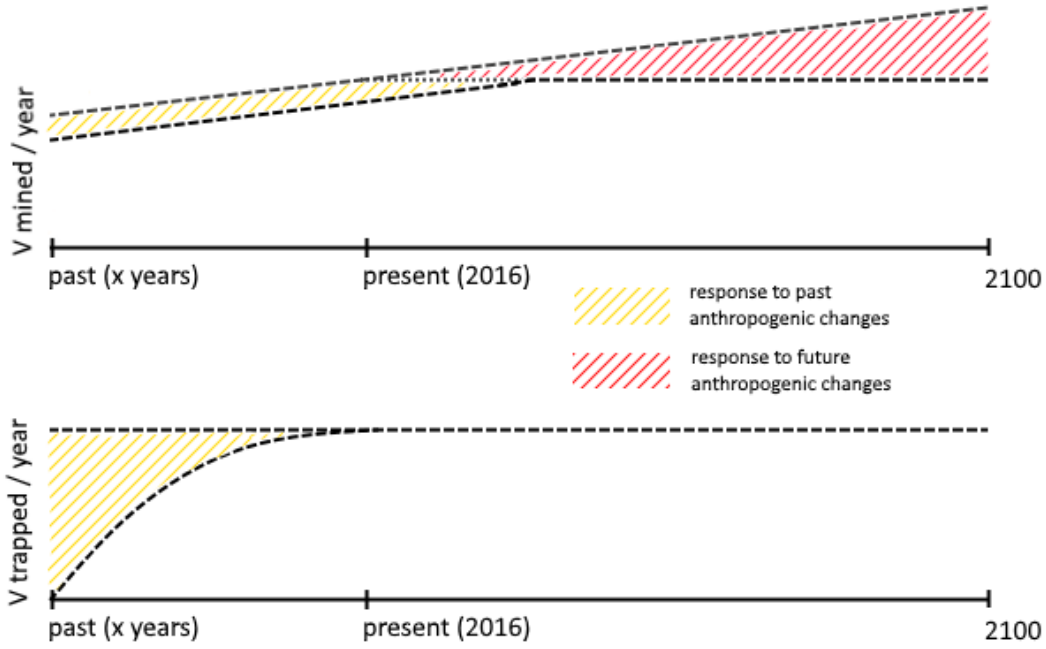

Figure 40: A simplied illustration of the assumptions regarding the R_{FS} component of the SMIC method for past and future anthropogenic changes to the fluvial sediment supply. Shaded shortages (have) result(ed) in coastline recession.

5.3.5. Measured Lengths of Affected Coastlines

Although the general littoral drift of coastal sediments along the South coast of Sri Lanka is from the West towards the East, the fluvial sediments supplied by the Nilwala Ganga river are alternatingly deposited to the West and to the East of the river mouth. Therefore the beach East of the Nilwala Ganga river mouth receives only a part the increase in annual fluvial sediment supply. At the Kalu Ganga river, a similar alternation between the North (Dayananda, 1992) and the South (Bamunawala et al., 2018) of the Kalu Ganga river mouth is reported. Examples of other shortcomings are coastal sediments bypassing the headland downdrift from the Batticaloa Lagoon and the temporary elongation of the affected coastline during high discharges by the Menik Ganga river.

5.4. Conclusions

5.4.1. Sea-level Rise Induced Coastline Recession

On average, the mean long-term recession by the Sri Lankan coastline is 16 m, 21 m, 23 m and 31 m, depending on the imposed RCP. However, the likelihood ranges in the sea-level rise projections result in considerable uncertainties in the coastline recession estimates. Moreover, the use of bathymetry measurements has resulted in both regional and local differences in the Bruun rule coastline recession estimates. Instances of local differences are found at shorelines protected by continuous offshore reefs (west of Point Pedro), sediment poor areas (Hikkaduwa) and beaches controlled by headlands (Pasikuda Headland). The latter may be the result of a lack of information regarding nearshore wave data.

5.4.2. Recession or Progradation at Inlet-basin Systems

Without significant freshwater inputs, the presence of intermittently closed to permanently open inlet-basin systems along the East and North-east coast of Sri Lanka is likely to result in mild to (dangerously) strong local coastline recession trends. Short-term, pronounced tidal flats in the basin of an inlet-basin system may alleviate the majority of the coastal sediment import by said system, but long-term basin infilling will dominate. Along the Northern coast, inlet-basin systems within the Jaffna Peninsula are expected to export sediments and downdrift coastlines are expected to progradate.

5.4.3. Mitigating or Accelerating Effects by Rivers

Climate change and continuing development of river catchments will result in increased volumes of fluvial sediments supplied to the Sri Lankan coast. The influx will mitigate sea-level rise induced coastline recession and, except for the Gal Oya and Deduru Oya rivers, is expected to result in short-term and long-term local coastline progradation.

Regarding the Gal Oya river, the high catchment-wide trapping efficiency drastically reduces the present annual fluvial sediment supply. Consequently, the limited increase is insufficient to compensate for the Bruun principle. Downdrift from the Deduru Oya, short-term coastline recession is expected before long-term coastline progradation will be observed. However, long-term coastline recession due to the infilling Chilaw Lake remains a possibility.

Future increases in present river mining activities are of dire importance to the future location of downdrift coastlines. Provided the mean RCP8.5 climate change scenario, possible future river mining activities are not expected to result in shortages of supplied fluvial sediments. However, the likelihood of future shortages increases with milder RCPs. Furthermore, coastline recession downdrift from rivers is the result of both the Bruun principle and future fluvial sediment supplies. Consequently, without a limit to future river mining activities, receding coastlines are possible.

6. Sea-level Rise Induced Beach Loss

Chapter 6 presents an answer to the fourth and final research question: *"What is the consequence of sea-level rise regarding the width of Sri Lankan beaches?"*. Future beachwidths are shown using two nation-wide graphs and four maps depicting beach widths for the year 2100 assuming the mean RCPs in IPCC (2013). Notable limitations and conclusions have been written in Paragraph 6.2 and 6.3 (resp.).

6.1. Future Beach Widths

To determine future beach widths, the active shoreface is allowed to migrate landwards until a (soft) barrier is reached. From that moment in time onwards, erosion is absent or in case of a soft barrier replenished with sediment from a cliff or dune (Udo & Takeda, 2017).

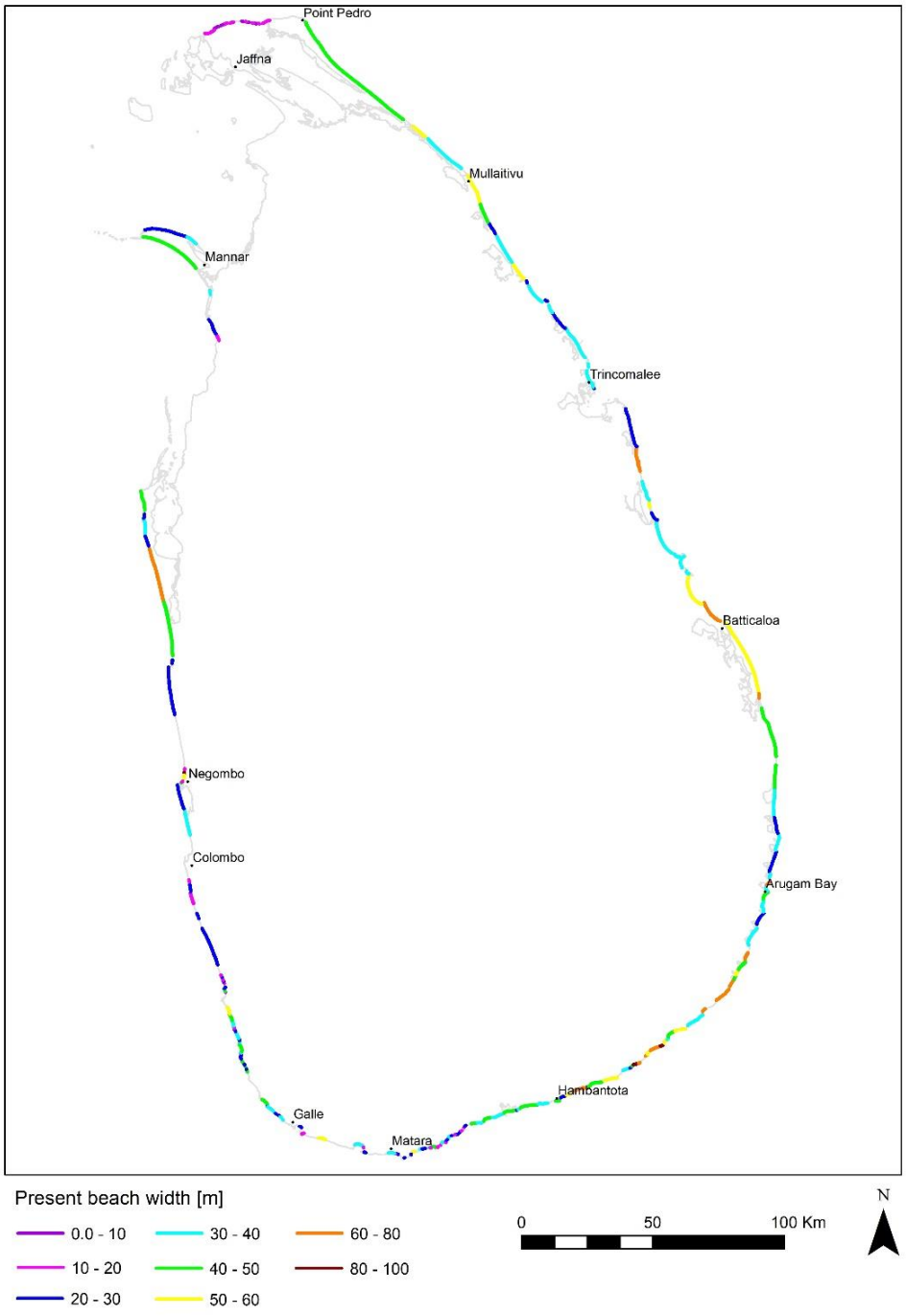

Figure 41: Present beach width per defined coastal zone [m]. Measurements have been taken from satellite images.

Omitting interrupted coastlines (Figure 23), nation-wide averaged future beach widths and nation-wide future distributions of beach widths have been plotted in Figure 42. Regarding the latter, the short-term and long-term mean RCP2.6 and RCP8.5 climate change scenario, the long-term 95% likelihood RCP2.6, and the long-term 5% likelihood RCP8.5 coastline recession estimates have been used.

Whereas the top frame in Figure 42 shows the nation-wide averaged remaining beach widths, the bottom frame displays the percentage of the uninterrupted coastline that has a remaining beach width equal to or smaller than a certain bin value. Therefore, the bottom can be used to assess the percentage of Sri Lankan coastline (almost) depleted of its beaches. Additionally, nation-wide maps depicting the projected long-term beach widths have been drawn for each mean RCP.

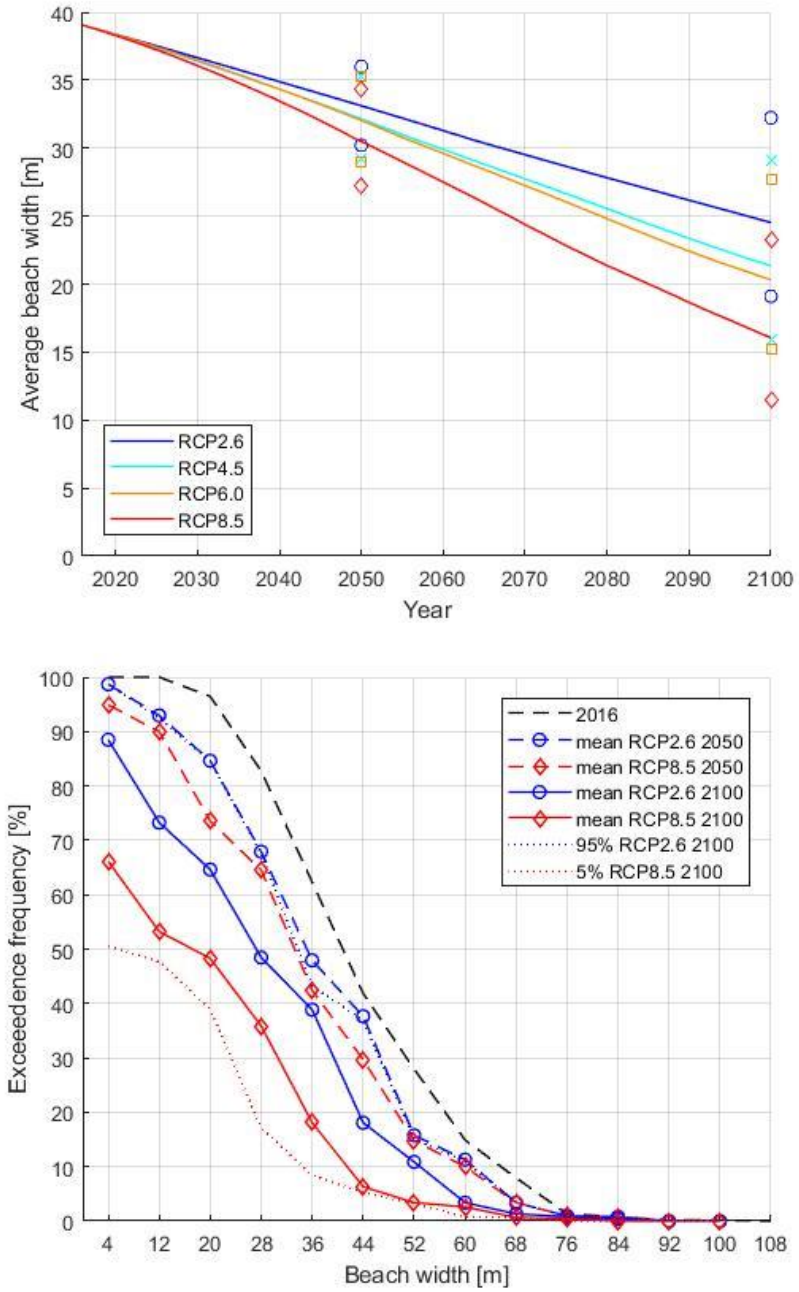

Figure 42: Estimated future nation-wide averaged beach widths at uninterrupted coastlines (top frame), and 2050 and 2100 nation-wide exceedance frequencies of beach widths according to the mean RCP2.6 and RCP8.5, 95% likelihood RCP2.6 and 5% likelihood RCP8.5 sea-level rise projections in IPCC (2013) *(bottom frame).*

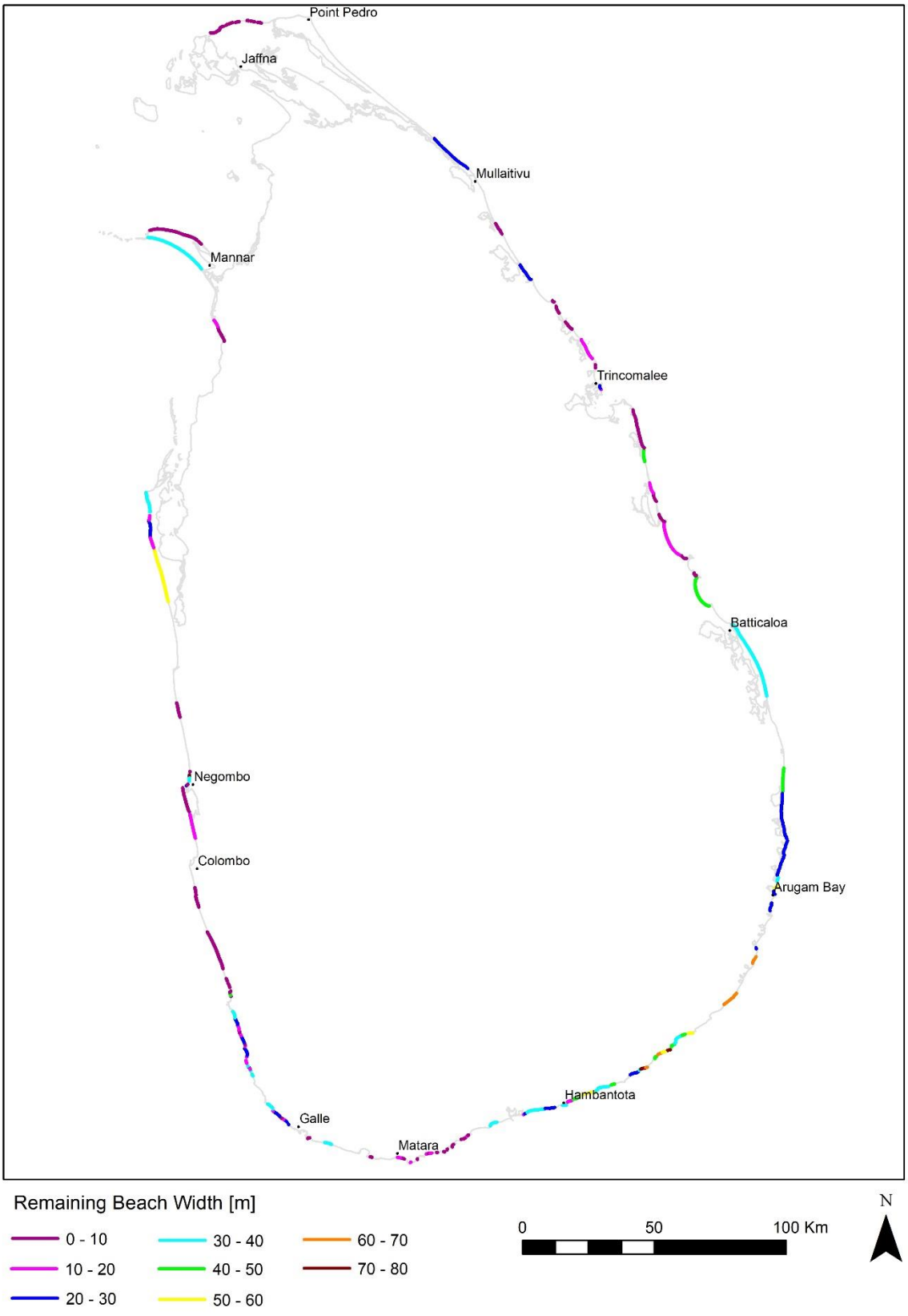

Figure 43: Remaining 2100 beach widths along the Sri Lankan coast provided the mean RCP2.6 sea-level rise projections.

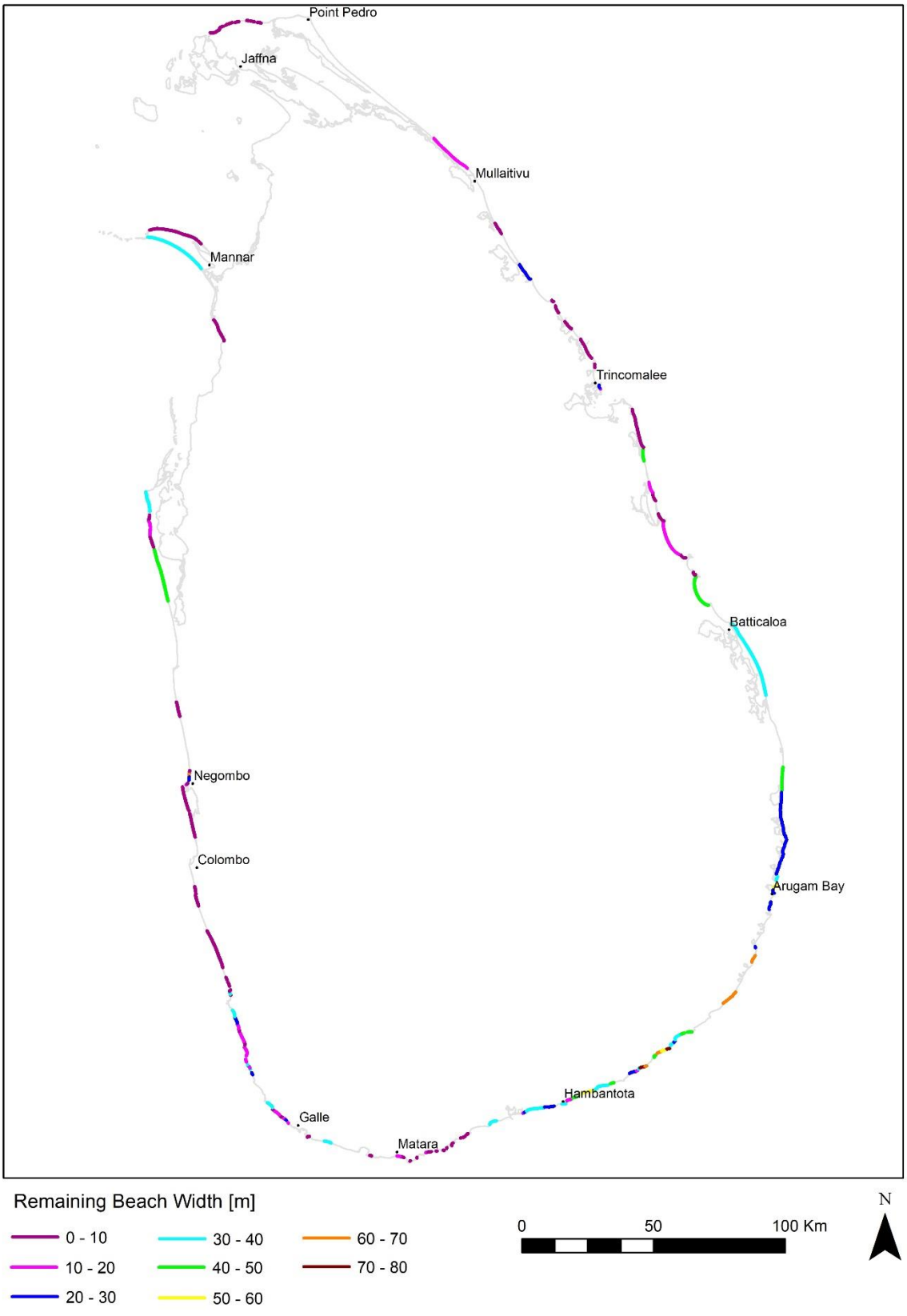

Figure 44: Remaining 2100 beach widths along the Sri Lankan coast provided the mean RCP4.5 sea-level rise projections.

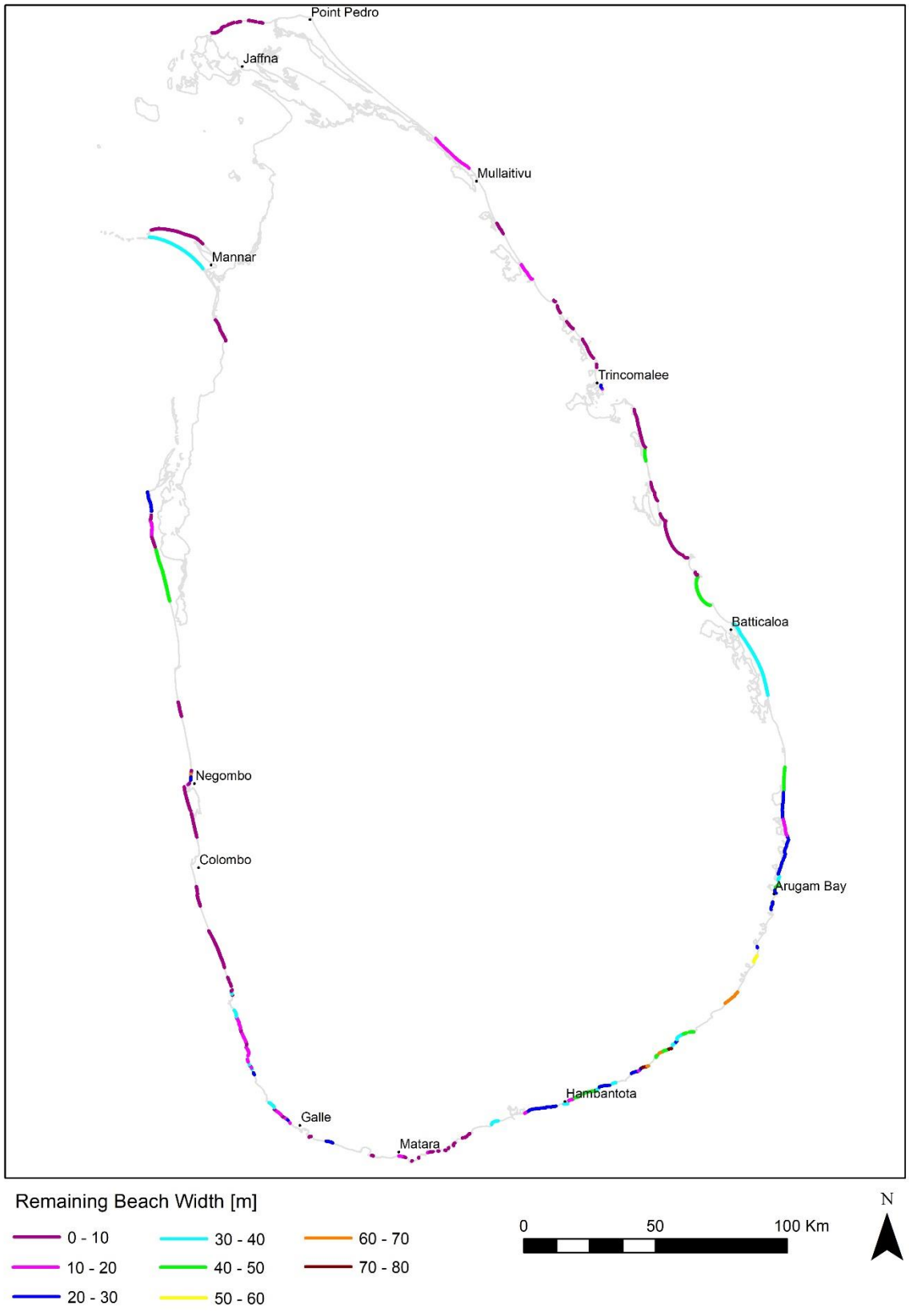

Figure 45: Remaining 2100 beach widths along the Sri Lankan coast provided the mean RCP6.0 sea-level rise projections.

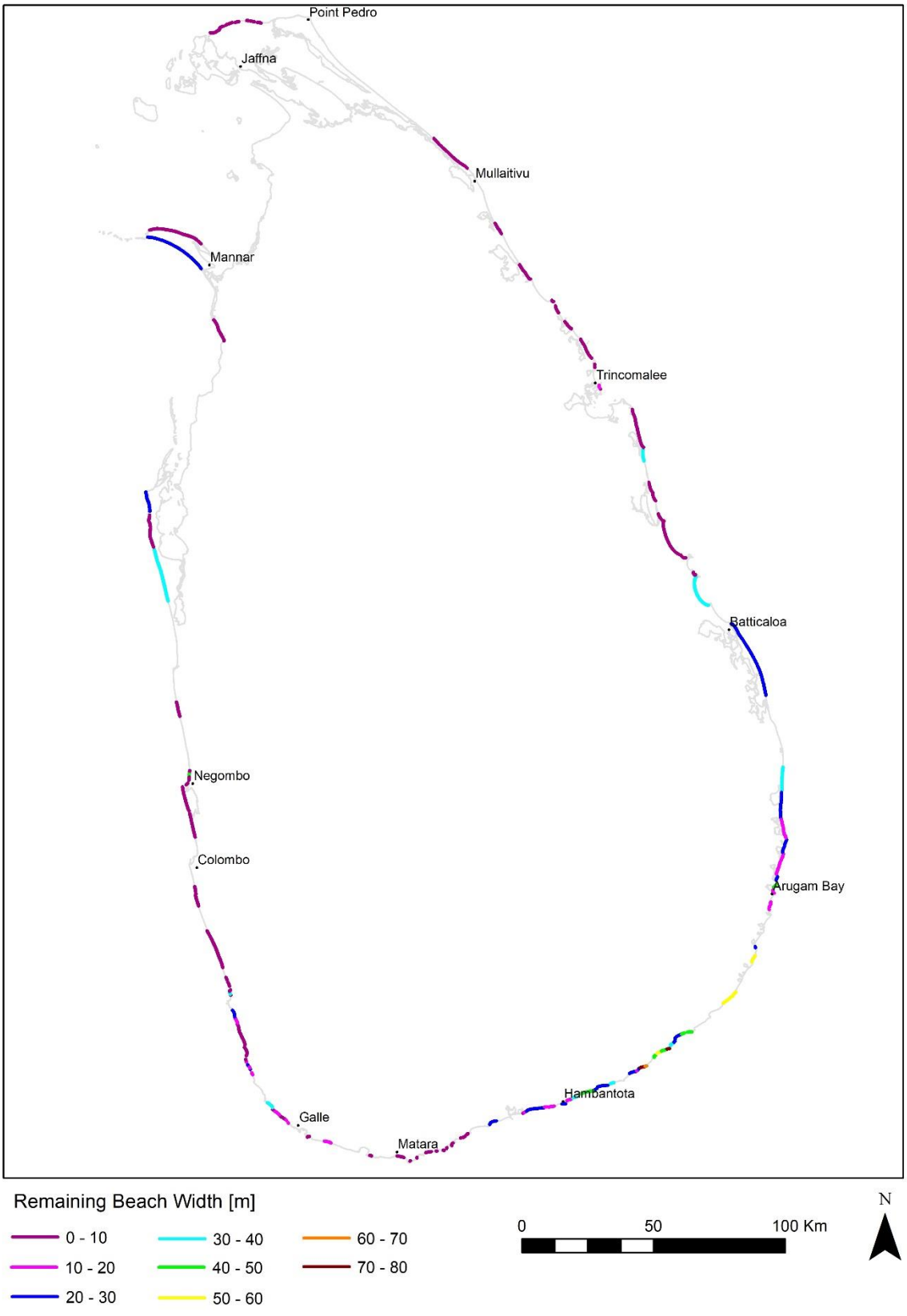

Figure 46: Remaining 2100 beach widths along the Sri Lankan coast provided the mean RCP8.5 sea-level rise projections.

6.2. Limitations

Firstly, present beach widths have been measured using satellite images that are not guaranteed to accurately provide the average position of the MSL mark of a cross-shore profile. Furthermore, outlining present beaches is a tedious and ambiguous process often hindered by variying satellite image qualities. Regions for which the image quality has been troublesome are the South-east coast, the top half of the North-east coast and the Northern coastline. Beach width measurements have been refined through multiple iterations, but remain prone to human error.

Secondly, depending on the landward barrier, the credibility of said barrier is high (dunes and built up area) medium (permanent vegetation line) or low (backshore).

Thirdly, the results in Chapter 5 show the future position of interrupted coastlines is strongly influenced by changes in the fluvial sediment supply of rivers, and/or coastal sediment import or export by inlet-basin systems. The beaches downdrift from rivers and/or intermittently closed to permanently open inlet-basin systems have been omitted in Paragraph 6.1. Consequently, the sandy coastlines along the South and North-east of Sri Lanka are poorly represented.

6.3. Conclusions

With the present landward limit to beaches locked in place, mean long-term sea-level rise will considerably decrease beach widths at uninterrupted coastlines to a national average of 25 m (RCP2.6), 22 m (RCP4.5), 20 m (RCP6.0) or 16 m (RCP8.5).

Along the Northern coast, short-term sea-level rise is expected to reduce beach widths to zero. Long-term sea-level rise and affiliated coastline recession may result in the disappearance of a considerable amount of beaches along most of the Sri Lankan coast. Results show that diminishing beach widths are not only limited to the more severe climate change scenarios. Long-term, the mean RCP2.6 climate change scenario sea-level rise will result in depleted beaches along the North and parts of the West coast of Sri Lanka as well.

7. General Conclusions

Chapter 7 summarises the answers to the posed research question given in the previous chapters.

RQ 1: *What is the validity of applying the Bruun rule in assessing the future position of the Sri Lankan coastline?*

The Bruun rule is a first-pass assessment of the coastline response to sea-level rise for approximately half of the total Sri Lankan coast. However, diverenges in the littoral drift or cross-shore sources or sinks influencing the coastal sediment balance cannot be precluded along respectively 78% and 51% of the sandy coastline. Moreover, the presence of numerous (large) rivers, lagoons and/or coastal lakes may result in deviations from the Bruun rule coastline recession estimates along 32% of the assessed coast.

RQ 2: *What is the predictive accuracy of the Bruun rule for the Sri Lankan coastline?*

Bruun rule coastline recession estimates should be interpreted as the sea-level rise induced recession of the average cross-shore location of the coastline. However, due to several limitations regarding the performed Bruun rule hindcast (using the Satellite Derived Shoreline trends by Luijendijk et al. (2018)) and the comparison between Bruun rule coastline recession estimates and the Probabilistic Coastal Recession method derived projections in Dastgheib et al. (2017), a clear answer to this research question cannot be provided.

RQ 3: *How far will the Sri Lankan coastline recede due to sea-level rise, and what influence have rivers and inlet-basin systems?*

On average, the mean long-term sea-level rise induced recession by the Sri Lankan coastline is 16 m, 21 m, 23 m or 31 m, depending on the imposed RCP. However, significant regional differences and uncertainties in the coastline recession projections are present and should be taken into account.

The East and North-east lagoons are likely to result in mild to (dangerously) strong local coastline recession trends. Along the Northern coast, inlet-basin systems within the Jaffna Peninsula are expected result in local coastline progradation.

Climate change and continuing development of catchments will result in increased volumes of fluvial sediments supplied to the Sri Lankan coast downdrift from mostly uncontrolled rivers. However, future surpluses in supplied fluvial sediments may be nullified by increased river mining activities. Consequently, strong local erosion trends at the beach adjacent to the Nilwala Ganga river mouth and along the coastline downdrift from the Deduru Oya river mouth cannot be debarred.

RQ 4: *What is the consequence of sea-level rise regarding the width of Sri Lankan beaches?*

Provided the landward limit to present beaches is locked in place, long-term sea level rise may significantly reduce the number of Sri Lankan beaches by the end of the 21st century. The mean RCP2.6 climate change scenario will result in diminished beachwidths limited to the North and parts of the West coast of Sri Lanka. However, provided the mean RCP8.5 climate change scenario, the absence of beaches will become a common phenomenon along most of the Sri Lankan coast.

8. Recommendations

The following recommendation are proposed to mitigate the impact of future coastline recession, enrich the projection in this report, and spark or help improvements and follow-up research linked to the used research method.

- Expecting mild to (dangerously) strong local erosion trends downdrift from the intermittently closed and permanently opened inlet-basin systems along the East and North-east coast of Sri Lanka, development of these coastlines should be discouraged or restricted to temporary structures and infrastructure.
- Similarly, developments close to the coastline downdrift from the inlet of Chilaw lake and the mouth of the Deduru Oya river are not adviseable.
- The landward limit to beaches must be allowed to migrate landwards where possible. The West to South coast of Sri Lanka is heavily developed and unfortunately said landward migration is often prohibited by property and infrastructure. Here nourishments of coastal sediment balances may provide a solution.
- The Coast Conservation Department Sri Lanka is encouraged to continue the measuring of the Sri Lankan coastline and increase the accuracy of the Bruun rule estimates. An important gap in their present bathymetry measurements ensemble is between Galle and Tangalle. Figure 20 can be employed to identify other gaps.
- The Coast Conservation Department Sri Lanka is urged to collaborate with the Geological Survey and Mining Bureau in determining present and future river mining activities in the catchments of the Deduru Oya and Nilwala Ganga rivers, and downstream from large reservoirs in the catchments of other rivers along the West to South-east coast.
- Originally this research aimed to include a (qualitative) analysis of sea-level rise related economic damages. However, due to missing crucial information, it is not possible to present a sufficiently complete overview of the following three dimensions to economic impact:
    - loss of property expressed as either the value of property lost (Dastgheib et al., 2017) or number of properties lost (Wadey et al., 2013);
    - damage to roads and railways expressed as the length of infrastructure affected (Wadey et al., 2013);
    - devaluation of beach related ecosystem services such as recreation and tourism, (commercial) fishery and amenity due to decreasing beach widths (Udo & Takeda, 2017) or beach surface area (Dastgheib et al., 2017).

  Although the Sri Lankan coast is heavily developed and the potential damages to property and infrastructure are considerable (Table 17), the comparison between the Bruun rule and the Probabilistic Coastal Recession method in Paragraph 4.2 has shown that the use of the Bruun rule (without the addition of interannual variability of storms) is not justifiable in an impact analysis regarding these two dimensions. To include intra-annual variability in the position of the shoreline, the approach by Toimil et al. (2017) and a the application of the Probabilistic Coastal Recession method without sea-level rise are both options. However, in data poor environments, scaling the Bruun rule (Table 17) may be the only option.

  Alternative to the Openstreetmap database, the Global Urban Footprint by the German Earth Observation Centre (or other satellite derived global urban area masks) can be used to determine the amount of built up area lost. However, due to the poor performance of the Global Urban Footprint in scarcely built up areas (Klotz et al., 2016; Mück et al, 2017), the applicability of the Global Urban Footprint is limited to medium or high urban density areas.

Table 17: Presence of railways and connecting roads (categorised using the Openstreetmap highway key) [km], and permanent building polygons within 100 m of the MSL mark at unprotected sandy shorelines | enveloped by scaled Bruun rule coastline recession estimates at uninterrupted coastlines or explained by the SMIC method (Openstreetmap database).

Coastal sector	Railways [km]	Roads [km]				Buildings polygons
		Trunk	Primary	Secondary	Tertiary	
Southern	- |	6.9 | 1.1	1.2 | 1.1	≈ 0 | -	0.3 | ≈ 0	793 | 195
South-eastern	- |	- | -	- | -	0.3 | -	0.6 | -	48 | 2
Eastern	- |	0.8 | -	0.4 | -	- | -	5.2 | 7.1	514 | 325
North-eastern	- |	- | -	- | -	1.6 | 0.2	6.2 | 1.0	1453 | 732
Northern	- |	≈ 0 | 0.2	2.4 | 1.9	0.4 | ≈ 0	- | -	15 | 10
North-western	≈ 0 | ≈ 0	- | -	1.1 | -	- | -	- | -	155 | 171
Western	27 | 1.3	2.4 | 0.9	- | -	1.1 | -	5.8 | 0.4	445 | 217
Southwestern	2.1 | 0.8	10 | 2.3	- | -	≈ 0 | -	0.3 | ≈ 0	153 | 56

.

- Using the third generation Simulating Waves Nearshore model developed at Delft University of Technology, offshore ERA-Interim reanalysed wave data (Dee et al., 2011) can be projected onto a nearshore grid. The resulting refined nearshore wave conditions can be used to estimate depth of closures more accurately. An example is found in Giardino et al. (2018).
- Alternative to the approach by Udo and Takeda (2017), the annual (nearshore) significant wave heights exceeded for 12 hours and affiliated wave periods may be used to build two generalised extreme value distributions. Said distributions can be used to determine the required wave conditions exceeded for 12 hours at timescales within and outside that of the employed (nearshore) wave data.
- Regarding the attenuation of the oceanic tide in large (with a wide inlet channel) inlet-basin systems here a simplification assuming no tidal attenuation has been used . It is recommended to either justify the simplication further or derive a new relation between the oceanic tide an the tidal amplitude within the basin for (both small and) large inlet-basin systems. Provided the aforementioned, the iterative approach by Bamunawala et al. (2018) is promising in modelling present and future ebb tide flow volumes for both type I and type II inlet-basin systems as it decreases the required variables to more easily observed variables such as inlet channel length and width.
- An improved scaling of the Global Human Footprint Index for use in the BQART model may be attained through the following steps:
    1. Determine the catchment-wide GHFI value of each catchments used by Syvitski and Milliman (2007) to derive the BQART model.
    2. Average the catchment-wide GHFI values of the catchments associated with each E_h class ($E_h = 0.3$, $E_h = 1.0$ or $E_h = 2.0$).
    3. Fit a line through the three datapoints that allows E_h to be a function of the GHFI.
- To accurately incorporate river mining activities and increase the applicability of the BQART model in other coastline recession studies a sound approach to combining the effects of reservoir siltation and river mining activities should be sought.
- Future comparisons between the Bruun rule and the Probabilistic Coastal Recession method is advised to use the annual average shoreline locations according to the Probabilisitc Coastal Recession method with Bruun rule estimates and repeat the comparison for sandy coastlines with different dimensions of the active shoreface.

References

Argus, D. F., Peltier, W. R., Drummond, R., & Moore, A. W. (2014). The Antarctica component of postglacial rebound model ICE-6G_C (VM5a) based on GPS positioning, exposure age dating of ice thicknesses, and relative sea level histories. *Geophysical Journal International*, *198*(1), 537–563. https://doi.org/10.1093/gji/ggu140

Ballu, V., Bouin, M.-N., Simeoni, P., Crawford, W. C., Calmant, S., Bore, J.-M., … Pelletier, B. (2011). Comparing the role of absolute sea-level rise and vertical tectonic motions in coastal flooding, Torres Islands (Vanuatu). *Proceedings of the National Academy of Sciences*, *108*(32), 13019–13022. https://doi.org/10.1073/pnas.1102842108

Bamunawala, J., Ranasinghe, R., van der Spek, A., Maskey, S., & Udo, K. (2018). Assessing Future Coastline Change in the Vicinity of Tidal Inlets. *Journal of Coastal Research*. https://doi.org/10.1007/s11947-009-0181-3

Brune, G. M. (1953). Trapping Efficiency of Reservoirs. *American Geophysical Union*, *34*(3), 407–419.

Bruun, P. (1962). Sea Level Rise as a Form of Shore Erosion. *Coastal and Ocean Engineering*, *88*(1), 117–130.

Camenen, B., & Larson, M. (2007). Predictive Formulas for Breaker Depth Index and Breaker Type. *Journal of Coastal Research*, *234*(4), 1028–1041. https://doi.org/10.2112/05-0566.1

Castelle, B., & Coco, G. (2012). The morphodynamics of rip channels on embayed beaches. *Continental Shelf Research*, *43*, 10–23. https://doi.org/10.1016/j.csr.2012.04.010

CCD. (2006). *Coastal Zone Management Plan (CZMP) 2004*. *Gazette Extraordinary of the Democratic Socialist Republic of Sri Lanka*. Retrieved from http://www.coastal.gov.lk/downloads/pdf/CZMP English.pdf

Cooper, J. A. G., & Pilkey, O. H. (2004). Sea-level rise and shoreline retreat: Time to abandon the Bruun Rule. *Global and Planetary Change*, *43*(3–4), 157–171. https://doi.org/10.1016/j.gloplacha.2004.07.001

Cowell, P. J., Stive, M. J. F., Niedoroda, A. W., Swift, D. J. P., De Vriend, H. J., Buijsman, M. C., … De Boer, P. L. (2003). The coastal-tract (part 2): Applications of aggregated modeling of low-order coastal change. *Journal of Coastal Research*, *19*(4), 828–848. https://doi.org/10.2112%2F0749-0208%282003%29019%5B0828%3ATCPAOA%5D2.3.CO%3B2

Cowell, P. J., Thom, B. G., Jones, R. A., Everts, C. H., & Simanovic, D. (2006). Management of Uncertainty in Predicting Climate-Change Impacts on Beaches. *Journal of Coastal Research*, *221*, 232–245. https://doi.org/10.2112/05A-0018.1

Da Cruz, C. M. (2018). *Stochastic Projections of Coastline Variations: Application to Hasaki Beach, Japan*. IHE-Delft Institute for Water Education.

Dastgheib, A., Jongejan, R., Mehvar, S. A., & Ranasinghe, R. (2017). *Coastal Risk Assessment Along the East Coast of Sri Lanka*.

Dayananda, H. V. (1992). *Shoreline Erosion in Sri Lanka's Coastal Areas*.

Dean, R. G. (1991). Equilibrium Beach Profiles : Characteristics and Applications. *Journal of Coastal Research*, *7*(1), 53–84. Retrieved from http://www.jstor.org/stable/4297805

Dean, R. G. (1995). Cross-shore sediment transport processes. *Coastal Engineering Manual*, *1*, 152–...

Dean, R. G., & Dalrymple, R. A. (2001). *Coastal processes with engineering applications* (2004th ed.). Cambridge: Cambridge University Press. Retrieved from http://marineman.ir/wp-content/uploads/2015/03/Coastal_Processes_with_Engineering_Applications__Cambridge_Ocean_Technology_Series_.pdf?v=d6392e39ad2a

Dee, D. P., Uppala, S. M., Simmons, A. J., Berrisford, P., Poli, P., Kobayashi, S., … Vitart, F. (2011). The ERA-Interim reanalysis: Configuration and performance of the data assimilation system. *Quarterly Journal of the Royal Meteorological Society*, *137*(656), 553–597. https://doi.org/10.1002/qj.828

Department of Irrigation Sri Lanka. (2018). Online Reservoir Status. Retrieved March 16, 2018, from http://www.irrigation.gov.lk/index.php?option=com_gmapfp&view=gmapfp&layout=categorie&catid=124&id_perso=0&Itemid=221&lang=en

Department of Meteorology Sri Lanka. (2016). Climate of Sri Lanka. Retrieved April 4, 2018, from http://www.meteo.gov.lk/index.php?option=com_content&view=article&id=94&Itemid=310&lang=en

Duong, T. M. (2015). *Climate Change Impacts on the Stability of Small Tidal Inlets*.

Duong, T. M., Ranasinghe, R., Walstra, D., & Roelvink, D. (2016). Assessing climate change impacts on the stability of small tidal inlet systems: Why and how? *Earth-Science Reviews*, *154*, 369–380.

https://doi.org/10.1016/j.earscirev.2015.12.001

Edelman, T. (1976). Dune erosion during storm surge conditions. *Hydro Delft*, *45*, *Dec.*, 2–3. https://doi.org/10.9753/icce.v13.%25p

Engle, V. D., Kurtz, J. C., Smith, L. M., Chancy, C., & Bourgeois, P. (2007). A classification of U.S. estuaries based on physical and hydrologic attributes. *Environmental Monitoring and Assessment*, *129*(1–3), 397–412. https://doi.org/10.1007/s10661-006-9372-9

Giardino, A., Schrijvershof, R., Nederhoff, C. M., de Vroeg, H., Brière, C., Tonnon, P. K., … Sloff, C. J. (2018). A quantitative assessment of human interventions and climate change on the West African sediment budget. *Ocean and Coastal Management*, *156*, 249–265. https://doi.org/10.1016/j.ocecoaman.2017.11.008

Global Energy Observatorium. (2018). No Title. Retrieved March 16, 2018, from http://globalenergyobservatory.org/select.php?tgl=Edit

Hallermeier, R. J. (1980). A profile zonation for seasonal sand beaches from wave climate. *Coastal Engineering*, *4*(C), 253–277. https://doi.org/10.1016/0378-3839(80)90022-8

Heinemarm, H. G. (1981). a New Sediment Trap Efficiency Curve for Small Reservoirs. *JAWRA Journal of the American Water Resources Association*, *17*(5), 825–830. https://doi.org/10.1111/j.1752-1688.1981.tb01304.x

IHE-Delft. (2016). *Delft3D model based alongshore sediment transport rates at Pesalai , Gurunagar , Point Pedro and Mullaitivu , Sri Lanka (Phase 2 Final Report)*. Delft.

IPCC. (2013). *Climate Change 2013: The Physical Science Basis*. New York. https://doi.org/10.1017/CB09781107415315.026

Jacobsen, P. R., Perera, N., & Jensen, K. B. (1987). *Master Plan for Coastal Erosion Management*. Retrieved from https://www.researchgate.net/publication/294306230_Master_plan_for_coast_erosion_management

Jarvis, A., Reuter, H. I., Nelson, A., & Guevara, E. (2008). Hole-filled SRTM for the globe Version 4, International Centre for Tropical Agriculture (CIAT), Available at: http://srtm.csi.cgiar.org.

Jayasekera, D. L., Kaluarachchi, J. J., & Villholth, K. G. (2011). Groundwater stress and vulnerability in rural coastal aquifers under competing demands: A case study from Sri Lanka. *Environmental Monitoring and Assessment*, *176*(1–4), 13–30. https://doi.org/10.1007/s10661-010-1563-8

Jayathilaka, R. M. R. M. (2015). *Large Scale Sediment Budgets in Data Poor Environments via Numerical Modelling*. UNESCO-IHE Institute for Water Education.

Jayawardena, U. de S., & Sarathchandra, M. J. (1995). Land subsidence and other environmental impacts due to groundwater extraction from fractured hard rocks in Sri Lanka. *Land Subsidence (Fifth International Symposium of Land Subsidence)*, (234), 439–444.

Jiménez, J. A., Sánchez-Arcilla, A., & Stive, J. F. (1993). Prediction of Storm Normal Beach Profiles. *Journal of Waterway Port Coastal and Ocean Engineering*.

Keulegan, G. H. (1967). *Tidal Flow in Entrances; Water-Level Fluctuations of Basins in Communication With Seas*.

Klotz, M., Kemper, T., Geiß, C., Esch, T., & Taubenböck, H. (2016). How good is the map? A multi-scale cross-comparison framework for global settlement layers: Evidence from Central Europe. *Remote Sensing of Environment*, *178*, 191–212. https://doi.org/10.1016/j.rse.2016.03.001

Komar, P. D. (1983). *CRC Handbook of Coastal Processes and Erosion*. Boca Raton: CRC Press.

Kummu, M., Lu, X. X., Wang, J. J., & Varis, O. (2010). Basin-wide sediment trapping efficiency of emerging reservoirs along the Mekong. *Geomorphology*, *119*(3–4), 181–197. https://doi.org/10.1016/j.geomorph.2010.03.018

Larson, M., Erikson, L., & Hanson, H. (2004). An analytical model to predict dune erosion due to wave impact. *Coastal Engineering*, *51*(8–9), 675–696. https://doi.org/10.1016/j.coastaleng.2004.07.003

Le Cozannet, G., Oliveros, C., Castelle, B., Garcin, M., Idier, D., Pedreros, R., & Rohmer, J. (2016). Uncertainties in Sandy Shorelines Evolution under the Bruun Rule Assumption. *Frontiers in Marine Science*, *3*, 49. https://doi.org/10.3389/fmars.2016.00049

Luijendijk, A., Hagenaars, G., Ranasinghe, R., Baart, F., Donchyts, G., & Aarninkhof, S. (2018). The State of the World's Beaches. *Nature Scientific Reports*, *8*, 1–11. https://doi.org/10.1038/s41598-018-24630-6

McCarroll, R. J., Brander, R. W., MacMahan, J. H., Turner, I. L., Reniers, A. J. H. M., Brown, J. A., … Sherker, S. (2014).

Evaluation of swimmer-based rip current escape strategies. *Natural Hazards*, *71*(3), 1821–1846. https://doi.org/10.1007/s11069-013-0979-1

McCarroll, R. J., Brander, R. W., Turner, I. L., Power, H. E., & Mortlock, T. R. (2014). Lagrangian observations of circulation on an embayed beach with headland rip currents. *Marine Geology*, *355*, 173–188. https://doi.org/10.1016/j.margeo.2014.05.020

Mendoza, E. T., & Jiménez, J. A. (2006). Storm-Induced Beach Erosion Potential on the Catalonian Coast. *Journal of Coastal Research*, (48), 81–88. https://doi.org/10.1061/40855(214)98

Mück, M., Klotz, M., & Taubenbock, H. (2017). Validation of the DLR Global Urban Footprint in rural areas: A case study for Burkina Faso. *2017 Joint Urban Remote Sensing Event, JURSE 2017*, 6–9. https://doi.org/10.1109/JURSE.2017.7924618

Nicholls, R. J., Birkemeier, W., & Hallermeier, R. (1996). Application of The Depth of Closure Concept. *Coastal Engineering*, 3874–3887.

Nicholls, R. J., Hanson, S. E., Lowe, J. A., Warrick, R. A., Lu, X., & Long, A. J. (2014). Sea-level scenarios for evaluating coastal impacts. *Wiley Interdisciplinary Reviews: Climate Change*, *5*(1), 129–150. https://doi.org/10.1002/wcc.253

Nicholls, R. J., Larson, M., Capobianco, M., & Birkemeier, W. A. (1998). Depth of closure: Improving understanding and prediction. *Proceedings of the 26th International Conference on Coastal Engineering*, *3*, 2888–2901. https://doi.org/10.1061/9780784404119.219

O'Neil, D. J. (1987). *Variations in Alsea River flow: implications for Alsea Spit and Inlet Stability*. Oregon State University.

Peltier, W. R., Argus, D. F., & Drummond, R. (2015). Space Geodesy Constrains Ice-Age Terminal Deglaciation: The Global ICE-6G_C (VM5a) Model. *J. Geophys. Res. Solid Earth*, *120*(1), 450–487. https://doi.org/10.1002/2014JB011176

Ranasinghe, R., Callaghan, D., & Stive, M. J. F. (2012). Estimating coastal recession due to sea level rise: Beyond the Bruun rule. *Climatic Change*, *110*(3–4), 561–574. https://doi.org/10.1007/s10584-011-0107-8

Ranasinghe, R., Duong, T. M., Uhlenbrook, S., Roelvink, D., & Stive, M. (2013). Climate-change impact assessment for inlet-interrupted coastlines. *Nature Climate Change*, *3*(1), 83–87. https://doi.org/10.1038/nclimate1664

Ranasinghe, R., & Stive, M. J. F. (2009). Rising seas and retreating coastlines. *Climatic Change*, *97*(3), 465–468. https://doi.org/10.1007/s10584-009-9593-3

Roelvink, D., Reniers, A., van Dongeren, A., van Thiel de Vries, J., McCall, R., & Lescinski, J. (2009). Modelling storm impacts on beaches, dunes and barrier islands. *Coastal Engineering*, *56*(11–12), 1133–1152. https://doi.org/10.1016/j.coastaleng.2009.08.006

Rosati, J. D., Dean, R. G., & Walton, T. L. (2013). The modified Bruun Rule extended for landward transport. *Marine Geology*, *340*, 71–81. https://doi.org/10.1016/j.margeo.2013.04.018

Silva, L. E. ., Katupotha, J., Amarasinghe, O., Manthrithilake, H., & Ariyaratna, R. (2013). *Lagoons of Sri Lanka: from the origins to the present*. Colombo: International Water Management Institute. https://doi.org/10.5337/2013.215

Sindhu, B., & Unnikrishnan, A. S. (2013). Characteristics of Tides in the Bay of Bengal. *Marine Geodesy*, *36*(4), 377–407. https://doi.org/10.1080/01490419.2013.781088

Stive, M. J. F., & Rakhorst, R. D. (2008). Review of empirical relationships between inlet cross-section and tidal prism. *Journal of Water Resources and Environmental Engineering*, *23*(23), 89–95.

Sunamura, T. (1975). Static relationships among beach slope, sand size and wave properties. *Geographical Review of Japan*, *48*(7), 485–489.

Sunamura, T. (1983). Coastal and beach changes by waves. *Transactions - Japanese Geomorphological Union*, *4*(2), 179–188.

Survey Department Sri Lanka. (1983). *National Atlas of Sri Lanka*. Colombo: Survey Department Sri Lanka.

Syvitski, J. P. M., & Milliman, J. D. (2007). Geology , Geography , and Humans Battle for Dominance over the Delivery of Fluvial Sediment to the Coastal Ocean. *The Journal of Geology*, *115*(1), 1–19. https://doi.org/10.1086/509246

Takeda, I., & Sunamura, T. (1983). *Formation and Spacing of Beach Cusps* (26th ed.).

Thompson, P. R., Piecuch, C. G., Merrifield, M. A., McCreary, J. P., & Firing, E. (2016). Forcing of recent decadal variability in the Equatorial and North Indian Ocean. *J. Geophys. Res. Oceans*, *121*(9), 6762–6778.

https://doi.org/10.1002/2016JC012132

Toimil, A., Losada, I. J., Camus, P., & Díaz-Simal, P. (2017). Managing coastal erosion under climate change at the regional scale. *Coastal Engineering*, *128*(November 2016), 106–122. https://doi.org/10.1016/j.coastaleng.2017.08.004

Udo, K., & Takeda, Y. (2017). Projections of Future Beach Loss in Japan Due to Sea-Level Rise and Uncertainties in Projected Beach Loss. *Coastal Engineering Journal*, *59*(02), 1740006. https://doi.org/10.1142/S057856341740006X

Velegrakis, F., & Schimmels, S. (2013). Predicting Beach Face rotation on a Meso Tidal, Steeply Sloping Beach. *Coastal Dynamics*, 1835–1846.

Verstraeten, G., & Poesen, J. (2000). Estimating trap efficiency of small reservoirs and ponds: methods and implications for the assessment of sediment yield. *Progress in Physical Geography*, *24*(2), 219–251. https://doi.org/10.1177/030913330002400204

Vörösmarty, C. J., Meybeck, M., Fekete, B., Sharma, K., Green, P., & Syvitski, J. P. M. (2003). Anthropogenic sediment retention: Major global impact from registered river impoundments. *Global and Planetary Change*, *39*(1–2), 169–190. https://doi.org/10.1016/S0921-8181(03)00023-7

Wadey, M. P., Roberts, H., & Harris, J. (2013). Impacts of climate change on built structures (onshore and coastal). *Marine Climate Change Impacts Partnership Science Review*, 284–294. https://doi.org/10.14465

Wickramaarachchi, B. (2010). *Spatial Analysis & Mapping, Maha Oya Low Land Corridor*.

Wickramagamage, P., Wickramanayake, N., Kumarihamy, K., Vidanapathirana, E., & Larson, M. (2012). A comparative study of elevation data from different sources for mapping the coastal inlets and their catchment boundaries. *Journal of the National Science Foundation of Sri Lanka*, *40*(1), 55–65. https://doi.org/10.4038/jnsfsr.v40i1.4169

Wijeratne, E. M. S. (n.d.). Sea Level Measurements and Coastal Ocean Modelling in Sri Lanka.

Wijeratne, E. M. S., & Pattiaratchi, C. B. (2017). Sea Level Variability in Sri Lanka Waters. Retrieved from http://wcrp.ipsl.jussieu.fr/Workshops/SeaLevel/Posters/2_1_WijeratneRevised.pdf

Wildlife Conservation Society - WCS and Center for International Earth Science Information Network - CIESIN - Columbia. (2005). Last of the Wild Project, Version 2, 2005 (LWP-2): Last of the Wild Dataset.

Zhang, K., Douglas, B. C., & Leatherman, S. P. (2004). Global warming and coastal erosion. *Climatic Change*, *64*(1–2), 41–58. https://doi.org/10.1023/B:CLIM.0000024690.32682.48

Appendix A

This appendix provides a qualitative description of the sediment sink and source terms found along the Sri Lankan coast. For ease of reading, the text has been split into paragraphs each linked to one coastal sector.

A.1 Southern Coastal Sector (Galle – Tangalle)

The West to East littoral current has drained the Southern coastal sector of most of its sediments. Consequently, beaches are mostly found in areas where the morphological control of headlands is sufficient to hold beaches in place or fluvial sediment supply is present.

Using a predictive formula for the breaker depth index (Camenen & Larson, 2007) and the breaking wave height (Sunamura, 1983) combined offshore mean wave conditions (Dee et al., 2011) and a constant beachslope (Dayananda, 1992) according to common grain sizes (Duong, 2015), surfzone widths during normal conditions between 25 m and 40 m have been predicted. A more elaborate explanation is written in Appenix B. Considering the limitations involved with predicting surf zone widths, the circulation of sediments at most small embayed beaches (up to approximately 400m in length (Castelle & Coco, 2012; McCarroll, Brander, MacMahan, et al., 2014)) is closed. Consequenlty, the sediment balance at these beaches is unaffected by the littoral drift of sediments. According to the criteria in Castelle and Coco, 2012, and McCarroll, Brander, MacMahan, et al., 2014, the circulation of sediments at larger embayed beaches in is Gandura Bay, Dikwella Bay, Nilewelli Bay and Mahawelli Bay (semi-)open.

Weligama Bay and Matara Bay receive large amount of fluvial sediments (Dayananda, 1992). Besides large fluvial systems, small systems (comparable to those investigated by Toimil et al. (2017)) are found at embayed beaches.

Figure A.1: Embayed beaches in Dikwella Bay. The distances between the headlands at the two beaches on the left and the beach on the right are less than 400 m (closed circulation of sediments). The distance between the headlands at the ends of the the middle beach is approximately 1100 m (open circulation of sediments) (Google Earth).

A.2 South-eastern Coastal Sector (Tangalle – Arugam Bay (Elephant Point))

Between Tangalle and Arugam Bay (Elephant Point), the prominence of headland formations results in a stable shoreline despite the littoral current going west to east (CCD, 2006; Dayananda, 1992). Consequently, no significant divergence in the littoral drift of sediments is expected. Most of the South-eastern shoreline is backed by large (mobile) dunes thus indicating the possibility of onshore loss of sediments due to aeolian transport. Then again, between Tangalle and Kirinda natural nourishment by offshore coral reefs (dependent upon the health of said reefs (CCD, 2006)) exists (Dayananda, 1992).

Fluvial sediments are mostly supplied by the Walawe Ganga, Kirindi Oya, Menik Ganga and Kumbukkan Oya rivers (Dayananda, 1992). Apart from lagoons immediately downdrift from headlands between Panama and Elepant Point, the multitude of inlet-basin systems not closed off by human activities appear closed on satellite images. However, according to conversations with officials of the CCD stationed in Pottuvil, these systems open during the South-west monsoon and are of great importance to the sediment budget of the South-east to East coast of Sri Lanka.

A.3 Eastern Coastal Sector (Arugam Bay (Elephant Point) – Trincomalee Bay)

Between Arugam Bay (Elephant Point) and Trincomalee bay, satellite images show without exception a Northwards longshore drift. Divergence in the littoral drift between Arugam Bay and Pasikuda Headland (North of Batticaloa Lagoon) allows the shoreline to progradate (CCD, 2006; Dayananda, 1992). Consequently, the vast amount of lagoons have to be manually opened to prevent flooding of the (low-lying (Dayananda, 1992) backshore. Prominent is the intermittently closed to permanently open Batticaloa Lagoon. North of Pasikuda Headland, nourishments by the littoral sediment drift are less prominent. Closely related, Google Earth satellite images show the inlet-basin systems here to be intermittently open.

Along the majority of the Eastern coastal sector partial nourishment of the shoreface from offshore sources exist (Dayananda, 1992). The commonly low-lying backshore results in onshore losses due to overwash. Evidence is predominantly found on satellite images towards the Northern end of the coastal sector.

A.4 North-eastern Coastal Sector (Trincomalee Bay – Point Pedro)

Trincomalee Bay may be assumed to block all sediments transported North from the Eastern coastal sector (Dayananda, 1992; Zhang et al., 2004). Regarding the direction of the longshore sediment drift within the coastal sector CCD, (2006), Dayananda (1992) and IHE-Delft (2016) give only a partial image. Based on the accretion and erosion patterns at headlands, and the shape of the sandspits, the dominant littoral drift of sediments between Tincomalee Bay and Nayaru Lagoon is without doubt towards the North. IHE-Delft (2016) calculate the presence of nodal point near Mullaitivu. Consequently, a point of confluence is expected between Nayaru Lagoon and Mullaitivu. North of Mullaitivu a North-east littoral drift until Point Pedro is generally agreed upon.

Along the North-east coast, multiple large permanently open inlet-basin systems are present. Coupled with a smooth coastline, most of the North-eastern coastal sector exchanges sediments with at least one permanently open inlet-basin systems. The basins contain varying amounts of tidal flats. One of the highest ratios between tidal flats and wet surface area is achieved by Nayaru Lagoon.

Due to the deep offshore bathymetry near Trincomalee Bay (CCD, 2006), possible offshore losses exist at Manayaweli Bay, Dutch Bay and Back Bay. With predicted surfzone widths during normal conditions between 15 m and 25 m, offshore loss of sediments can reasonably be debarred at Manayaweli Bay. North of Mullaitivu a low backshore may result in overwash of coastal sediments.

A.5 Northern Coastal Sector (Point Pedro – Vaddukoddai)

West of Point Pedro until Dabakolapatuna the shoreline is protected by (continuous) partially live reefs positioned approximately 65 m offshore. The source of sediments from these reefs is limited (Dayananda, 1992) but necessitate the truncation of the active shoreface to their offshore distance to the MSL mark (Ranasinghe et al., 2012). The longshore sediment drift is towards the West and feeds the Vaddukkodai sandspit. Between Point Pedro and the Vaddukoddai sandspit the coastline is interrupted once by the inlet of Thondammanaru Lagoon.

A.6 North-western Coastal Sector (Mannar Island – Kandakuliya)

Near Vankalaippadu on the North side of Mannar Island, IHE-Delft (2016) calculates the presence of a nodal point in the littoral drift of sediments. Across the entire length of the Gulf of Mannar (the south side of Mannar Island) sediments are transported in the Northern direction. Likely due to said littoral drift, the coast here is exceptionally sediment poor. Sandy beaches are present in the more sheltered parts of the coast, downdrift of fluvial systems, or held in place by headlands or jetties. South of Marichchukkaddi the mainland coast is behind several islands and consequently the ERA-Interim offshore wave conditions are likely not applicable.

A.7 Western Coastal Sector (Kandakuliya – Bentota)

Except for the area immediately South of the Kalu Ganga river mouth (Bamunawala et al., 2018), the littoral drift moves sediments towards the North. The straight coastlines leave beaches in the western coastal sector vulnerable to longshore sediment losses (CCD, 2006; Dayananda, 1992).

Equally important to the coastal sediment balance is the supply of fluvial sediments. Past human activities in the river catchments have resulted in receding coastlines downdrift from most large fluvial systems (CCD, 2006; Dayananda, 1992; Jayathilaka, 2015; Wickramaarachchi, 2010) . The Bruun rule cannot be applied along long stretches of the heavily engineered Western coast. Beaches downdrift from the Kalu Ganga river mouth and the Negombo Lagoon inlet sustained by the construction of breakwaters can been evaluated but must be assumed to be closed circulating embayed beaches.

A.8 South-western Coastal Sector (Bentota – Galle)

The nodal point related to the South-west monsoon is, according to Jayathilaka (2015), between Hikkaduwa and Dodanduwa. Therefore, this area experiences large losses of sediments to the start-up of the littoral sediment drift going around most of the island. North of Ambalangoda, headland formations (similar to those in the South-eastern coastal sector) define the shape of the shoreline. Therefore, at this location, little longshore losses of sediments are expected. Nourishment from offshore coral reefs has been witnessed North of Ambalangoda (Dayananda, 1992).

Apart from the Bentota Ganga river (which only supplies a limited amount of fluvial sediments (Dayananda, 1992)) and the Gin Ganga river, multiple coastal lakes with fixed inlets are present along the South-west coast. However, due to the many headlands, jetties and breakwaters the longshore lengths of affected coastline remain small.

Appendix B

Appendix B describes the method that has been used to define the criteria by Castelle and Coco (2012), McCarroll et al (2014) for embayed beaches with a closed, semi-open and open circulation of coastal sediments.

Firstly, the sinusoidal empirical function by Camenen and Larson (2007) is composed:

$$f_*(m, \lambda_\infty) = A_1 + A_2 \, sin\left[\frac{\pi}{2}\left(\frac{m}{m_{max}}\right)^{\alpha}\right] \qquad (B.1)$$

with m [-] the beach slope, λ_∞ [-] the offshore wave steepness, $A_1 = 0.87$, and A_2 and α coefficients that can be calculated using:

$$A_2 = 0.32 + 14\,\lambda_\infty \qquad (B.2)$$

$$\alpha = -(1 + 20\,\lambda_\infty) \qquad (B.3)$$

The use of Equation B.3 requires:

$$m > m_{max} = 0.10 + 1.6\,\lambda_\infty \qquad (B.4)$$

Once f_* has been calculated it is inserted into:

$$\gamma_b = \frac{0.284}{\sqrt{\lambda_\infty}}\, tanh\left(f_*\, \pi \sqrt{\lambda_\infty}\right) \qquad (B.5)$$

found Camenen and Larson (2007) to determine the breaker depth index (γ_b).

Secondly, the breaking wave height is calculated using Sunamura (1983):

$$H_b = \left[tan(m)^{0.2} \left(\frac{H_s}{L_s}\right)^{-0.25}\right] H_s \qquad (B.6)$$

with H_s [m] the mean significant wave height, and L_s [m] the mean significant wave length.

Lastly, the width of the surf zone is calculated by dividing the breaking wave height with the breaker depth index and the beach slope:

$$X_S = \frac{H_s}{\gamma_b\, m} \qquad (B.7)$$

The Irribaren number dictates a sensitivity of γ_b to the beach slope (Camenen & Larson, 2007). Moreover, Camenen and Larson (2007) report an error in γ_b by 20% and 10% in respectively 15% and 50% of their validations. Satellite images show that actual surf zone widths are within the higher part of the range in X_S values found with offshore ERA-Interim reanalysed wave data (Dee et al., 2011) and a beach slope between 0.070 and 0.105 (Dayananda, 1992). Therefore, the upper limit has been used to define the criteria by Castelle and Coco (2012), and McCarroll et al. (2014).

Appendix C

Future shortages in fluvial sediments supplied to the coast by rivers and volumes of coastal sediments imported by inlet-basin systems.

Deduru Oya

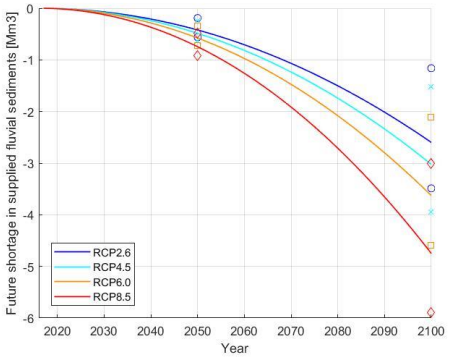

Kelani Ganga

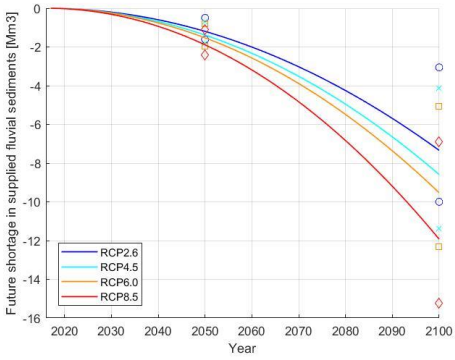

Kalu Ganga

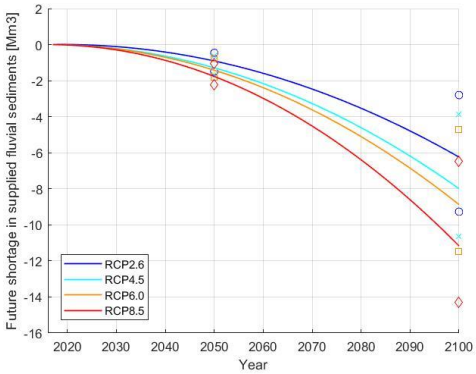

Ging Ganga

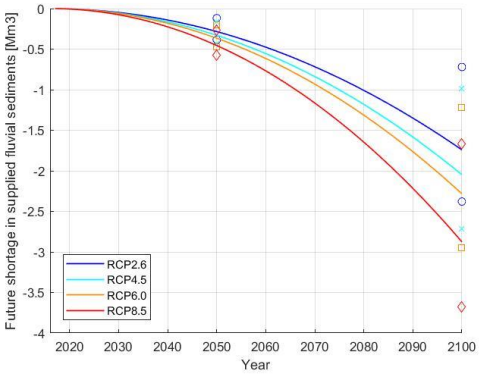

Nilwala Ganga

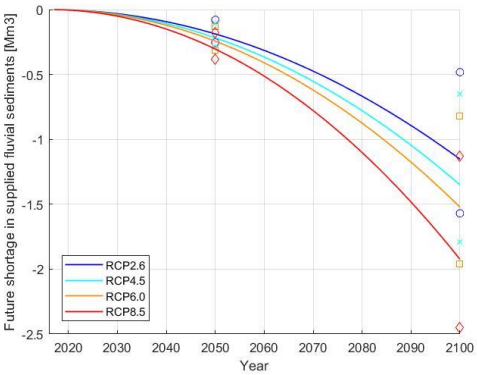

Walawe Ganga

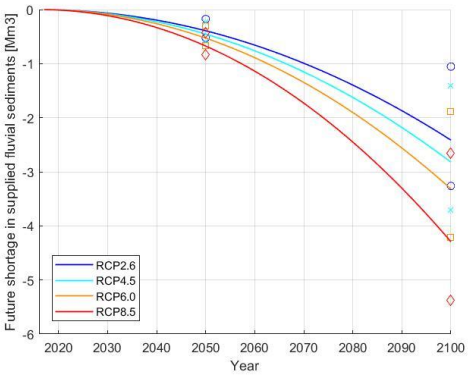

Kirindi Oya

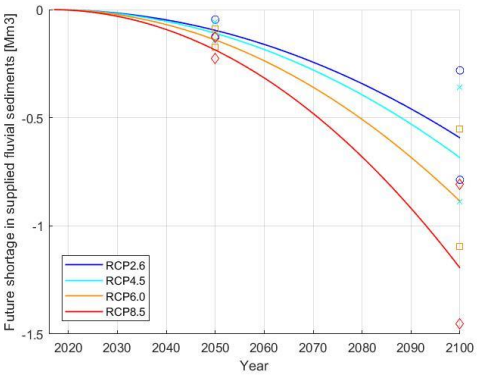

Menik Ganga

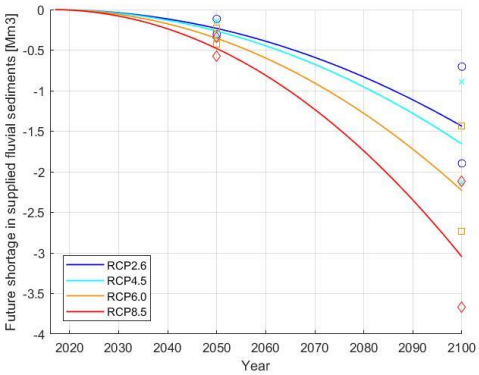

Kumbukkan Oya

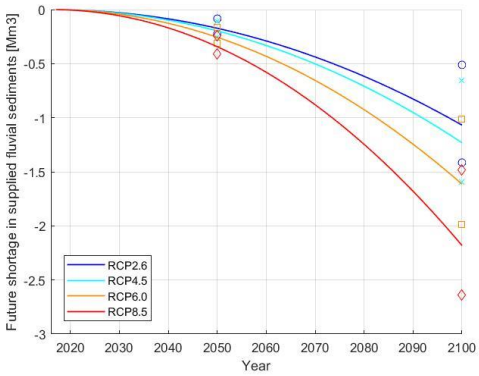

Gal Oya

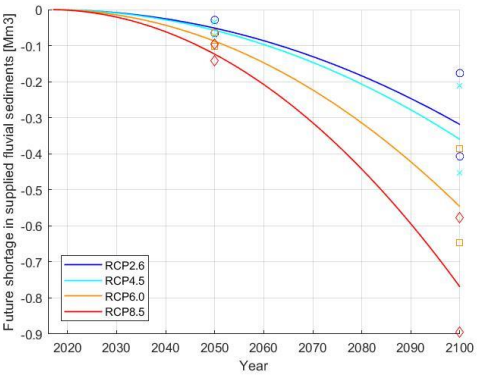

Chilaw Lake

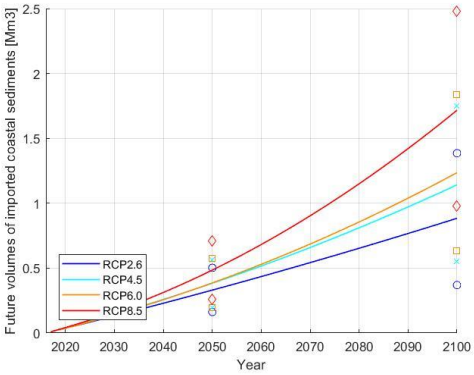

Batticaloa Lagoon

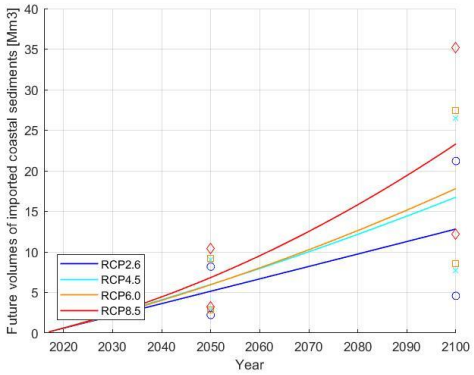

Kokkilai Lagoon

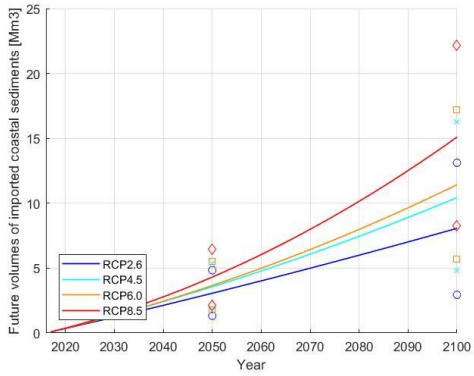

Nayaru Lagoon

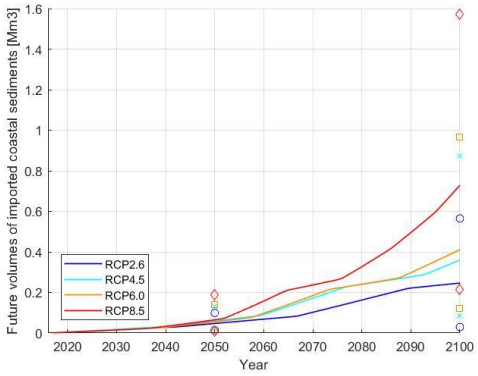

Thondamannaru Lagoon

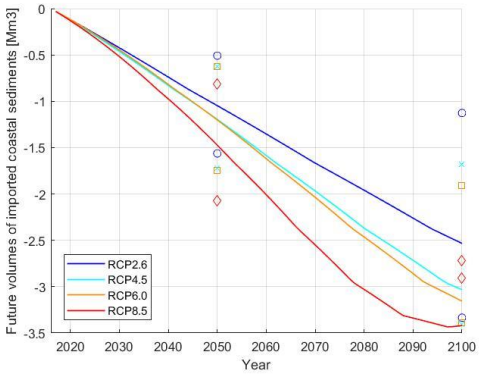

Appendix D

Future shortages in fluvial sediments supplied to the coast by rivers after substracting legal river mining volumes ($V_{m\ legal}$) (frames on the left) and river mining volumes including illegal mining activities ($V_{m\ total}$) (frames on the right). River mining volumes have been extrapolated using the reported mining volumes and the present annual fluvial sediment supply for the Kalu Ganga river.

Deduru Oya

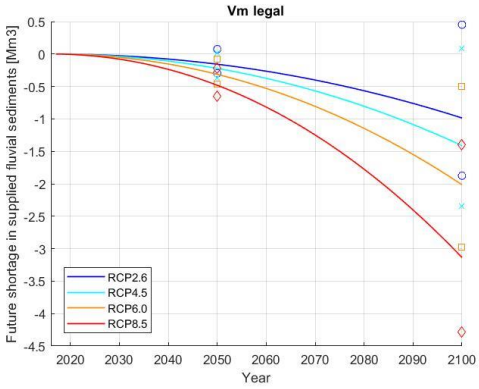

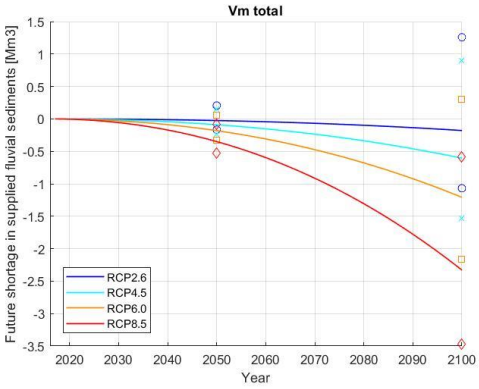

Kelani Oya

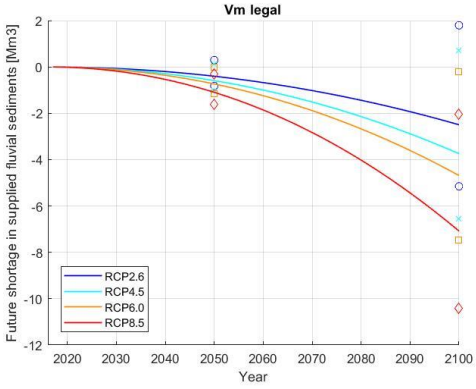

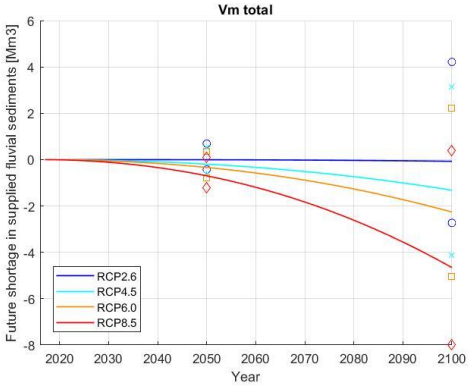

Kalu Ganga

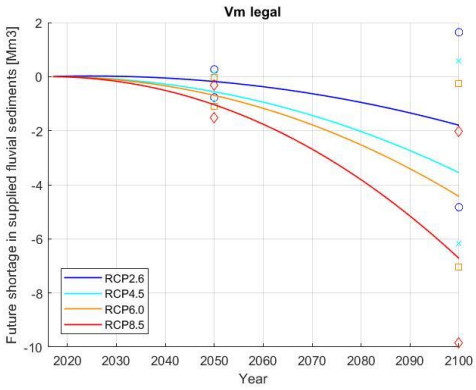

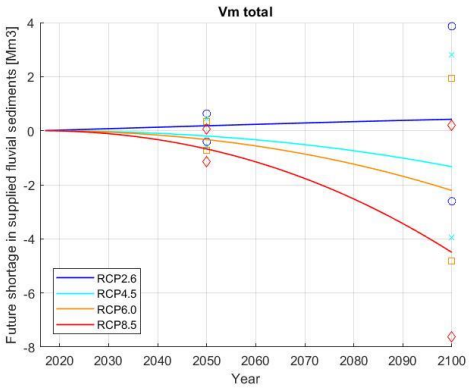

Gin Ganga

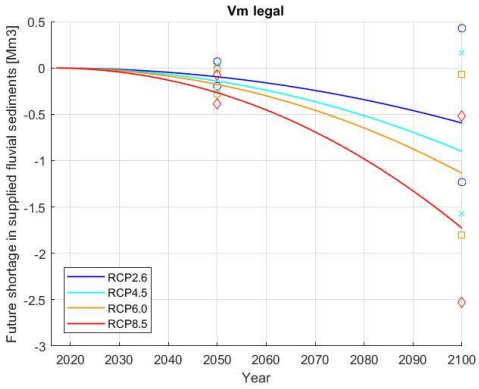

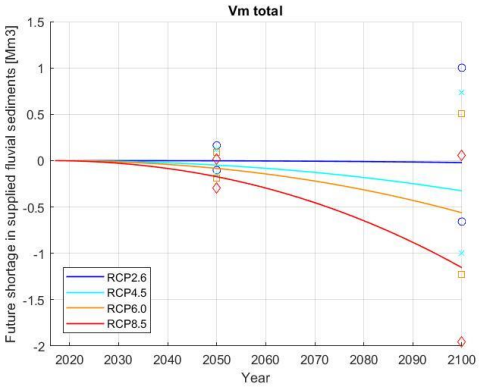

Nilwala Ganga

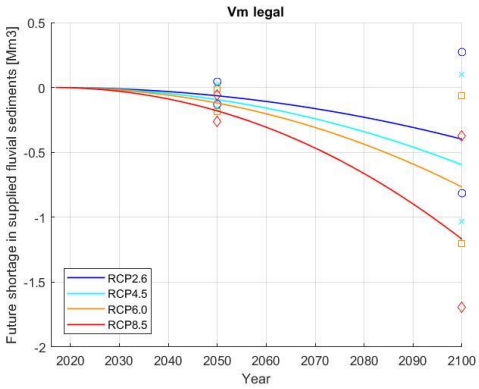

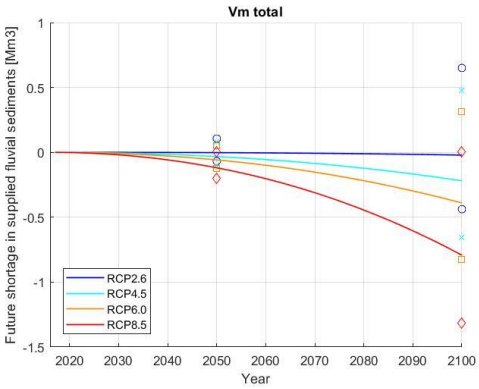

Menik Ganga

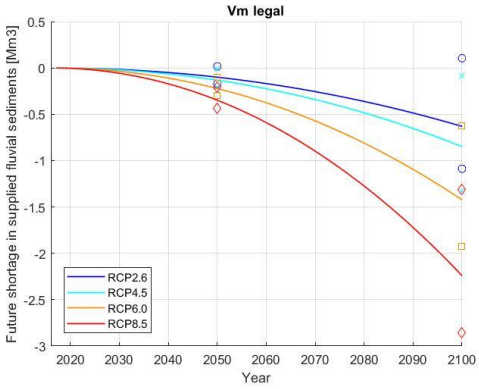

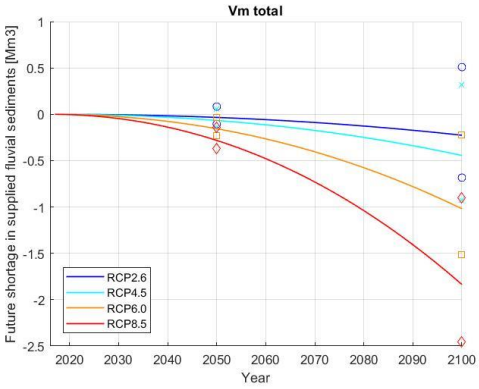

Kumbukkan Oya